Process Intensified Gas-to-Liquids Technology Enhanced by Microfibrous Entrapped Catalyst Structure

by

Xinquan Cheng

A dissertation submitted to the Graduate Faculty of
Auburn University
in partial fulfillment of the
requirements for the Degree of
Doctor of Philosophy

Auburn, Alabama
December 15, 2018

Keywords: Fischer-Tropsch Synthesis, Hydrocracking, Syngas-to-DME (STD), Syngas-to-Gasoline (STG), Microfibrous Entrapped Catalysts (MFEC), Heat Transfer and Mass Transfer

Approved by

Bruce J. Tatarchuk, Chair, Professor of Chemical Engineering
Andrew J. Adamczyk, Assistant Professor of Chemical Engineering
Selen Cremaschi, Associate Professor of Chemical Engineering
Maria Soledad Peresin, Assistant Professor of School of Forestry and Wildlife Sciences

Abstract

The increasing demand for liquid fuels draws attention to synthetic fuels. Currently, two well-known Gas-to-Liquids technologies are used to convert syngas to liquid fuels. One is Fischer-Tropsch Synthesis (FTS); the other one is the methanol-based approach. It can be Syngas-to-Gasoline (STG), which is based on methanol synthesis and Methanol-to-Gasoline (MTG). The MTG process composed of methanol dehydration to form Dimethyl Ether (DME) and DME converts on zeolites to synthesize gasoline. If we combine methanol synthesis with methanol dehydration, the Syngas-to-DME (STD) process could be formed, which is also an effective method to generate synthetic fuel. Although DME is not in liquid phase under atmosphere pressure, it can be liquefied with minor pressure (0.5 MPa). Also, DME is an excellent diesel fuel alternation with high cetane number. Hence, people treat DME as a liquid fuel, and DME synthesis is also discussed in this dissertation. In short, the two major approaches of gas-to-liquids are FTS and methanol-based approach including STD and STG.

These two approaches have their advantages and disadvantages. FTS process produces a broad spectrum of high value-added products including liquefied petroleum gas, gasoline, jet fuels, diesel, and waxes. Typically, it requires complex and expensive subsequent processes to upgrade the initial products to meet liquid fuel specifications. For instance, the heavy wax products need to be hydrocracked or thermally cracked into middle distillates to maximize liquid fuels production. The FTS and hydrocracking process can be integrated into a single reactor by physically mixing FTS catalysts and hydrocracking catalysts. The problem is that both FTS (ΔH^0 = -165.0 kJ/mol) and hydrocracking processes are highly exothermic processes, and the product distribution of FTS is strongly dependent on the reaction temperature. High temperatures favor the formation of undesirable light products like methane. Therefore, a reactor system with an

excellent heat transfer property is necessary for process intensifying these two highly exothermic processes together.

Both the STD and STG approaches need to go through multiple reaction steps to synthesize the final liquid fuels. It typically consists of methanol production from syngas and dimethyl ether production via methanol dehydration. For the STD process, the reaction is stopped at methanol dehydration and DME as the final product. If for the STG process, an additional reaction step needs to be added to convert DME to gasoline. The STD process can produce high quality DME that used as diesel fuel alternation. The STG process can synthesize high quality gasoline with high selectivity, but it cannot produce jet fuels or diesel. Also, methanol synthesis is a reversible pressure dependent reaction and is subject to an equilibrium limitation. Moreover, every reaction step requires independent reactor systems, relevant product separation systems, and recycle loops. Hence, the conventional STD or STG process is not an efficient process to convert syngas to liquid fuels. There is a great opportunity to integrate methanol synthesis and methanol dehydration reaction, which overcomes the pressure dependent equilibrium yield of methanol and push the reaction forward. It must be noted that both methanol synthesis (ΔH^0 = -90.8 kJ/mol) and methanol dehydration (ΔH^0 = -23.6 kJ/mol) are highly exothermic reactions. In addition, Water-Gas-Shift (WGS) reaction is another highly exothermic reaction (ΔH^0 = -41.1 kJ/mol), which is unavoidable occur with methanol synthesis reaction. The net reaction of STD is an extremely exothermic process (ΔH^0 = -246.3 kJ/mol). Therefore, a reactor system must have an efficient heat transfer mechanism to accommodate the added thermal load from integrating these highly exothermic reactions into a single reactor.

As we mentioned before, the STG process is operated in three consecutive reaction steps: methanol synthesis, methanol dehydration to form DME, DME converts to gasoline. Every

reaction step needs their own reactor system, heating system, product separation system, and recycle loops, etc. Therefore, the STG process is complex and expensive if operating in the traditional method with multiple reaction steps. However, there are two novel process intensified approaches. Since the first two reaction steps could be integrated together, then the STG process can be reduced to a two-step process. Furthermore, if we can continue to process intensification of the two-step STG process into a single-step STG process, we could greatly reduce the CAPEX & OPEX. The key issue is like the one-step STD process, all these reactions in the STG process are highly exothermic reactions. When compared with the one-step STD process, the single-step STG process is even more exothermic because one more exothermic reaction has been added. All in all, new means of enhancing intra-bed heat transfer are required to intensify these highly exothermic reactions.

Microfibrous Entrapped Catalyst (MFEC) structure is a novel catalyst structure developed by our group, which is a micron-sized metal fibers network with high thermal conductivity. Previous efforts on this unique catalyst structure have shown significant enhancement in intra-bed heat transfer and mass transfer. Especially for highly exothermic reactions like FTS, Cu MFEC structure can efficiently transfer the reaction heat out of the reactor, maintain a stable reaction temperature, and improved FTS product selectivity and process stability.

This dissertation is focusing on process intensification of FTS and hydrocracking process together, process intensification of the STD into a one-step process, and process intensification of the conventional STG process into a single vessel. The Cu MFEC structure has been used to handle the added thermal load, to maintain a stable reaction temperature, and to scale up the tubular reactor to a larger scale. In the first part, a highly active and stable iron-based FTS catalyst (Fe-FTS) has been developed. Based on that, a hybrid catalyst was formed by physically

mixing the Fe-FTS with an equal mass of mesoporous aluminosilicate. This hybrid catalyst demonstrated FTS and hydrocracking activity simultaneously. Furthermore, the reaction has been scaled up to a large tubular reactor (34.0 mm I.D.) packed with Cu MFEC. It demonstrated a radial temperature gradient of less than 5 ºC, while the comparative packed bed (34.0 mm I.D.) reached a radial temperature gradient around 54 ºC. In the second part, the direct STD process was carried out in a 34.0 mm I.D. tubular reactor with the assistance of Cu MFEC structure. As a result, the one-step STD process demonstrated a stale temperature profile throughout the entire reaction process, and the radial temperature deviation is around 7.6 ºC. In contrast, the comparable packed bed showed a temperature deviation of 37.5 ºC. The direct STD process has been carried out under different reaction conditions (H_2:CO ratio, GHSV or WHSV, T, reactor size and type). The results showed that it offers a high per pass conversion (68.8 %) and high carbon productivity (0.51 g of C/$g_{catalyst}$/h) when a reactor packed (34.0 mm I.D.) with Cu MFEC structure and operated at H_2:CO = 1:1, WHSV = 4.18 L/$g_{catalyst}$/h, and T = 275 ºC. In the third part, a single vessel STG (SV-STG) with multiple reaction zones has been developed. The SV-STG demonstrated a high gasoline selectivity of 74.8 wt% under a high CO conversion of 78.3 % in a small tubular reactor (9.0 mm I.D. Moreover, Cu MFEC structure has been successfully used to scale up SV-STG to a large tubular reactor (41.mm I.D.) without compromising the reaction activity or gasoline selectivity. The SV-STG packed with Cu MFEC structure exhibited a maximum radial temperature gradient of less than 5 ºC, while the comparable packed bed showed a maximum radial temperature gradient around 40 ºC. This difference has only been demonstrated in a bench scale reactor (41.0 mm I.D. tubular reactor), and the difference can be much greater in a larger diameter tube. Furthermore, Cu MFEC structure has high voidage (60 – 80 vol%) which prevents the bed from experiencing severe

pressure drop even when using small catalyst particles (80 – 170 mesh). Therefore, the Cu MFEC structure is greatly heat transfer medium, which enables process intensification of these highly exothermic reactions, significantly reduces CAPEX and OPEX and enhances scalability and modularity.

Acknowledgments

First of all, I would like to express my great appreciation to my advisor Dr. Bruce J. Tatarchuk for his tremendous experience and broad knowledge has guided me through my Auburn career. I have learned a lot from Dr. Tatarchuk, not only in research related knowledge and skills but also in the way of thinking and doing things. I would also like to express my sincere appreciation to my committee members, Dr. Selen Cremaschi, Dr. Andrew J. Adamczyk, and Dr. Maria Soledad Peresin, and Dr. Bart Prorok for their guidances and support in my dissertation. I am very thankful to IntraMicro Inc. for providing the microfibrous materials and supporting my research, especially Dr. Hongyun Yang, Dr. Paul S. Dimick, Troy Barron, and Harrison Wright. They have been helped me a lot; I could not move my research forward without constant support from them. I would like to thank all the CM3 group members, especially Dr. Wenhua Zhu, Dwight Cahela, Peng Cheng, Phillip Martin. They are always helpful, and I had a great time working with them. Also, I would like to thank all my friends in Auburn and my church friends; they have made my life full of enjoyment and caring. The most important, I want to think my family including my parents, brothers, sisters, and my lover Yidan Zhang. Without the support and love from them, I am not able to accomplish all the things I did in the past five and a half years. I am very grateful to have them as my family and my lover. Finally, I really want to thank God for leading me through everything.

Table of Contents

List of Figures

List of Tables

Chapter I: Introduction of Gas-to-Liquids Technology

Abstract

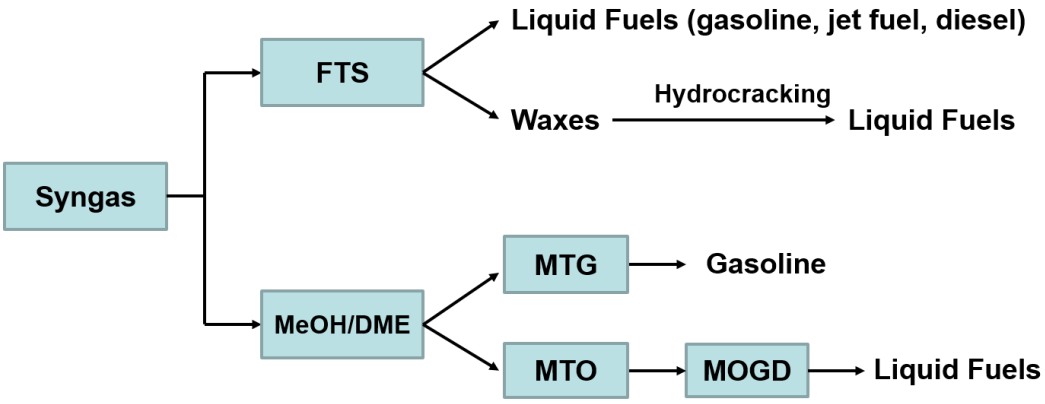

Figure I.1 Processes for syngas to liquid fuels

Gas-to-liquids (GTL) technology is a process that converts natural gas or other gaseous sources into liquid fuels including gasoline, jet fuel, and diesel. Also, GTL technology can produce waxes. One of the most common techniques used at GTL plants is Fischer-Tropsch Synthesis (FTS). Although FTS has been around for nearly a century and has been commercialized worldwide, it still the focus of much research. However, another technique that has also received interest in recent decades is syngas-to-methanol followed by methanol-to-gasoline (MTG). The process starts with syngas and ends with gasoline, so it has been named syngas-to-gasoline (STG). As we can see from Figure I.1, the FTS process can make both liquid fuels and waxes, so it has a broad spectrum of products. The initial wax products must be upgraded by subsequent processes to maximize the production of liquid fuels. The MTG process can only produce gasoline, but with some modifications, its major products will be olefins via a process called methanol-to-olefins (MTO). With a further process called Mobil olefins-to-gasoline and

distillates (MOGD), jet fuels and diesel can be produced. The above approaches are the two major methods used to convert syngas to liquid fuels.

I.1 History and Development

I.1.1 Fischer-Tropsch Synthesis (FTS)

Fischer-Tropsch synthesis (FTS) is a well-known technique for converting syngas containing hydrogen and carbon monoxide to hydrocarbon products. In 1922, two Germany scientists Franz Fischer and Hans Tropsch discovered this technique, and the FTS process has been highly developed through recent decades [1–3]. In 1927, the problems of chemical engineering had been tackled under the supervision of Roelen, and then a series of fixed bed and circulating bed reactors were developed. These improvements in the reactor design prepared well for the later industrialization of the FTS process. In 1934, the FTS process was first licensed by Ruhrchemie and reached an industrial scale in two years. In 1936, the first large-scale FTS plant was built in Braunkohle-Benzin. Due to the lack of domestic petroleum reservoirs, the German government encouraged the development of the FTS process to serve as an alternative fuel resource. By the end of the 1940s, Germany had a capacity of 660,000 tons of primary products per year. During World War II, large-scale fixed bed FTS reactors were developed by Arbeitsge-meinschaft Ruhrchemie und Lurgi (ARGE). At the same period, the circulating catalyst bed was proposed by Kellog. Both the ARGE and Kellog techniques were realized by Sasol in South Africa and were used to build several plants in the later time [4–7].

In the 1980s, the global interest was drawn back to FTS by the problems of increased crude oil price, environmental concerns, and utilization of natural gas. FTS process has been considered as a part of the Gas-to-Liquid (GTL) technology, which converts cheap natural gas to

more valuable middle distillates and lubricants. Under this situation, a lot of new FTS plants have been built, such as the Shell Bintulu, Sasol Oryx, SasolChevron in Nigeria, and ShellExxon in Qatar and so on [5]. In short, through the efforts of past decades, FTS technology has become a highly developed and full-scale industry.

I.1.2 Syngas-to-Gasoline (STG)

Syngas-to-Gasoline (STG) is a continuous integrated reaction loop including three major reactions in a series in which syngas is converted to gasoline [8]. The first reaction is methanol synthesis in which carbon monoxide and hydrogen are converted to methanol. The second reaction is DME synthesis in which the methanol is dehydrated into dimethyl ether (DME). The last step is gasoline synthesis in which DME is converted to hydrocarbons including paraffins, olefins, aromatics, and naphthenes. Typically, gasoline produced from STG process has a carbon number ranging from C_5 to C_{10}, which means the STG product spectrum limited to a maximum carbon number of C_{10}. Therefore, the STG process has a very narrow product distribution pattern compared with the FTS process [9].

Major Reactions of STG:

1. Methanol Synthesis: $CO + 2H_2 \leftrightarrow CH_3OH$
2. DME Synthesis: $2CH_3OH \leftrightarrow CH_3OCH_3 + H_2O$
3. WGS reaction: $CO + H_2O \leftrightarrow CO_2 + H_2$
4. Gasoline Synthesis: DME $\rightarrow$ Light Olefins + H_2O

   Light Olefins + DME $\rightarrow$ Heavy Olefins + H_2O

   Heavy Olefins $\rightarrow$ Aromatics + Paraffins

   Aromatics + DME $\rightarrow$ Higher Aromatics + H_2O

STG process is mainly based on the MTG process. MTG process was discovered by ExxonMobil scientists in the 1970s [10]. In the MTG process, methanol is converted to hydrocarbons and water, and the hydrocarbons are primarily high quality gasoline range fuels. Then, in late 1985, the first commercial MTG plant was constructed in New Zealand. This plant was scheduled to produce 570,000 tons of high quality gasoline with an average of 92 to 94 research octane number, which is about one-third of New Zealand's gasoline consumption [11]. ExxonMobil successfully commercialized the MTG process that was a milestone in synfuels development, because this is the first new synfuels technology after the commercialization of the FTS process. In the late 1990s, ExxonMobil led a second generation MTG technology with significant improvements in heat integration and process optimization compared to the operation experience of the New Zealand MTG plant. These improvements resulted in a prospective capital reduction of 15–20 % compared with the original design in New Zealand. The first second-generation MTG plant was constructed in China by Jincheng Anthracite Mining Group. The original design is 100,000 tonnes per year, but the second stage of this plant expected to extend to 1,000,000 tonnes per year [10]. Recently, ExxonMobil planned to build some new MTG plants in the United States [8]. For instance, the new plant designed to be built in Wyoming can produce 20,000 to 22,000 barrels of gasoline per day. Another similar plant proposed by Transgas Development Systems (TGDS) has an expected annual production of 6.5 million barrels of gasoline. Furthermore, several other new MTG plants are being planned across the world. Therefore, the MTG process is gaining commercialization and producing significant economic yields.

I.2 Reactants

The major reactants for both FTS process and STG process are syngas. Usually, syngas can come from natural gas, coal, and biomass. The reservoirs of natural gas and coal are very large, and these can be converted into syngas by either steam reforming or partial oxidation processes. FTS or STG is the key step for converting these different sources of syngas into liquid fuels (Figure I.2). The syngas H_2/CO ratio is dependent on the source of the syngas. Typically, syngas from natural gas has an H_2/CO ratio of 1.7 – 2.0, which is a suitable ratio for Co-based FTS. However, syngas from coal gasification and biomass usually have a lower H_2/CO ratio (0.6 – 1.0), which is an acceptable ratio for both the Fe-based FTS process and STG process due to the water-gas-shift reaction. Hence, different sources of syngas could choose different GTL process to construct plants.

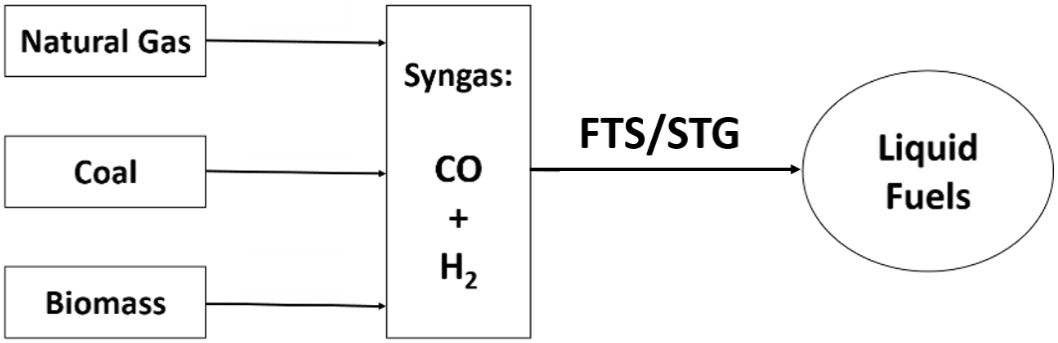

Figure I.2 Reaction processes for producing syngas

I.3 Catalysts

I.3.1 Catalysts for FTS Process

All metals in group VIII have noticeable FTS activity. Ruthenium is the most active metal followed by cobalt, iron, and nickel [12]. However, ruthenium is very expensive, and its worldwide

reserves are insufficient for large-scale industrial utilization. Nickel-based catalysts produce too much methane under low operating pressure and generate a volatile nickel carbonyl at high operating pressure. Cobalt and iron are the most common catalysts used in the industrial area for FTS. Co-based catalysts are more expensive than Fe-based catalysts. At a high conversion, Co-based catalysts are significantly more active than Fe-based catalysts, but the activities of these two metals are comparable under a low conversion. However, the water-gas-shift reaction is more significant on Fe-based catalysts than on Co-based catalysts. Hence, Fe-based catalysts are more suitable to operate on syngas derived from coal with low H_2/CO ratio [13,14].

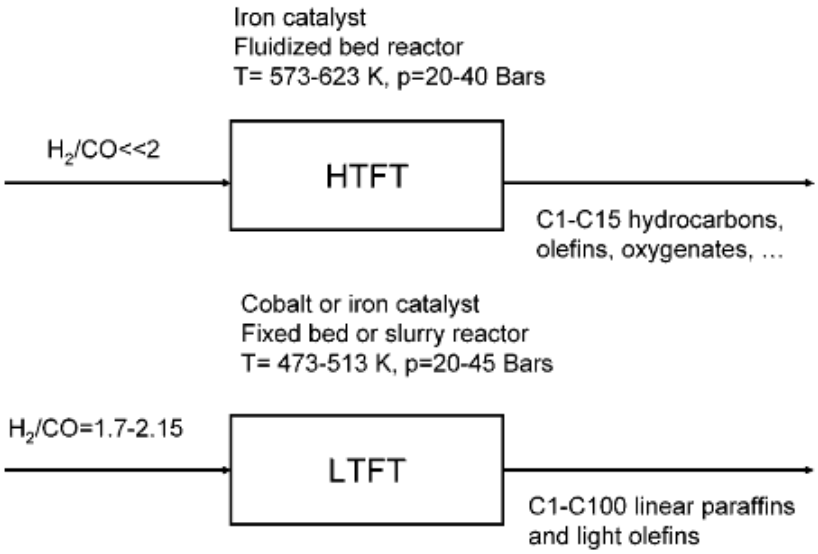

Figure I.3 High- and low-temperature FT processes

The FTS operation can be separated into two categories depending on the operation temperature: high-temperature FT processes (HTFT) and low-temperature FT processes (LTFT) [13]. Typically, the HTFT is operated at 573 – 623 K (Figure I.3) and Fe-based catalysts are used to produce hydrocarbons in the range of C_1 – C_{15}. This process is primarily utilized to produce liquid fuels, while some byproducts also can be extracted from the synthetic crude oil, such as α-olefins, alcohols, and ketones and so on. The LTFT process is operated at 473 – 513 K and both

Fe- and Co-based catalysts can be used for synthesizing long-chain hydrocarbons. High quality sulfur-free diesel fuels can be produced in this process, which is a great blending source for lowering the sulfur content transportation fuels extracted from crude oil. Compared with Fe-based catalysts, Co-based catalysts are better choices for the synthesis of long-chain hydrocarbons in the LTFT process, considering the stability, per pass conversion, and hydrocarbon productivity.

I.3.2 Catalysts for STG Process

Since a typical STG process is composed of three major reaction processes in sequence, there are different kinds of catalysts used for different reaction process. For the methanol synthesis, typical catalysts are copper-based such as $Cu/ZnO/Al_2O_3$ and $Cu/ZnO/Cr_2O_3$ [15,16]. In addition, researchers demonstrated that the performance of Cu-based catalysts could be enhanced if an appropriate preparing process has been used. For example, Chu et al. reported that if tetraethylammonium hydroxide is employed instead of polyethylene glycol as the precipitating agent, the catalyst's activity and stability improved to the best level for $Cu/ZnO/Al_2O_3$ catalysts [17]. Furthermore, another very important way to improve the catalysts' performance is the preparation of the catalysts into nano-scale particles, which enhanced catalysts' adsorption and activation properties toward CO [8].

The DME synthesis is simply a methanol dehydration reaction. This reaction can be catalyzed on a lot of solid-acid catalysts such as γ-Al_2O_3, silica and phosphorous modified alumina, and zeolites [18]. For STG process, the most important part is the step of DME to gasoline. The catalysts can be used at this step are mainly zeolites, and the most widely used

zeolite is ZSM-5. However, some literature showed that non-zeolite catalysts could also catalyze this process. Here, we will focus on and discuss ZSM-5.

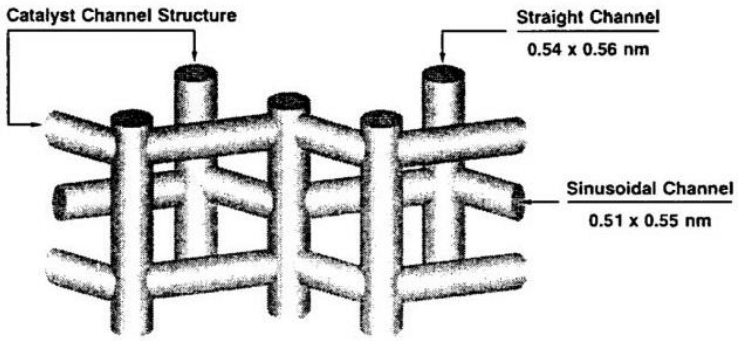

Figure I.4 Structure of ZSM-5 [19]

ZSM-5 was developed by ExxonMobil's scientists in the 1970s. It belongs to the pentasil family, and ZSM-5 is the trade name of a pentasil-zeolite. ZSM-5 is a synthetic crystalline material composed of arranged SiO_4 tetrahedra, and part of aluminum atoms are replaced by silica atoms in the framework, which produces active acid sites due to the unequal charges between silica and aluminum [19]. ZSM-5 has an MFI type of framework, and it has two kinds of channels (Figure I.4); one is a straight channel (0.54 x 0.56 nm), and another one is a zigzag channel (0.51 x 0.55 nm). The catalytic reactions occur in these channels will add unique shape selective constraints to the products, and that is why the product spectrum of the MTG process has been limited to a maximum carbon number of C_{10}.

I.4 Product Distribution

I.4.1 FTS Product Distribution

The FTS has a very broad product distribution pattern including a complex multicomponent mixture of linear and branched hydrocarbons and oxygenated products. The major products are

linear paraffins, α-olefins, and oxygenated products [20]. The corresponding reactions are listed as follows:

$$\text{Paraffin: } (2n+1)H_2 + n\,CO = C_nH_{2n+2} + nH_2O \quad \text{(Eq.I.1)}$$

$$\text{Olefin: } 2nH_2 + n\,CO = C_nH_{2n} + nH_2O \quad \text{(Eq.I.2)}$$

$$\text{Alcohol: } 2nH_2 + n\,CO = C_nH_{2n+1}OH + (n-1)H_2O \quad \text{(Eq.I.3)}$$

where n is the average carbon number. The FTS product stream consists of various types of fuels, such as LPG, gasoline, diesel, jet fuel, etc.. The definitions for the composition and names of the different types of fuels are given in Table I.1.

Table I.1 Conventions of fuel names and composition [3]

Name	Synonyms	Components
Fuel Gas		$C_1 – C_2$
LPG		$C_3 – C_4$
Gasoline		$C_5 – C_{12}$
Naphtha		$C_8 – C_{12}$
Kerosene	Jet fuel	$C_{11} – C_{13}$
Diesel	Fuel oil	$C_{13} – C_{17}$
Middle distillates	Light gas oil	$C_{10} – C_{20}$
Soft Wax		$C_{19} – C_{23}$
Medium Wax		$C_{24} – C_{35}$
Hard Wax		$C_{35}+$

The FTS process can produce sulfur and aromatic free fuels. Hence the fuels produced from the FTS process are excellent blending resources for conventional fuels derived from crude oil that contain very high sulfur or aromatic content. Moreover, some by-products of the FTS

process can be separated and upgraded to valuable products, such as ethylene, propene, α-olefins, alcohols, ketones, etc.

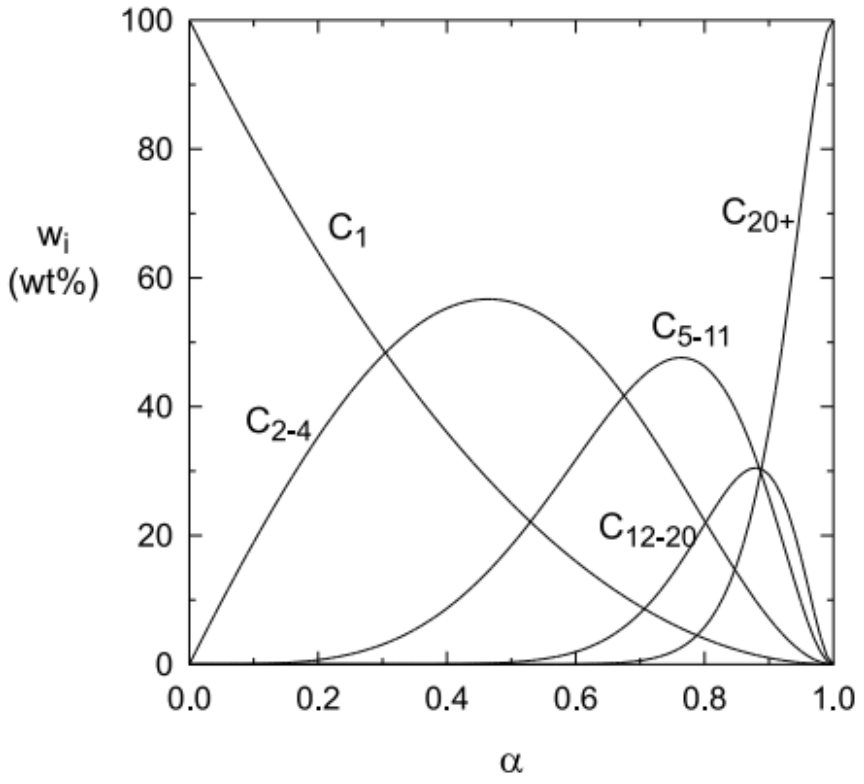

Figure I.5 Hydrocarbon selectivity as a function of the chain growth probability factor α [12,21]

The product distribution of the FTS process can be described by the Anderson-Schulz-Flory (ASF) equation [12,21]:

$$m_n = (1-\alpha)\cdot\alpha^{n-1} \quad \text{or} \quad \frac{W_n}{n} = (1-\alpha)^2\cdot\alpha^{n-1} \qquad \text{(Eq.I.4)}$$

where m_n is mole fraction, W_n weight fraction, and α is chain growth probability factor. α is independent of n and m_n, and it is defined by:

$$\alpha = R_p/(R_p + R_t) \qquad \text{(Eq.I.5)}$$

where R_p and R_t are the rate of propagation and termination, respectively. As Figure I.5 shows, the α value represents the total carbon number distribution of the FTS products. α is dependent

on the catalyst types and reaction conditions. According to Dry's report, the typical value of α on Ru-, Co-, and Fe-based catalysts is 0.85 – 0.95, 0.70 – 0.80, and 0.50 – 0.70, respectively. The α value highly depends on the reaction temperature. α decreases with an increase in the reaction temperature, which means more light products are produced.

I.4.2 STG Product Distribution

Table I.2 Hydrocarbon yields of MTG process

	Low T FTS	High T FTS	MTG (fixed bed)	MTG (fluid bed)
Reaction Temperature (℃)	200 – 240	300 – 350	300 – 400	300 – 480
Hydrocarbon Product (wt%)				
Light Gas	7.6	18.0	1.4	5.6
Propane	2.8	2.0	5.5	5.9
Propylene	2.0	12.0	0.2	5.0
Butane	2.2	2.0	11.9	16.2
Butene	3.0	9.0	1.1	7.3
Gasoline	22.5	40.0	79.9	60.0
Diesel	15.0	7.0	0.0	0.0
Heavy Hydrocarbons	41.0	4.0	0.0	0.0
Oxygenates	3.9	6.0	0.0	0.0
Total	100.0	100.0	100.0	100.0

As we mentioned above, STG process is based on the MTG process. A typical STG process composed of several reactors in a series. The first reactor converted syngas to methanol and then utilizing the MTG process to convert methanol to gasoline. Hence, STG's product distribution is the same as the MTG process. According to Table I.2 [12,19,22,23], the MTG's products can be

separated into several streams including light gas ($C_1 – C_2$), LPG ($C_3 – C_4$), and gasoline ($C_5 – C_{10}$). For an adiabatic fixed bed reactor, gasoline's selectivity can reach 79.9 wt%, but a fluid bed has a lower gasoline selectivity (60.0 wt%) which is still much higher than the gasoline selectivity of FTS process including both low temperature and high temperature FTS. Moreover, gasoline produced by the MTG process has very high quality. Typically, its octane number can be over 90, which means it can be directly used as automobile fuel. However, MTG process does have some drawbacks. One of the unfavorable aspects is that MTG products contain a higher concentration of 1,2,4,5-tetramethyl benzene (durene) than traditional gasoline refined from crude oil. At low ambient temperature, the high concentration of durene can cause some problems due to its high melting point (80 ºC). To deal with this issue, ExxonMobil developed a heavy gasoline treatment (HGT) process to hydrogenate the heavy fraction of the MTG gasoline. The HGT process has been tested on vehicles and has been shown to be very successful [19,22].

In the literature, there are many direct comparisons between FTS and MTG. Considering the capital and operational costs, there are not too many differences between these two processes until the primary products leave the reactors. The major differences are on the down streams because FTS produces a broad spectrum of products which requires complex and expensive subsequent refinery processes to upgrade the initial products to meet fuel specifications. In contrast, MTG's products are mainly gasoline, and the other products require very few treatments. Considering the FTS process has been discovered and well researched for a long period, but MTG process is relatively young and still under development. We have the reasons to believe that the MTG process will have a bright future in the areas of synthetic fuels development when compared with the traditional FTS process.

I.5 Reaction Mechanism

I.5.1 FTS Reaction Mechanism

The FTS reaction is a surface polymerization reaction. Although tremendous research effects have been spent on it, there is still much debate about its reaction mechanism. In general, there are two widely accepted major mechanisms [12,24]. One is the carbide mechanism (Figure I.6a), and another one is the CO insertion mechanism (Figure I.6b). Both mechanisms follow similar reaction steps: (1) reaction adsorption; (2) chain initiation; (3) chain growth; (4) chain termination; (5) product desorption; (6) readsorption and further reaction. Figure I.6a shows the carbide mechanism including the initiation, growth, and termination of chains. According to this mechanism, the generation of CH_2 intermediate initiates the reaction. The CH_2 intermediate is formed by dissociation of the C-O bond of adsorbed CO. Chain growth occurs by inserting the monomer CH_2 into a growing alkyl species. Chain termination can take place by abstracting hydrogen to an alkene or adding hydrogen to form an alkane. For the CO insertion mechanism, the first two steps (reaction adsorption and chain initiation) are the same as the carbide mechanism, but its chain growth step is two separate steps instead of one. First, another CO inserts into the initially generated CH_2 intermediate. Then the C-O bond dissociated and an initial C_2H_y species is formed. Further chain growth occurs by repeating these two steps of CO insertion and C-O bond cleavage. The chain termination step of the CO insertion mechanism is also similar to the carbide mechanism.

I.5.2 STG Reaction Mechanism

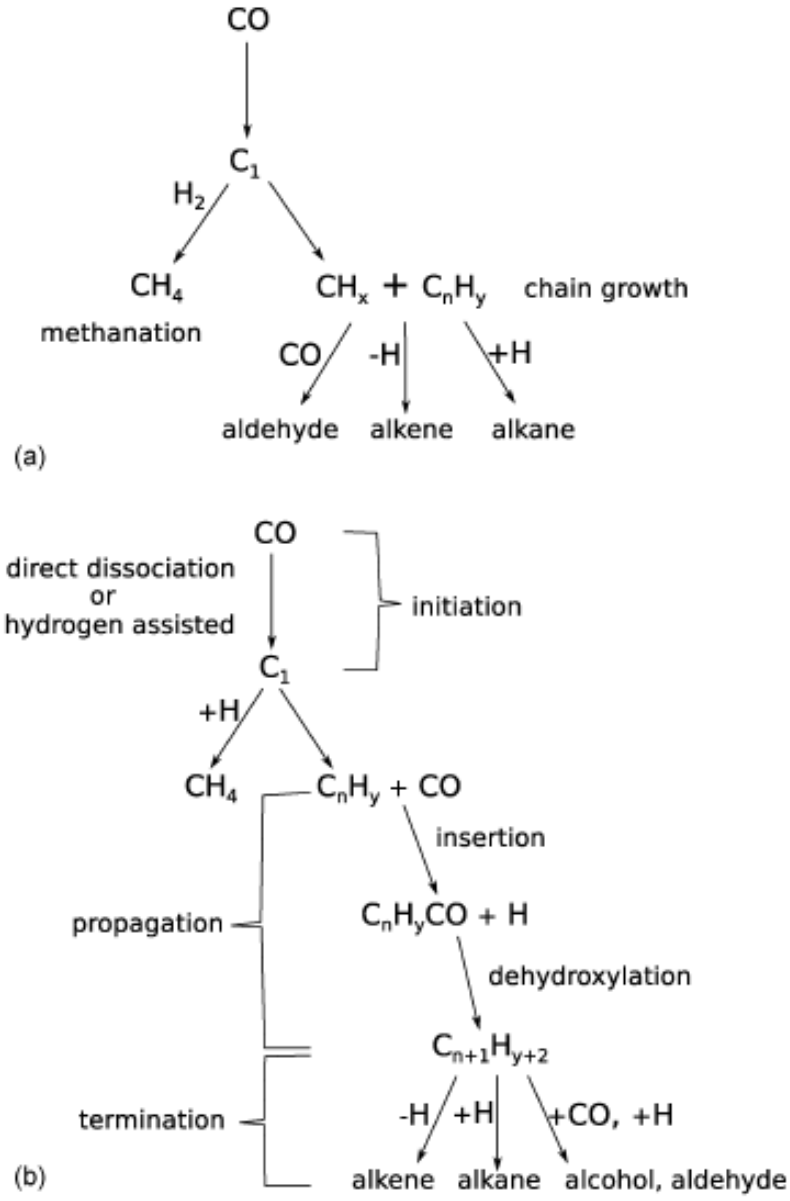

Figure I.6 Reaction mechanisms of the FTS process: (a) carbide mechanism; (b) CO insertion chain growth mechanism [24]

Since the STG process can be separated into two sequential processes (methanol formation from syngas and MTG process), the reaction mechanism of STG process will also be separated into two parts. The first part is the reaction mechanism of methanol formation. Methanol formation

reaction used the same reactants (syngas) as FTS. Also, methanol is a very important intermediate in the FTS reactions. Therefore, like the mechanism of FTS reaction, one of the biggest debates is that whether or not CO will dissociate to form methanol. Corresponding to this debate, there are two major mechanisms for methanol synthesis: dissociation mechanism and non-dissociation mechanism. Jones et al. proposed the following dissociation mechanism (from Eq.I.6 to Eq.I.13) [25,26]. Firstly, H_2 was adsorbed and dissociated to H(a), and CO was also adsorbed and dissociated to C(a) and O(a). Then, C(a) was reacted with two H(a) to form CH_2(a) which reacted with another H(a) species to form a CH_3(a) species. At the same time, dissociated H(a) species were reacted with O(a) to form OH(a). Finally, CH_3(a) was reacted with OH(a) to produce CH_3OH(a), and then CH_3OH(a) was desorbed from the active sites to release CH_3OH. On the other hand [27–29], the nondissociative mechanism claimed that the adsorbed CO(a) species was directly reacted with H(a) to form COH_2(a) (Eq.I.14), and COH_2(a) was reacted with another H(a) to form COH_3(a) (Eq.I.15). After that, COH_3(a) was reacted with H(a) again to produce CH_3OH(a) (Eq.I.16).

$$H_2 \leftrightarrow 2H(a) \quad \text{(Eq.I.6)}$$

$$CO \leftrightarrow CO(a) \quad \text{(Eq.I.7)}$$

$$CO(a) \leftrightarrow C(a) + O(a) \quad \text{(Eq.I.8)}$$

$$C(a) + 2H(a) \leftrightarrow CH_2(a) \quad \text{(Eq.I.9)}$$

$$CH_2(a) + H(a) \leftrightarrow CH_3(a) \quad \text{(Eq.I.10)}$$

$$O(a) + H(a) \leftrightarrow OH(a) \quad \text{(Eq.I.11)}$$

$$CH_3(a) + OH(a) \leftrightarrow CH_3OH(a) \quad \text{(Eq.I.12)}$$

$$CH_3OH(a) \leftrightarrow CH_3OH \quad \text{(Eq.I.13)}$$

*(a) denotes the adsorbed state

$$CO(a) + 2H(a) \leftrightarrow COH_2(a) \quad \text{(Eq.I.14)}$$

$$COH_2(a) + H(a) \leftrightarrow COH_3(a) \quad \text{(Eq.I.15)}$$

$$COH_3(a) + H(a) \leftrightarrow CH_3OH(a) \quad \text{(Eq.I.16)}$$

In order to clarify this debate, Atsushi Takeuchi and James Katzer [26] designed a thoughtful experiment by using an isotopic mixture of $^{13}C^{16}O$ and $^{12}C^{18}O$ both in 50 % to run the methanol synthesis reaction. According to the above reaction mechanisms, we should see an isotopic scrambling in the methanol products if the reaction follows the dissociative mechanism. On the contrary, if it follows the nondissociative mechanism, we should expect the methanol products composed with $^{13}CH_3{}^{16}OH$ and $^{12}CH_3{}^{18}OH$ and keep at a similar isotopic ratio as the ratio in the reactants. The experimental results shown the methanol products contained mainly the ^{13}C-^{16}O and ^{12}C-^{18}O pairs and kept the same ratio as in the CO reactant, which strongly approved the nondissociative mechanism.

The second part of the STG mechanism is the reaction mechanism of methanol-to-gasoline (MTG). MTG is a complex process, and the overall chemistry can be separated into five stages [30]. The first stage is the equilibrium among methanol, DME, and water. The second stage is a kinetic induction period of a fresh catalyst. The third stage is the formation of the first carbon-carbon bond, which is also the central step of MTG reactions. The fourth stage is the secondly reactions that convert the primary products to other hydrocarbons. The final stage is catalyst deactivation. The reaction pathways of MTG might be different depending on the catalyst type (including acid strength and density, catalyst topology, and crystallite size), reaction temperature, and process conditions. Nevertheless, they all follow the five stages of reaction processes.

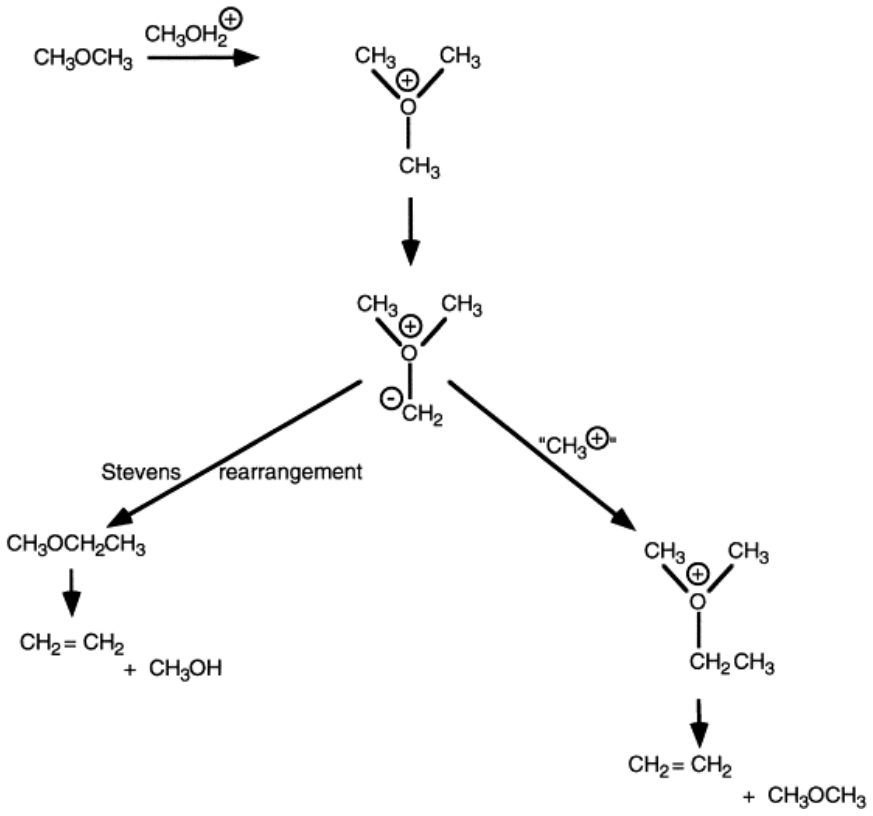

Figure I.7 Scheme of first C-C bond formation [31]

In the past several decades of research, more than twenty distinct mechanisms have been proposed. There are extensive discussions about these reaction mechanisms; one of the most intense debate is "How does the first C-C bond form?". Here we listed several very popular mechanisms to explain how the first C-C bond formed. Van den Berg et al. [32,33] suggested an oxonium ylide mechanism, and it is shown in Figure I.7. First, a DME molecule interacts with a Bronsted acid site of ZSM-5 to form a dimethyl oxonium ion. Then, this ion continues to react with another DME molecule to form a trimethyl oxonium ion which is further deprotonated on a basic site to form a dimethyl oxonium methyl ylide species. After that, it can start an intra-molecular Stevens rearrangement or an intra-molecular methylation. Both pathways will form ethylene through β-elimination. Chao et al. [31] used isotopic labeled methanol and DME to study the conversion of methanol to hydrocarbons over ZSM-5. The results showed that ethylene was

the primary hydrocarbon product. Also, the oxonium related mechanism was supported by other evidence. For instance, several investigations demonstrated that the activity of hydrocarbon formation is linearly dependent on zeolite's Bronsted acidity [34–36].

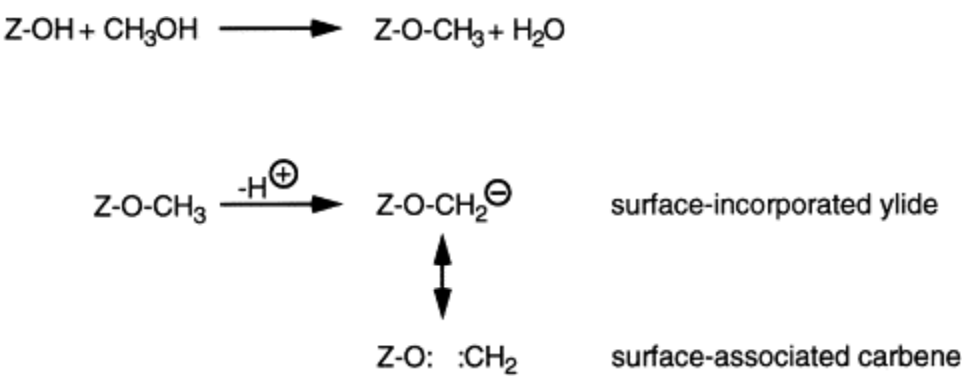

Figure I.8 Scheme of the oxonium ylide mechanism [31]

In short, the oxonium ylide mechanism can be summarized as follows (Figure I.8) [31,37]: 1) form a surface-bound methyl-oxonium intermediate over the active site of zeolite; 2) deprotonate to a surface-bound methylene-oxonium ylide; 3) form an initial C-C bond through further methylation.

I.6 Commercialized Reactors

Since the discovery of the FTS process, a large variety of reactors have been proposed, and some of them have been commercially applied. However, FTS reactor design is not straightforward. It must compromise various characteristics, including some conflicting requirements. One of the biggest and most common issues for both FTS and STG processes is thermal management. Both processes employ highly exothermic reactions, and the product selectivity and catalyst activity are highly depended on the reaction temperature. For instance, temperature overshooting can easily deactivate Co-based FTS catalysts and produce mostly methane. Similarly, for STG process temperature overshooting in the section of methanol synthesis could lead to mostly

methane, and in the section of MTG which could quickly deactivate the zeolite catalysts due to the fast formation of coke. Therefore, maintaining a stable reaction temperature is extremely important for both processes. In the following sections, the advantages and disadvantages of some important commercialized reactors will be discussed.

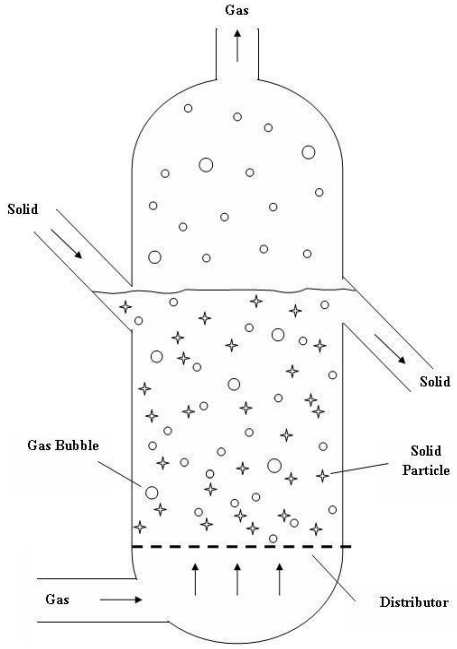

Figure I.9 Basic diagram of fluidized bed reactor

Fluidized-bed reactors (FBR) [38–41]**:** The working principle of FBR is that the solid catalyst particles are supported by a porous plate called a distributor. The fluid is forced through the distributor to contact with the solid catalyst particles. When the fluid is at a low velocity, the catalyst particles remain in place as the fluid passes through the material. This is known as the traditionally packed bed reactor. However, when the fluid velocity is large enough to lift the catalyst particles and make it like an agitated tank, the reactor is known as a fluidized bed (Figure I.9). For FBR the turbulent flow of reactant gas increases the convection heat transfer and minimizes the formation of the stagnant gas and liquid film on the walls of heat exchange. Moreover, the heat transfer efficiency can be significantly increased when there is a frequent

direct physical contact of hot catalyst particles with heat exchange fluid. Therefore, the FBR has excellent heat transfer ability and can easily remove the reaction heat from the reactor and maintain a stable reaction temperature. Furthermore, the intra-particle mass transfer limitation has been considered negligible as particle sizes of catalysts in the order of 100 μm. The physical strength of the catalyst is very important in fluidized systems, while the catalyst stability is less critical since the catalyst can be refreshed continuously. However, the presence of liquid products in the reactor can cause catalyst particles to agglomerate. To avoid this, the operation temperature and pressure must be chosen above the dew point of the hydrocarbons. Hence, the FBR is usually used for high-temperature FTS with light hydrocarbons as the major products.

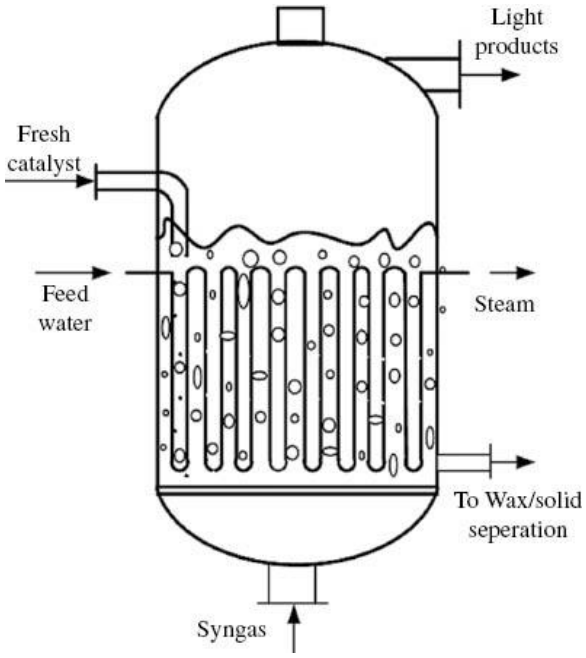

Figure I.10 Basic diagram of a slurry bubble column reactor [38]

Slurry bubble column reactors (SBCR) [38,42]: The SBCR is similar to FBR, both of them have been broadly used in the industrial area. In 1993, SASOL introduced this technology with a capacity of 2500 bbl/day in a unit. The working principle of SBCR is that reactant gas is bubbled through a slurry of heavy liquid products and catalyst particles. During the reaction, the

unreacted gas and light products outflow the reactor in a gas phase, while the liquid products are removed as a part of the slurry (Figure I.10). One of the biggest advantages of SBCR is the well-mixed liquid phase resulting in a nearly isothermal operation. It is obvious that a well-mixed liquid phase has a higher thermal conductivity than a continuous gas phase in an FBR. However, an associated disadvantage for SBCR is the back-mixing of the gas phase when the reactant gas bubbling through the slurry. Previous research shows that back-mixing in SBCR leads to significant decreases in per pass conversion and reactor productivity. Another very serious issue for SBCR is catalyst attrition and product separation, especially when catalyst particle size is very small. The stability of catalyst is another very important topic, but continuous refreshing is available for SBCR. Usually, SBCR is used to produce middle distillates.

Table I.3 Comparison of different reactor types [40,43]

Feature	Fluidized Bed(circulating)	Slurry	Fixed Bed
Operation	Complex	intermediate	simple
Temperature control	Good	good	poor
Heat exchanger surface	15 – 30m^2 per 2000 m^3	50 m^2 per 1000 m^3 feed	240 m^2 per 1000 m^3
Max. reactor diameter	Large	large	< 80 mm
CH_4 formation	High	as a fixed bed or lower	low
Flexibility	Little	intermediate	high
Product	low mol. Weight	full range	full range
Space-time yield (C_2+)	4000 – 12000 kg/m^3 day	1000 kg/m^3 day	> 1000 kg/m^3 day
Catalyst effectivity	highest	intermediate	lowest
Back mixing	intermediate	large	little
Minimum H_2/CO feed	highest	lowest	as a slurry or higher
Construction		simplest	

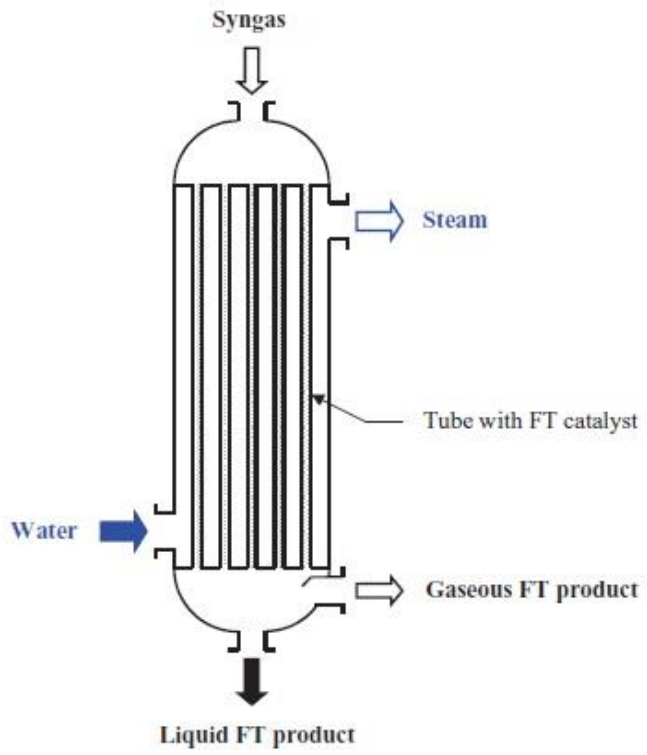

Figure I.11 Basic diagram of the multi-tubular fixed-bed reactor [44]

Multi-tubular fixed-bed reactors (MTFBR) [40,43,44]: To increase productivity and to solve the heat transfer issue, MTFBR were developed based on the tubular fixed-bed reactors. An MTFBR is just a combination of many small tubular fixed-bed reactors. Each tubular reactor is identical, independent, and surrounded by boiling water to efficiently transfer the reaction heat out of the reactor (Figure I.11). The MTFBR can better solve the heat removal problem compared with fixed-bed, but it still suffers from many heat transfer related issues. For instance, the fixed-bed based reactors have a limited catalyst particle size that can be applied. When the particle size is too small, it can cause a very high pressure drop over the reactor. In contrast, too large particles result in loss of reaction activity and product selectivity. Therefore, it is essential for the fixed-bed based MTFBR technology to reach a compromise between short diffusion

lengths and acceptable pressure drop. Another very important issue is that the catalysts need to have very high stability because changing the catalysts is extremely time consuming.

The three types of reactors presented above are the common reactors used in industry. All the reactors have their unique advantages but also suffer from some disadvantages as it shows in Table I.3. For example, the FBR is not suitable for producing middle distillates since it is mostly utilized for high-temperature FTS. The SBCR technology suffers from the back-mixing of the gas phase. Also, the catalyst attrition and separation is a key problem for SBCR. The MTFBR requires the catalysts have excellent stability and a balanced particle size for the sake of keeping a balance between mass transfer and pressure drop. In addition, per pass conversion of MTFBR cannot be very high to better manage the heat transfer and maintain the reaction temperature.

I.7 Challenges and Improvements

I.7.1 Challenges in Mass Transfer and Heat Transfer

One of the biggest challenges for the FTS process is how to manage the heat transfer since FTS reaction is a highly exothermic process. Traditionally, fixed-bed was used as the FTS reactor because it has many advantages, including high volumetric catalyst loading, no need of subsequent processes to separate products from catalyst particles, easy operation, and a wide temperature range. The biggest disadvantage of fixed-bed is its poor heat transfer ability, which greatly limits the reactor size and influences reaction activity and product selectivity. Furthermore, the fixed-bed reactor suffers from mass transfer limitation within the catalyst pores. In the following parts, these two kinds of major limitations of fixed-bed reactors will be discussed.

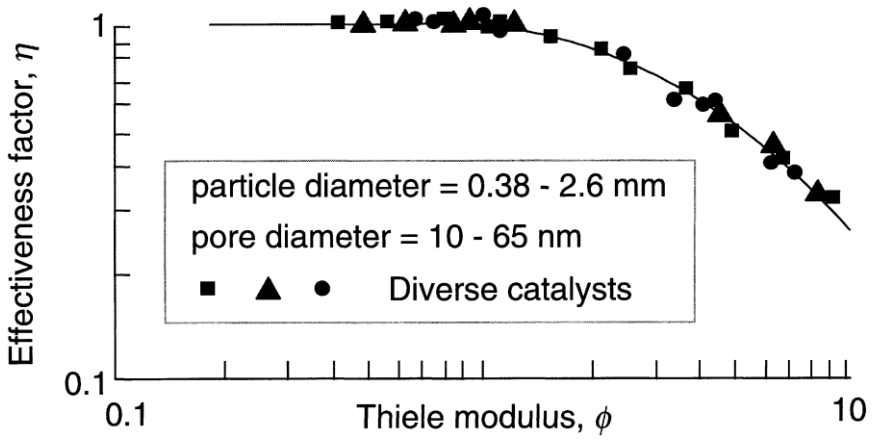

Figure I.12 Catalyst effectiveness as a function of the Thiele modulus for various cobalt- and iron-based catalysts [41]

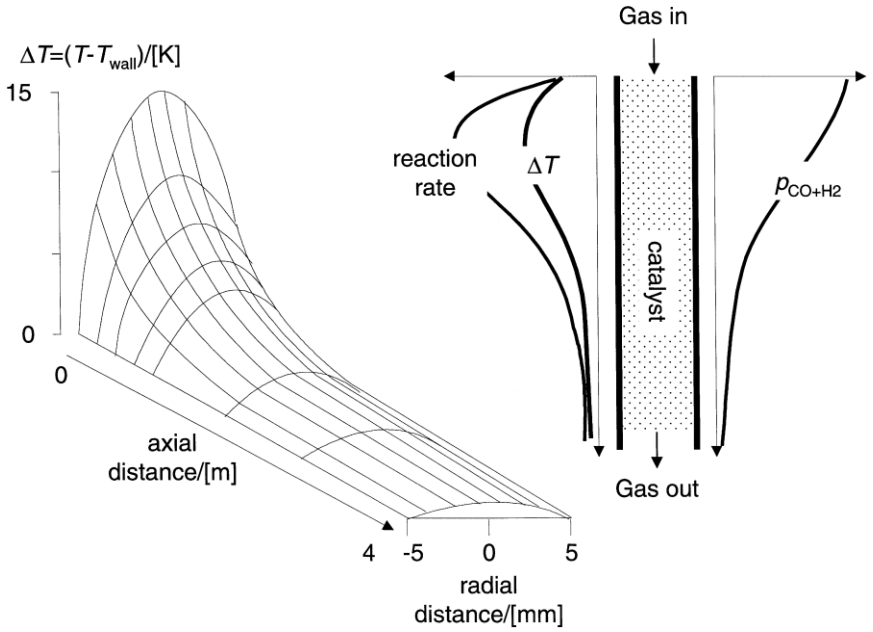

Figure I.13 Concentration and temperature profiles in a tubular fixed-bed reactor of FTS [41]

Mass transfer limitation [41]: Catalysts in a conventional fixed-bed usually have diameters larger than about 1.0 mm to avoid high pressure drop. However, studies showed that the diffusion of reactants and products through liquid filled pores is the key factor in intra-particle mass transport. As we can see from Figure I.12, the catalyst effectiveness decreased significantly below 1 as the Thiele modulus increased to more than 1. In a typical FTS process, the intra-

particle diffusion starts to play a role for particle size larger than 0.5 mm. Therefore, intra-particle diffusion limitation is an important factor to be considered in choosing catalyst particle size and shape for a conventional fixed-bed FTS reactor.

Heat transfer limitation [41]**:** As we can see from Figure I.13, there is a very high temperature gradient along the radial direction in the region near the inlet. This is because of the high reaction rate in this region. Further down the reactor tube, the radial temperature became more even due to a lower reaction rate as the reactants are being consumed. However, these data were received from a tubular reactor with a diameter of 10.0 mm. When the reactor size is increased the temperature difference is increased significantly. In an extreme case, the reactor can become unstable and the reaction temperature may run away. These phenomena are mainly caused by the relatively poor heat transfer abilities between catalyst particles to catalyst particles and catalyst particles to the reactor wall. Even for the relatively stable operation region, it is very hard to avoid the formation of hot spots on catalyst particles, which may give rise to the formation of light products and accelerated catalyst activity decline.

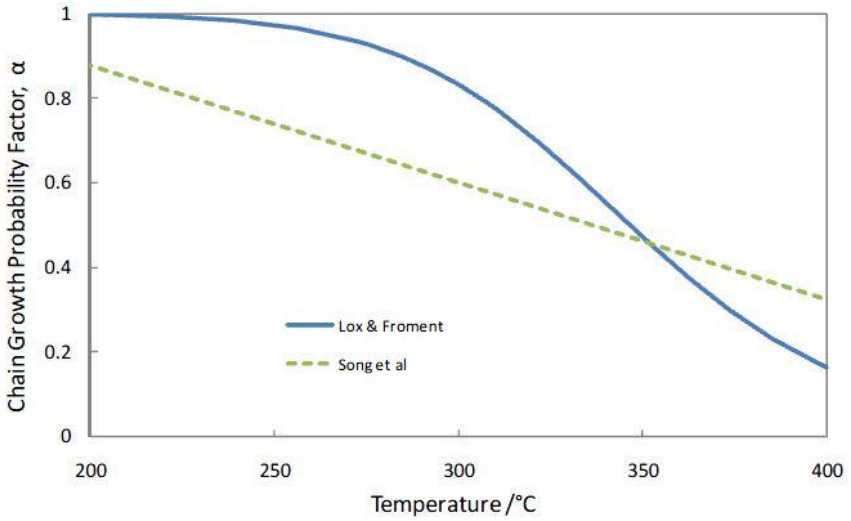

Figure I.14 The relation between the chain growth probability factor α and the reaction temperature [43]

According to the literature reports, the FTS product distribution strongly depends on the catalyst surface temperature. Figure I.14 shows that the α value decreases dramatically as the temperature increases, which means the product distribution shifts to lighter hydrocarbons. It turns out that the selectivity of desired heavy hydrocarbons decreased significantly. Hence, maintaining a uniform reaction temperature throughout the catalyst bed is crucial for FTS reactor designs.

I.7.2 Improvements in Reactor Design

To overcome these issues, various reactors have been designed and developed. The most famous examples are the above commercialized FTS reactors. In addition to these commercialized reactors, some advanced technologies have also been applied to the traditional fixed-bed reactor to increase its heat transfer ability.

Supercritical media [45–47]**:** By injecting a supercritical fluid into the FTS reactor, the heat transfer and mass transfer inside the reactor can be enhanced. A supercritical fluid is formed when the temperature and pressure are higher than its critical point, then the vapor and liquid phase became indistinguishable. Usually, a supercritical fluid has a gas-like viscosity and liquid-like diffusivity; these enhance the in-situ extraction of liquid products from catalyst pores. Also, the overall product distribution shifts to the heavier hydrocarbon range. Furthermore, Roberts et al. reported that 1-olefin contents in the supercritical phase of hexane solvent were always higher than in a traditional fixed-bed. In short, the benefits of utilizing supercritical media for FTS process can be listed as follows: 1) increased reaction rate; 2) enhanced heat and mass transfer; 3) extended catalyst lifetime; 4) easier separation and so on. Despite these benefits, this technique is not commercially feasible due to the extremely high pressure required.

Monolithic reactors [42]**:** Monolithic catalyst is one type of structured catalyst geometries which is characterized by a non-randomly order fixed-bed of catalysts. Typically, monolithic catalysts (Figure I.15) are ceramic structures with parallel channels composed of cordierite or catalyst supports like alumina or silica. Monolithic catalysts consist of various identical and parallel channels, and the diameters of the channels can vary depending on the cell density of the monolithic structure. The wall thickness of the monolithic catalyst is around 0.1 to 0.3 mm. The monolithic catalyst structures are characterized by a large surface area. For instance, a 600 cpsi monolithic catalyst structure with an open frontal area of 82 % can provide a surface area of 3476 m^2/m^3. Therefore, the geometric surface area per unit reactor of monolithic structure is very high and can be compared with most types of particle sizes applied in fixed-bed. Also, monolithic catalysts usually have a very low pressure drop due to their structure.

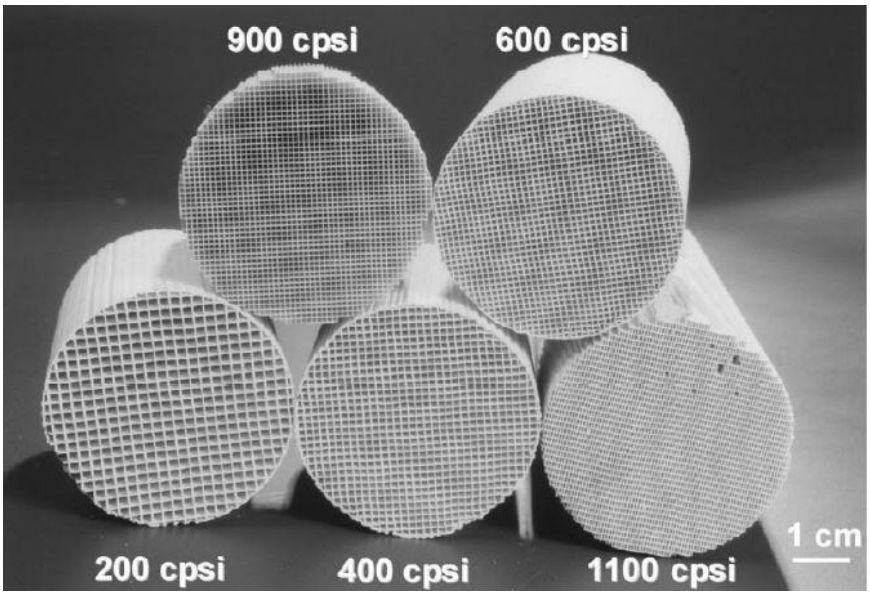

Figure I.15 Photo of several monolithic structures [42]

Several methods can be used to deposit the active metals onto the monolithic structure. A washcoating process is a common way to do this. The type of flow that occurs in the channels of a monolith can be in different flow regimes depending on the gas and liquid velocities. For gas-

liquid-solid catalysis, a Taylor flow or a slug flow is a preferable flow for the FTS process. This flow regime is characterized by a consecutive flow of gas and liquid slugs through the channels, and the typical flow rate is from 0.1 to 1.0 m/s. The liquid slugs fill the monolithic channels and friction with the channel walls, so circulation occurred within the liquid slugs which enhances the gas-liquid mass transfer. The thickness of the catalyst layer is also adjustable to reach a very high catalyst effectiveness factor (close to 1). In short, the external mass transfer of monolith structures can be increased by their large geometric surface area and can further be increased by choosing an optimal flow regime inside the channels.

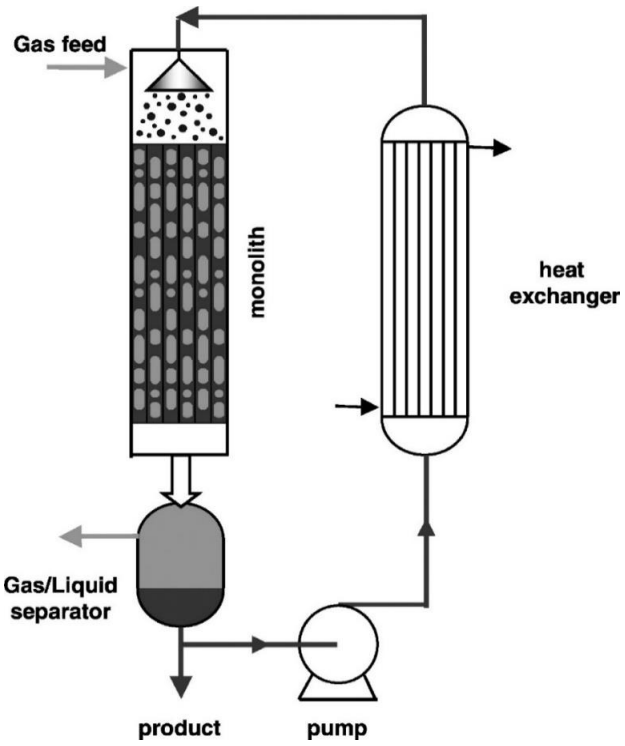

Figure I.16 Schematic drawing of a monolithic loop reactor with a liquid recycle [48]

However, the monolithic structure has a very poor radial heat transfer ability. To solve this problem, an external heat exchanger has been used to remove the reaction heat. Also, Moulijin et al. [41,50] suggested to limit the reaction temperature rise by recycling heavy liquid products

from the FTS process. For this reason, a new type of reactor named monolithic loop reactor has been designed in which liquid products are recycled through the monolithic reactor and the external heat exchanger (Figure I.16). Under this circumstance, the heat removal is relatively independent of the reactor design itself; this allows independent scaling of both the monolithic reactor and the external heat exchanger. In the early development of fixed-bed, people also used an external heat exchanger to remove the reaction heat, like the BASF Schaumverfahren. However, the very high pressure drop caused a big problem for fixed-bed systems. In contrast, the monolithic structure does not suffer from this issue since it can prevent from a high pressure drop. In this case, the gas phase does not need to be recycled if the conversion per pass is chosen high enough to ensure plug flow for the reactants and the gaseous reaction products.

Gas lift recycle reactor [42]**:** A gas lift recycle reactor (Figure I.17) is like a slurry bubble column reactor; catalysts are presented as fine particles in a slurry of liquid reaction products. The reactant gases are bubbled through the slurry to produce a concurrent flow upwards through the riser reactor. All the gas phase products and the unreacted reactant gases are removed from the top of the reactor while the slurry flows downwards to an external heat exchanger to bring out the reaction heat. One of the biggest benefits of this reactor system is the plug-flow behavior, which means all the gas, liquids, and solids within the reactor are moved in plug flow. The liquids are maintained in mixed mode by recirculation, and higher recirculation rates can result in higher mass transfer efficiency and heat transfer efficiency. According to the reports of Ghotage et al., there is very limited temperature rise for the gas lift recycle reactor even at an almost full conversion of the reactant gas. In addition, the catalyst distribution over the height of the reactor is more uniform in the gas lift recycle reactor than in the conventional slurry bubble

column reactor. Nevertheless, the problems of catalyst attrition and separation are still not solved in the gas lift recycle reactor.

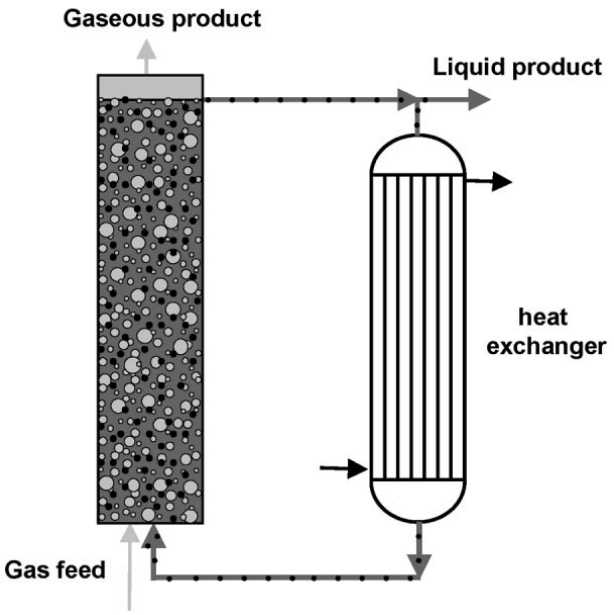

Figure I.17 Schematic drawing of a gas lift recycle reactor [42]

Designing an FTS reactor is not an easy task since various conflicting requirements need to be addressed. Through the development in recent decades, impressive improvements have been made to FTS reactor design. Some of them have been successfully applied to industry. For instance, Shell utilizes the fixed-bed reactors for all the existing and planned plants. The fixed-bed reactor can be scaled up easily and by conducting research on a single tubular reactor. Sasol developed the bubble column reactor that can efficiently remove the reaction heat. This allows for a uniform temperature distribution profile, which is a key concern for the FTS process. Also, there are some alternative novel reactors, such as supercritical media assisted fixed-bed reactors, monolithic reactors and gas lift recycle reactors. The most popular alternative reactor is the monolithic reactor since it appears to succeed in solving some of the problems of the conventional FTS reactors.

I.8 Microfibrous Entrapped Catalyst Structure

The above improvements of the FTS reactors can only partially solve the problems in the FTS process; sometimes they may also draw in some new problems. For instance, the monolithic reactor seems to solve the problems of the conventional reactors successfully. It combined the advantages of a slurry system with the advantages of a fixed system. However, it requires a washcoating process to load the active metals and cannot be used for pre-manufactured catalysts. Microfibrous entrapped catalyst (MFEC) structure is a novel technique developed by Auburn University and now is commercially available at IntraMicron Inc. [49–54]. MFEC is a type of catalyst structure which consists of sintered micron-sized metal, glass, or polymer fibers with small catalyst particles entrapped inside. The MFEC media entrapped with catalyst particles will be loaded into a tubular reactor. Therefore, the MFEC structure is similar to the conventional packed bed because they are both based on a fixed-bed system. However, previous research has shown that the fixed-bed loaded with MFEC media is different from the traditional packed bed. The MFEC structure demonstrates very high void volume, which significantly reduces pressure drop compared with a packed bed. Moreover, intra-particle heat transfer and mass transfer are enhanced in MFEC structure since small particles are used with an acceptable uniform particle distribution. When compared with monolithic reactors, one of the biggest advantages of MFEC is that MFEC can be used for pre-manufactured catalyst particles. This unique advantage greatly extends the applications of the MFEC structure to many other reactions. The original optimized catalyst recipes can be directly used without seeking a new recipe for a washcoating process.

Chapter II: Microfibrous Entrapped Hybrid Iron-based Catalysts for Fischer-Tropsch Synthesis

Abstract

Fischer-Tropsch synthesis (FTS) is a highly exothermic reaction, and an FTS reactor must have an efficient heat transfer mechanism to maintain a stable reaction temperature. Copper microfibrous entrapped catalyst (Cu MFEC) has demonstrated an excellent intra-bed heat transfer ability for FTS thermal management. The porous structure of Cu MFEC can entrap any pre-manufactured catalyst particles, while its counterpart approaches such as metallic foams or monolith reactor structures are typically based on washcoating process and require the details about catalyst formulation and preparation procedure to proceed. In this investigation, a highly active and stable iron-based FTS (Fe-FTS) catalyst, i.e. iron supported on γ-alumina and promoted with copper and potassium, has been developed. The apparent reaction rate constant of Fe-FTS and its productivity at 27.7 % of CO conversion are 167 mmol $(H_2 + CO)/g_{cat}/h$ and 0.30 g of $C_5+/g_{cat}/h$, respectively; these are comparable to the most active unsupported Fe-based catalyst. When Fe-FTS was physically mixed with an equal mass of mesoporous aluminosilicate (MAS) loaded with 0.3 wt% Pt, a hybrid catalyst was formed. This hybrid catalyst demonstrated an extremely low CO_2 selectivity (27.7 C-%) and a high selectivity (38.1 C-%) to liquids products (C_5-C_{20}). The result suggested that FTS and hydrocracking process simultaneously took place within a single reactor. Furthermore, FTS was carried out in a larger tubular reactor (34.0 mm I.D.) packed with Cu MFEC. It demonstrated a radial temperature gradient of less than 5 ºC and similar reactivity and product selectivity as those obtained in a small FTS reactor (9.5 mm I.D.). While with the same catalyst loading density and the same test conditions, the comparative

packed bed (34.0 mm I.D.) reached radial temperature gradient around 54 ºC. It was also found that the FTS based Cu MFEC required a negligible amount of time to reach its steady state compared with the packed bed. With these attributes and advantages, Cu MFEC approach is a promising alternative to the traditional packed bed for exothermic reactions such as FTS.

Keywords: Microfibrous Entrapped Catalysts, Fischer-Tropsch Synthesis (FTS), Hydrocracking, Supported Fe-based FTS Catalyst, Hybrid Catalyst, Mesoporous aluminosilicate.

II.1 Introduction

Fischer-Tropsch synthesis (FTS) is a well-known Gas-to-Liquid technique for converting natural gas or syngas into liquid fuels. However, FTS is a highly exothermic reaction which causes many heat transfer issues for FTS intensification since FTS was established in the 1920s [55]. First, the reaction temperature is easy to run away due to extensive heat generation, which can lead to some severe quality and even safety problems. More importantly, FTS is a temperature sensitive reaction, and its product distribution is strongly dependent on the reaction temperature. Undesirable gaseous products like methane, ethane, etc. will be produced at high temperatures. For the maximum selectivity to desired liquid products, the FTS reactor should be well controlled at a single stable temperature for the entire reactor. In addition, the high reaction temperature could deactivate the catalysts by sintering its active metal sites. As a result, efficient heat transfer is the key to solve FTS related issues.

In the past, researchers put tremendous efforts to develop various heat transfer structures for FTS to avoid reaction temperature overshoot and formation of hot spots. The major representative works are fluidized reactor and slurry reactor. Both of them have been successfully used in research and industrial areas [40,41,56–59]. For other types of reactors, including

metallic foams and metal monolith catalyst structures, some successful applications also existed in their infant stage [60–64]. However, they all have disadvantages. For instance, fluidized reactors require catalysts with good mechanical strength and complicated downstream recovery processes [56]. The serious issues for slurry reactors are back-mixing of the gas phase, catalyst attrition and separation from the liquid and wax products [65]. For metallic foams and monolith reactor structures, catalysts need to be prepared either directly on the reactor structure or via a washcoating process to load catalytic components [66,67]. Hence, these two kinds of reactor structures are not suitable for pre-manufactured catalysts. Through persistent efforts, our group developed a novel catalyst structure called microfibrous entrapped catalyst (MFEC) structure which is now commercially available at IntraMicron Inc. MFEC is a structured catalyst, and it consists of a highly porous network of micron-sized metal, glass, or polymer fibers with small catalyst particles entrapped inside [68–71]. One of the biggest advantages of MFEC when compared with metallic foams or monolith reactor structures is that MFEC can be used for pre-manufactured catalyst particles. This unique advantage greatly extends the applications of MFEC on many heterogeneous reactions by using the original optimized catalyst recipes, instead of seeking a new recipe for washcoating support [72,73]. Previous efforts have found out that MFEC demonstrates high void volume, which significantly reduces pressure drop compared with the packed bed. Moreover, intra-particle heat transfer and mass transfer are enhanced in MFEC structure since small particles are used, and acceptable uniform particle distribution are achieved. This unique catalyst structure has been widely used in various fields. For instance, Yang et al. studied the effects of microfibrous media on external mass transfer in desulfurization [74,75]. Zhu et al. discussed the electrical conductivity of metal microfibrous in fuel cell [76,77]. Gu et al. built a computational fluid dynamics pressure drop model for an MFEC filter [78]. Sheng et al.

investigated and simulated the thermal properties of MFEC and applied to FTS reaction [49,54,79]. According to Sheng et al.'s investigation, copper MFEC can significantly enhance intra-bed heat transfer and maintain a stable reaction temperature for highly exothermic reactions like FTS.

FTS produces a broad spectrum of products including gas, liquid, and wax [80,81]. To maximize the amount of hydrocarbons in the range of liquid fuels suitable operating conditions are required. For example, cobalt-based catalysts typically require 220°C and 20 bar to produce hydrocarbon liquids with the maximum selectivity. To further enhance hydrocarbon liquid fraction, paraffinic wax formed during FTS is hydrocracked to form more liquids. Traditionally, the complicated and expensive process of hydrocracking is performed downstream in a separate reactor. However, by physical mixing of an FTS catalyst with an acidic zeolite component, the FTS and hydrocracking process can simultaneously occur in a single reactor [82–84]. The common FTS catalysts used in the industry are cobalt and iron-based catalysts [6,12]. Iron-based catalysts are more favorable to produce long chain hydrocarbons from coal or biomass (low H_2/CO ratio) due to their high water-gas shift activity, low cost and low methane selectivity [58]. Typically, unsupported iron catalysts promoted with copper and potassium are used in the industry. These catalysts provide high activity and selectivity to hydrocarbons. However, the unsupported Fe-based catalysts generally lack physical strength and durability. In contrast, alumina-supported Fe-based catalysts, although having low activity and high methane selectivity, are stronger and more attrition resistant than unsupported Fe-based catalysts [85].

In the current investigation, a highly active and stable γ-alumina supported Fe-based catalyst was prepared and tested for FTS, and a mesoporous aluminosilicate (MAS) was synthesized as a hydrocracking catalyst. A hybrid FTS catalyst that physically combined these two components has been developed to be applied on FTS and hydrocracking reactions simultaneously within a

single reactor. The results revealed that this type of hybrid catalyst could produce wax-free liquid fuels (C_{23}+ less than 5 wt%), but the $C_5 – C_{20}$ selectivity was relatively low. Also, the selectivity of light hydrocarbons ($C_1 – C_4$) was significantly high. Recently, the addition of 0.3 wt% of Pt to the MAS for the formation of a new hybrid FTS catalyst greatly enhanced $C_5 – C_{20}$ selectivity and reduced the selectivities to CO_2 and the light hydrocarbons ($C_1 – C_4$).

Typical tubular reactors filled with active FTS catalysts will experience thermal runaway at a large reactor diameter due to inefficient radial heat transfer through the packed bed. However, the Cu MFEC structure successfully scaled up the FTS reaction to this larger degree without losing catalyst activity and major product selectivity by significantly enhancing heat transfer and maintaining a stable reaction temperature. To demonstrate the benefits of the MFEC structure, a tubular reactor with a large inside diameter (I.D.) of 34.0 mm I.D. has been designed and tested for FTS using hybrid FTS catalysts.

II.2 Experimental

II.2.1 MFEC Structure and Catalyst Preparation

II.2.1.1 Fabrication of Cu MFEC

A traditional paper-making technique was developed to prepare MFEC by Auburn University. The detailed process can be found in the literature [54]. Briefly, micro-sized copper fibers and cellulose fibers were dispersed in an aqueous suspension. Then, the resulting mixture was cast into a paper-making model, and a preformed sheet was formed by removing the water. A two-sided MFEC sheet can be fabricated by stacking two pieces of performed sheets together, which are made of copper microfibers with different diameters. The top layer was made by 12 μm

diameter copper microfibers, and the bottom layer was 4 μm diameter copper microfibers (IntraMicron, Auburn, AL, USA). After drying these two layers, a self-supporting two-sided sheet has been created. Subsequently, this preformed sheet was pre-oxidized in flowing air at 500 ºC for 30 min to remove the bulk of cellulose. Then, the pre-oxidized sheet was sintered in a flow of hydrogen at 700 ºC for 60 min to form fiber-fiber junctions. These junctions can form a sinter-locked network through the fiber media, which greatly enhances heat transfer in this media. The final step was loading catalyst particles with certain sizes into this porous microfiber media. After sintering, the top layer of media became very fluffy, and the bottom layer was much more compact since it was made of fibers with a smaller diameter. The catalyst particles can be easily loaded into the top layer of this microfiber media, and the bottom layer prevents catalyst particles from leaking or moving out from the microfiber media.

II.2.1.2 Preparation of Fe-based FTS Catalyst

The Fe-based FTS catalyst was supported on a commercial gamma-alumina (Alfa Aesar, γ-Al_2O_3 #43832). The metal precursors were iron (III) nitrate nonahydrate (Alfa Aesar, ACS grade, 98.0-101.0 wt%), copper (II) nitrate hemipentahydrate (Alfa Aesar, ACS grade, 98.0 – 102.0 wt%), and potassium hydrogen carbonate (Alfa Aesar, ACS grade, 99.7 – 100.5 wt% dried basis). In a typical procedure, γ-Al_2O_3 was ground and sieved to 60 – 80 mesh (177 – 250 μm), and then calcined in static air at 750 ºC for 5 hours to remove the hydroxyl groups on the surface. Then, 9.3 g $Al(NO_3)_3 \cdot 9H_2O$, 2.555 g $Cu(NO_3)_3 \cdot 2.5H_2O$, and 0.954 g $KHCO_3$ were dissolved in 36.0 mL of deionized water. An excess solution impregnation method was used to load the metal solution on 3.0 g calcined γ-Al_2O_3 in three steps [86,87]. In each step, one-third of the above metal solution was added to the support while kept on a shaker and dried slowly in air. After drying, the sample was calcined at 300 ºC for 5 hours in static air. Then, the previous steps were

repeated two times to load the remaining metal solution. It must be noted that each loading was followed by calcination. Finally, an iron-based FTS catalyst with a nominal composition of 100 Fe/7.5 Cu/4 K/233 Al_2O_3 (mass basis) was fabricated and was named as Fe-FTS.

II.2.1.3 Synthesis of MAS and Pt-MAS

A sol-gel synthetic method was used to synthesize this mesoporous aluminosilicate (MAS) [88]. Aluminum nitrate nonahydrate (ANN, J.T. Baker, ACS grade, 98.7 wt%) and tetraethylorthosilicate (TEOS, Alfa Aesar, 99.9 wt%) were used as the alumina and silica sources, respectively. Cetyltrimethylammonium bromide (CTAB, Spectrum Chemical MFG. Corp., 98 – 101 wt%) was used as the templating agent. Also, ammonium hydroxide (NH_4OH, BDH Chemicals, 30 wt%) and ethyl alcohol (C_2H_5OH, EMD Chemicals Inc., ACS grade, 99.5 wt%) were used. The molar composition of the synthesis mixture was as followed: 1.0 TEOS:0.13 ANN:40 H_2O:8 C_2H_5OH:0.25 CTAB:10 NH_4OH. In a typical synthesis, 4.88 g ANN was dissolved in 46.7 mL C_2H_5OH and then mixed with 22.3 mL TEOS. Meanwhile, 9.1 g CTAB, 72.0 mL water, and 116.8 g NH_4OH solution were mixed together under constant stirring. After 30 min, the TEOS solution was added to the CTAB mixtures drop by drop while stirring. After all the solution was added, the mixture was increased to and kept at 60 ºC under stirring for 3 days. The resulting gel was filtered and washed with an excess amount of water to remove unreacted components. After drying overnight at 100 ºC, the resulting sample was calcined at 540 ºC for 6 hours to remove the template.

An incipient wetness impregnation method was used to prepare 0.3 wt% Pt-MAS by using tetraammineplatinum (II) nitrate (Alfa Aesar, ACS grade, 99 wt%) as the Pt source. After drying at 120 ºC for 6 hours, the sample was calcined at 500 ºC for 4 hours in static air.

II.2.1.4 Preparation of Hybrid Catalysts

Hybrid catalysts were composed of two parts. One part is the FTS catalyst mentioned above, Fe-based catalyst (Fe-FTS), with a nominal composition of 100 Fe/7.5 Cu/4 K/233 Al_2O_3 (based on mass). The other part is the hydrocracking catalyst which is ZSM-5 (Zeolyst, CBV 8014, Si/Al=80:1), or MAS, or Pt-MAS. In a typical process, a physical powder mixture of 50 wt% Fe-FTS catalyst and 50 wt% hydrocracking catalyst was pressed into extrudate form, and then the extrudates were crushed and separated to 60 – 80 mesh particles. The resulted hybrid catalysts were named as Fe-FTS/ZSM-5, Fe-FTS/MAS and Fe-FTS/Pt-MAS for the three hydrocracking catalysts, respectively. It is worth noting that the ZSM-5 was activated at 540 ºC for 3 hours before using.

II.2.2 Catalyst Characterization

Nitrogen adsorption/desorption isotherms were recorded at -196 ºC on a Micromeritics TriStar II 3020 instrument. Before the measurement, samples were degassed at 200 ºC under N_2 flow overnight. The total surface areas of samples were calculated via the Brunauer-Emmett-Teller (BET) equation. Average pore diameter and pore size distribution were calculated by using the Barrett-Joyner-Halenda (BJH) method. The surface morphologies of Cu MFEC structure before and after catalyst loading were characterized on a JEOL JSM-7000F scanning electron microscope (SEM).

II.2.3 FTS Reaction Measurements

II.2.3.1 Packed Bed

The FTS experiments in this paper can be separated into two groups. One tested FTS catalysts in packed beds and the other evaluated these catalysts in the Cu MFEC structure. For packed bed tests, usually 0.5 g of Fe-FTS catalyst (60 – 80 mesh) was diluted with a certain amount of glass beads (Alfa Aesar, acid washed, 60 – 80 mesh). For hybrid catalyst tests, 1.0 g of hybrid catalysts were used for the reaction to keep the Fe-based FTS catalyst in the same amount. Before applying the FTS reaction, the catalysts were pre-reduced in situ at 120 ºC for 2 hours in flowing ultra-high purity hydrogen (Airgas, HY UHP300). Then, the temperature was slowly increased to 280 ºC for another 10 hours which was followed by gradually increasing the temperature to 320 ºC for another 4 hours. After that, the catalysts were cooled down to 260 ºC to initiate the FTS reaction. All the experiments in this paper were carried out at 260 ºC and 2.0 MPa by using a syngas with an H_2/CO ratio of 2:1. This syngas was purchased from Airgas with 1.5 vol% nitrogen as the internal standard. The outlet stream went sequentially through a hot trap (150 ºC) and a cold trap (2 ºC) to collect heavy hydrocarbons and liquid products, respectively. The residual gas products were analyzed on an online gas chromatograph (GC, Agilent 6890) equipped with a packed column (Hayesep-DB 100/120). A thermal conductivity detector (TCD) was used to determine the concentrations of CO, CO_2, and $C_1 – C_6$ using nitrogen as the internal standard. In the same GC, there was a capillary column (DB-5) connected with a flame ionization detector (FID) which was used to analyze liquid and wax products. The collected wax products were dissolved and diluted in carbon disulfide (Alfa Aesar, ACS grade, >99.9 wt%) and then shot into the FID.

II.2.3.2 Cu MFEC Structure

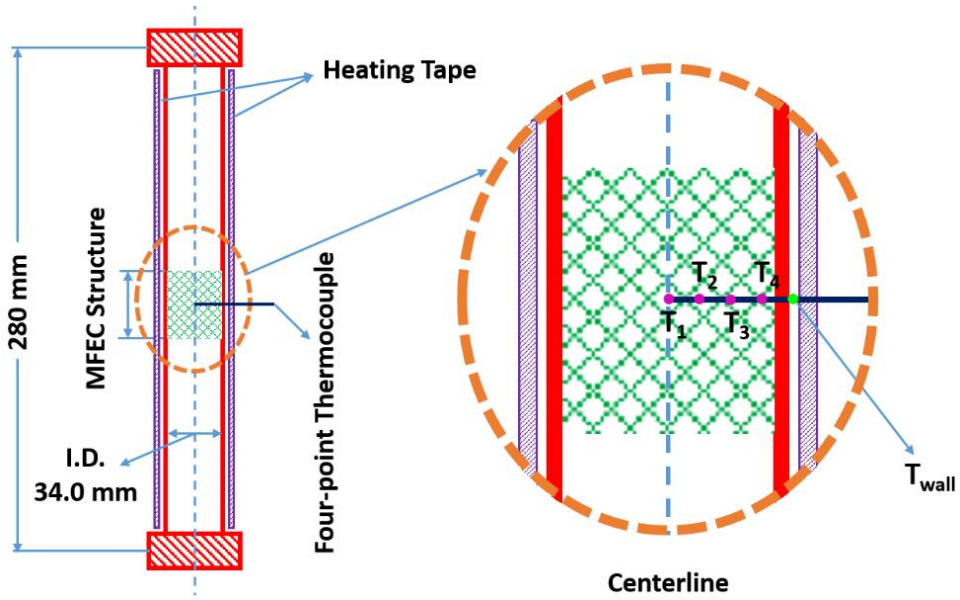

Figure II.1 The Cu MFEC reactor structure (From T_1 to T_4, the intervals between each point are 10.0 mm, 2.0 mm, and 5.0 mm, respectively. T_{wall} is the outside reactor temperature)

The Cu MFEC structure was only used in the large reactor (34.0 mm I.D.). First, the calcined catalyst particles were entrapped into a sintered copper microfiber media to form a Cu MFEC structure. Next, circular disks with a diameter of 36.0 mm were punched out from the Cu MFEC to pack into the tubular reactor. The disk size (36.0 mm) was 6 % larger than the inside diameter of the tubular reactor (34.0 mm) this offers tremendous contact points between the copper fiber media and the reactor wall. By doing this, the inside wall heat transfer coefficient was significantly increased when compared with the traditional packed bed. As shown in Figure II.1, a four-point thermocouple was inserted into the reactor from the outside wall of the reactor when the reactor was loaded half-way, and then the other half of the bed was loaded. In that way, the radial temperature distribution profiles were measured precisely. For Cu MFEC structures, all the reaction conditions and product analysis system were the same with the above mentioned packed bed.

II.3 Results and Discussion

II.3.1 Catalyst Activity and Selectivity

II.3.1.1 Small Reactor for Catalyst Screening

Table II.1 Nitrogen sorption data

Sample	BET Surface Area (m^2/g)	Pore Volume (cm^3/g)	Average Pore Diameter (nm)
Calcined γ-Al_2O_3	216	0.75	11.7
Fe-FTS	74	0.25	10.7
MAS	1108	1.00	3.5
Pt-MAS	1061	0.95	3.5
ZSM-5[a]	450	0.27	0.56

[a] The sorption data of ZSM-5 was referenced from the literature [89,90].

Fe-FTS is an iron-based FTS catalyst that is supported on calcined γ-alumina and promoted with copper and potassium. The porous structures of alumina support and Fe-FTS have been measured by N_2 sorption (Figure II.2). As shown in Table II.1, after metals loading, the support's BET surface area was significantly decreased from 216 to 74 m^2/g, and the pore volume was also drastically reduced from 0.75 to 0.25 cm^3/g due to the very high iron loading ratio (30 wt%). The average pore diameter was slightly decreased from 11.7 to 10.7 nm (Table II.1). The Fe-FTS catalyst was tested in a small tubular reactor (9.5 mm I.D.) under a typical FTS reaction condition (260 ºC, 2.0 MPa, and H_2/CO = 2:1). At a CO conversion of 27.7 % (SR-1 in Table II.2), the apparent reaction rate constant of Fe-FTS was 167 mmol $(H_2 + CO)/g_{cat}/h$ and the corresponding productivity was 0.30 $gC_5+/g_{cat}/h$. These values are higher than those obtained on typical supported Fe-based catalysts and comparable to those achieved on most active unsupported Fe-based catalysts [91]. Also, the selectivity to methane was very low (5.2 C-%) and a

high α value (0.81) was calculated by following the Anderson-Schulz-Flory distribution (Figure II.3). The selectivity of CO_2 was very high, which is a common phenomenon for Fe-based FTS catalyst because of the water-gas shift reaction [92]. Furthermore, the Fe-FTS catalyst was very stable, and no catalyst deactivation was observed during the 120 hours of operation (Figure II.4). Therefore, Fe-FTS is a highly active and stable γ-alumina supported Fe-based FTS catalyst.

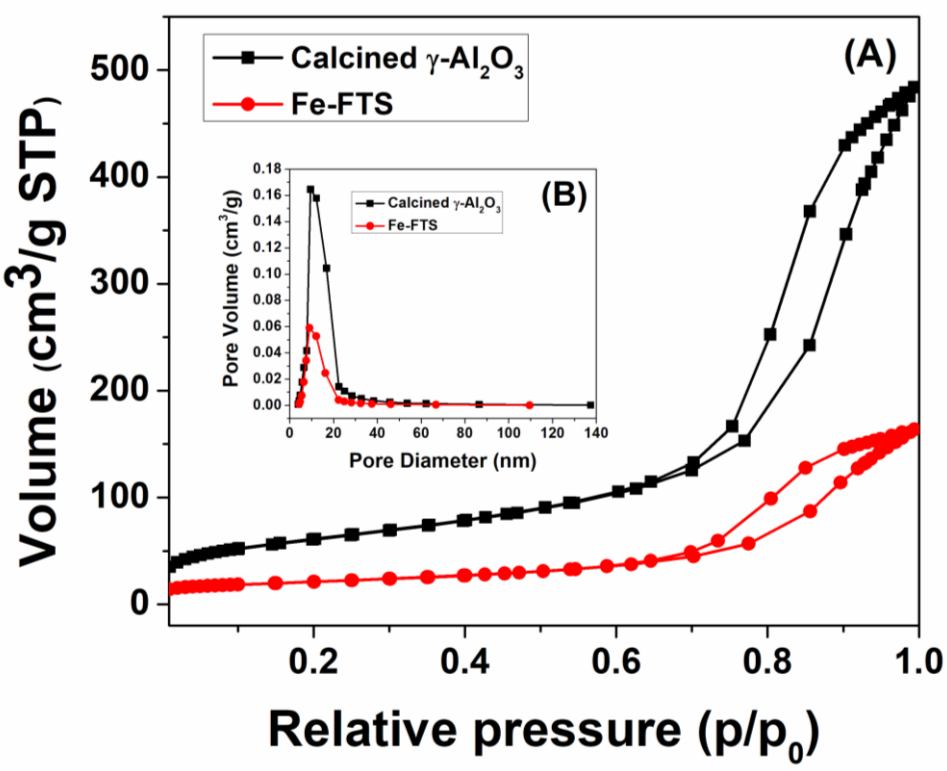

Figure II.2 N_2 sorption data (A) adsorption/desorption isotherms of calcined γ-Al_2O_3 and Fe-FTS; (B) pore size distribution patterns of calcined γ-Al_2O_3 and Fe-FTS

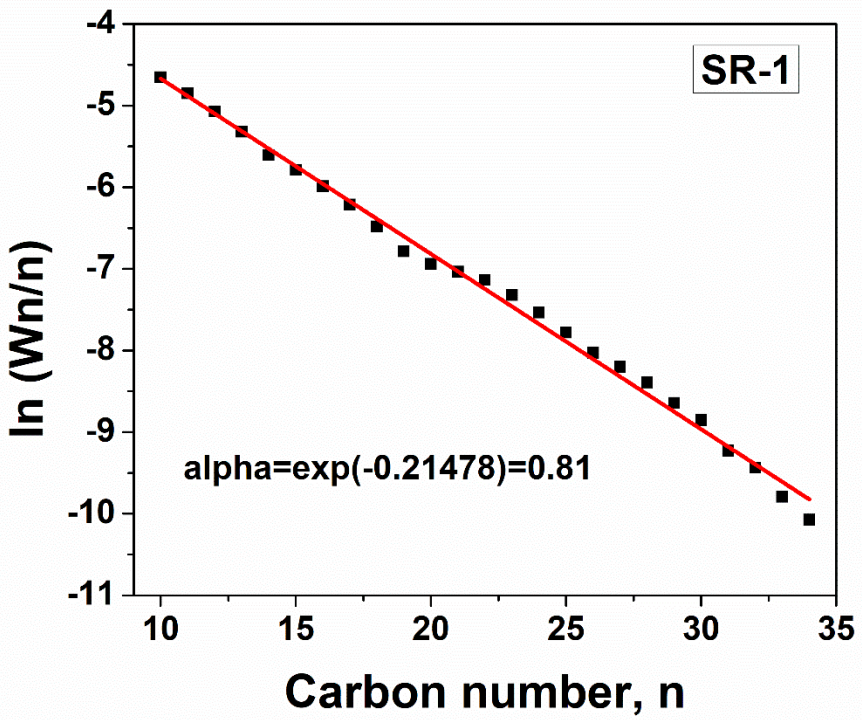

Figure II.3 N_2 sorption Anderson-Schulz-Flory diagram of data from SR-1

One of the major reasons for this high activity is that the alumina support was pretreated at 750 ºC for 5 hours, before loading metals, to remove the hydroxyl groups on the surface. Decreasing the surface hydroxyl groups can reduce the formation of $FeO \cdot Al_2O_3$ surface spinel, which cannot be reduced to the FTS active species under the typical reduction conditions [85]. Moreover, this Fe-based FTS catalyst had very high iron loading (30 wt%) and was promoted by copper and potassium. It is well known that Cu promoter facilitates the dispersion and reduction of iron species, and potassium promoter enhances the CO adsorption and carburization. All these facts contributed to the high reaction activity and high productivity. Apparently, supported Fe-based catalyst have many advantages over unsupported ones under a similar reaction activity and product selectivity [85].

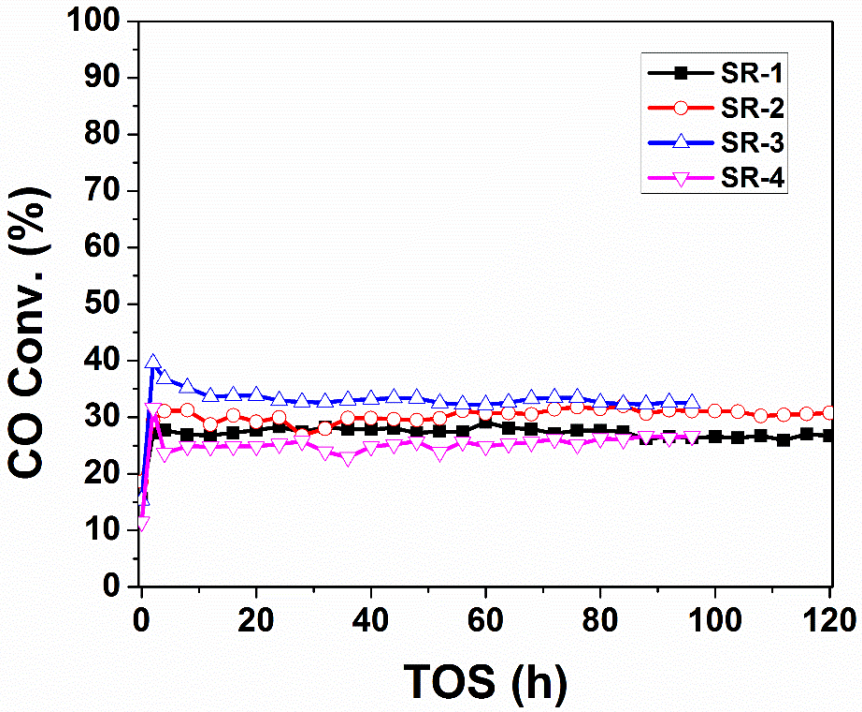

Figure II.4 CO conversion vs. time on stream for four experiments carried out in the small reactor: SR-1 for Fe-FTS; SR-2 for Fe-FTS/ZSM-5; SR-3 for Fe-FTS/MAS; SR-4 for Fe-FTS/Pt-MAS (solid dot for FTS catalyst and empty dot for hybrid catalysts)

Based on this highly active and stable Fe-based FTS catalyst (Fe-FTS), three hybrid catalysts were prepared by physically mixing Fe-FTS with ZSM-5, MAS, and Pt-MAS, and were named as Fe-FTS/ZSM-5, Fe-FTS/MAS, and Fe-FTS/Pt-MAS, respectively. The corresponding experiments were named SR-2, SR-3, and SR-4, respectively. All the experiments (from SR-1 to SR-4) in the small reactor (9.5 mm I.D.) were operated at the same reaction conditions, and the reaction activities and selectivities of these catalysts were obtained at similar CO conversion levels of 26 – 33 %. Hence, the measured values of activity and selectivity for these catalysts are directly comparable. As shown in Table II.2, all the hybrid catalyst demonstrated much different product distributions compared with that of plain Fe-FTS catalyst. Due to the hydrocracking activity of ZSM-5 [93], the hybrid catalyst Fe-FTS/ZSM-5 (SR-2 in Table II.2) demonstrated a high selectivity of 32.8 C-% to light chain hydrocarbons (C_1 – C_4) and a low selectivity of 1.5 C-

% to C_{21}+, compared with those obtained by Fe-FTS at 21.9 C-% and 7.4 C-%, respectively (SR-1 in Table II.2). Because the decreased selectivity to C_{21}+, the catalyst production rate to C_5+ slightly decreased from 0.3 to 0.28 $gC_5+/g_{cat}/h$, even at a higher reaction rate and higher CO conversion. In addition, the liquid product selectivity ($C_5 – C_{20}$) in SR-2 was almost the same as that in SR-1. Therefore, Fe-FTS/ZSM-5 is not an ideal hybrid catalyst for liquid hydrocarbon production.

According to the literature [90], hydrocracking selectivity to long chain hydrocarbons can be improved significantly if the pore size of hydrocracking catalyst can reach mesoporous range. Considering this, a mesoporous aluminosilicate (MAS) with a larger pore size (3.5 nm) was synthesized as the hydrocracking catalyst. The N_2 adsorption/desorption isotherm shows the presence of an H2 hysteresis loop with an abrupt step around $P/P_0 = 0.52$ in the desorption branch of MAS (Figure II.5A). This is a typical mesoporous adsorption and desorption isotherm. As shown in Figure II.5B, MAS has a narrow pore size distribution, and the average pore diameter is 3.5 nm. Moreover, MAS has a very high surface area (1108 m^2/g) and its pore volume reach of 1.00 cm^3/g (Table II.1). Therefore, MAS could be an excellent candidate as a hydrocracking catalyst, and the experimental results confirmed this expectation. Hybrid catalyst Fe-FTS/MAS (SR-3 in Table II.2) significantly increased the selectivity of $C_1 – C_4$ to 47.9 C-% and reduced the $C_5 – C_{20}$ selectivity to 20.6 C-%. Moreover, the catalyst productivity dropped to 0.22 g of $C_5+/g_{cat}/h$. This is due to the large pore size of MAS can fit in the long chain hydrocarbons, which greatly increased the chance of heavy products to be hydrocracked to short chain hydrocarbons. These results also suggest Fe-FTS/MAS is not a suitable catalyst for the selective production of FTS liquids.

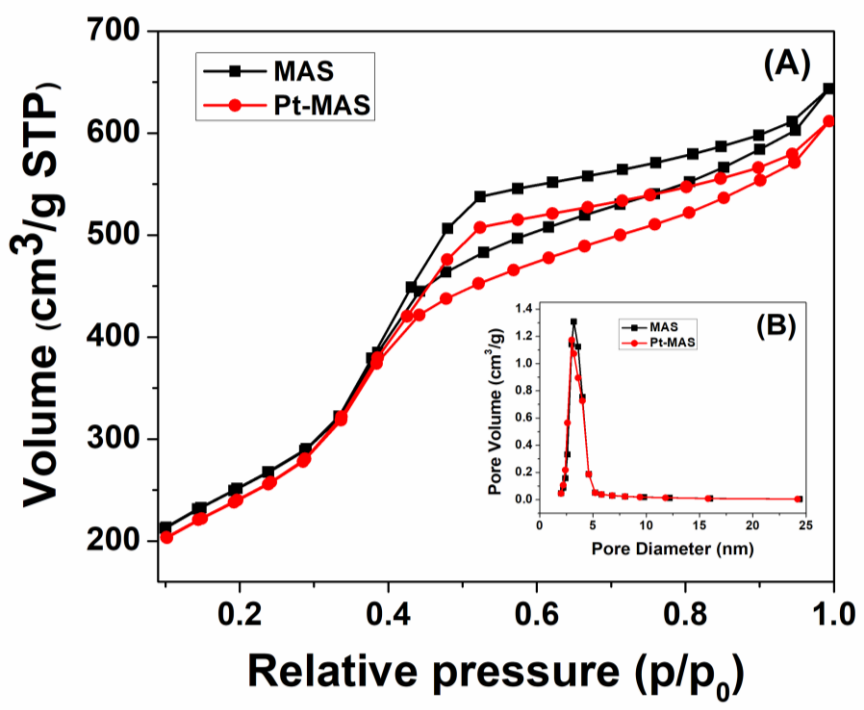

Figure II.5 N_2 sorption data (A) adsorption/desorption isotherms of MAS and Pt-MAS; (B) pore size distribution patterns of MAS and Pt-MAS

It must be noted that the CO_2 selectivity in SR-3 decreased to 31.1 C-% which is much less than the CO_2 selectivity in SR-1 (41.3 C-%). One possible reason is that the acid components of MAS provided active protons (H^+) to terminate the active oxygen (O^{2-}) that dissociated from CO or H_2O, which suppressed the formation of CO_2 [94]. If this assumption is correct, the production of H_2O should be increased. To prove that, the mass ratio of H_2O to liquid oils was calculated. The results show that the mass ratio of H_2O/oil was around 1.0 for Fe-FTS catalyst (SR-1), but it increased to 1.9 when hybrid catalyst Fe-FTS/ZSM-5 was used (SR-2 in Table II.2). The mass ratio further rose to 7.0 when hybrid catalyst Fe-FTS/MAS (SR-3 in Table II.2) was used. This is an extremely high H_2O/oil mass ratio, and the very low C_5+ selectivity (21.0 C-%) contributed to this. These results verify our argument that the acid component can suppress the water-gas shift reaction activity and promote water production.

Table II.2 Performance of different catalysts in both packed bed and Cu MFEC structure

Reactor size [a]	I.D. 9.5 mm				I.D. 34.0 mm			
Reactor structure [b]	PB				MFEC	MFEC	MFEC	PB
Experiment number [c]	SR-1	SR-2	SR-3	SR-4	LR-1	LR-2	LR-3	LR-4
Catalyst composition [d]	Fe-FTS	Fe-FTS /ZSM-5	Fe-FTS /MAS	Fe-FTS /Pt-MAS	Fe-FTS	Fe-FTS	Fe-FTS /Pt-MAS	Fe-FTS
Voidage, %	43.9	39.0	33.3	33.4	65.6	64.6	44.8	45.3
HSGV, Nl/g_{Fe}/h	5.7	5.7	5.7	5.7	5.7	3.3	3.3	5.7
Time on stream, h	120	120	96	96	60	60	60	60
CO conversion, %	27.7	30.1	33.2	25.7	18.5	24.2	18.1	50.4
Rate constant [e]	167	181	231	186	143	108	94	284
Product selectivity, C-%								
CO_2	41.3	36.4	31.1	27.7	37.3	40.3	24.3	44.7
CH_4	5.2	9.9	16.0	12.3	7.9	8.7	10.8	8.3
$C_2 – C_4$	16.7	22.9	31.9	19.9	19.2	22.6	23.4	20.6
$C_5 – C_{20}$	29.4	29.3	20.6	38.1	28.8	22.8	39.0	24.6
C_{21}+	7.4	1.5	0.4	2.0	6.8	5.6	2.5	1.8
Catalyst productivity [f]	0.30	0.28	0.22	0.32	0.21	0.14	0.18	0.40
α value [g]	0.81	—	—	—	0.80	0.76	—	0.79
H_2O/oil mass ratio [h]	1.0	1.9	7.0	4.1	1.0	1.0	3.6	0.8

[a] Two kinds of tubular reactors were used, their inside diameters are 9.5 mm and 34.00 mm, respectively;

[b] PB means packed bed and MFEC means copper MFEC structure;

[c] The experiments operated on the small reactor (9.5 mm I.D.) named as SR- and on the large reactor (34.00 mm) named as LR-;

[d] Four kinds of catalysts were used, Fe-FTS is only for Fischer-Tropsch reaction, and hybrid catalysts were fabricated from Fe-FTS by physically mixed with ZSM-5, or MAS, or Pt-MAS;

[e] Apparent reaction rate constant means mmol (H_2 + CO)/g_{cat}/h. For hybrid catalyst, g_{cat} means per gram of Fe-FTS without counting the equal mass of hydrocracking catalyst;

[f] Catalyst productivity means g of C_5+/g_{cat}/h and g_{cat} still means the weight of Fe-FTS catalyst for hybrid catalysts;

[g] Calculated by using ASF equation (Figure II.5);

[h] The mass ratio of collected water to oil.

(All the experiments in this table were carried out at 260 ºC and 2.0 MPa by using a syngas with H_2/CO ratio equals to 2:1)

Because monofunctional cracking catalysts, e.g. MAS usually produce mostly short and unsaturated hydrocarbons, Fe-FTS/MAS is not an ideal hybrid catalyst for the maximum production of liquid hydrocarbons. In contrast, bifunctional hydrocracking catalysts can maximize the production of middle distillates by making a balance between the acid and the metal functions [95,96]. Typically, noble metals such as Pt or Pd are used to build bifunctional hydrocracking catalysts due to their higher hydrogenating activity. This property can improve the yield of middle distillates as well as reduce the light hydrocarbons formation. In addition, a strong hydrogenation function can enhance catalyst stability through suppressing the formation of coke precursors [97].

Considering the aforementioned fundamentals, 0.3 wt% of Pt was loaded on MAS to form a bifunctional hydrocracking catalyst (Pt-MAS). The texture property of Pt-MAS was characterized by N_2 sorption (Table II.1). When compared with MAS, the BET surface area of Pt-MAS slightly decreased to 1061 m^2/g, and its pore volume was also slightly reduced to 0.95 cm^3/g. While its average pore diameter remained almost unchanged, since Pt loading content was low. The hybrid catalyst Fe-FTS/Pt-MAS was tested for FTS performance (SR-4 in Table II.2). The results showed that the $C_1 - C_4$ selectivity and CO_2 selectivity of Fe-FTS/Pt-MAS were 32.2 C-% and 27.7 C-%, respectively, which are much lower than those achieved by Fe-FTS/MAS, 47.9 C-% and 31.1 C-%, respectively. Its $C_5 - C_{20}$ selectivity reached 38.1 C-%, which is much higher than that of Fe-FTS/MAS (20.6 C-%) and is the highest among all three hybrid catalysts selective to the liquid fraction. Moreover, the catalyst productivity was increased to 0.32 $gC_5+/g_{cat}/h$ even at a slightly lower CO conversion. In a word, Fe-FTS/Pt-MAS is a good hybrid catalyst formulation for the maximum liquid hydrocarbon production compared with the hybrid

catalysts with ZSM-5 and MAS. Therefore, the best hybrid catalyst has been screened out and can be used for further study in Cu MFEC structure.

II.3.1.2 Large Reactor for Cu MFEC Structure

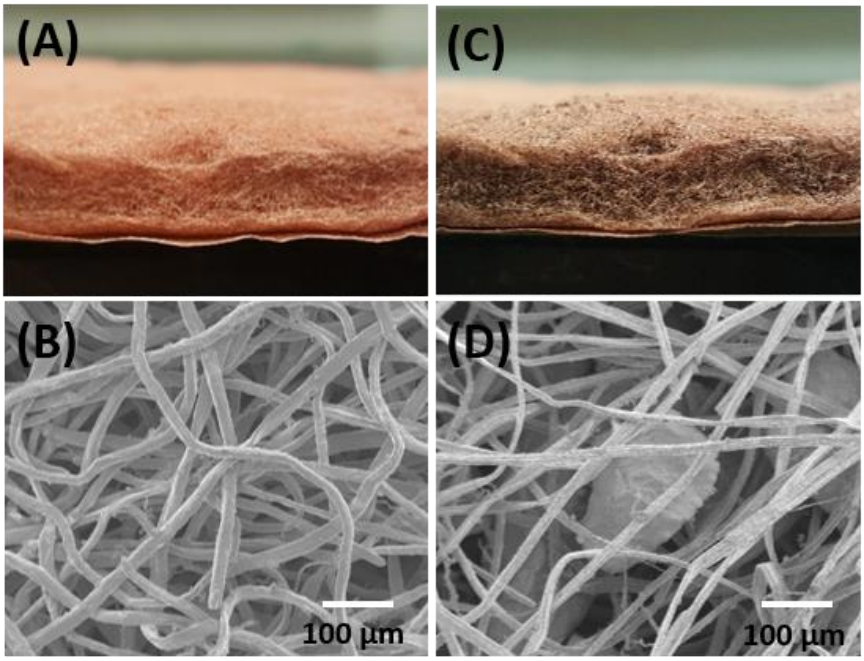

Figure II.6 Images of Cu MFEC structure: (A) Picture of Cu MFEC before catalyst loading; (B) SEM image of Cu MFEC before catalyst loading; (C) Picture of Cu MFEC after catalyst loading; (D) SEM image of Cu MFEC after catalyst loading

In the catalyst screening step, all the evaluations were performed in a small tubular reactor (9.5 mm I.D.). Since the Cu MFEC structure can greatly enhance radial heat transfer, a larger reactor could demonstrate this benefit more markedly. Therefore, a much larger tubular reactor with a 34.0 mm I.D. was used to construct the Cu MFEC reactor. Figure II.6A shows a picture of copper microfiber media which has a very fluffy structure at the top layer, hence catalyst particles can easily migrate into the fiber media by utilizing a shaker, resulting in an acceptable dispersion (Figure II.6C). After loading, the catalyst particles were immobilized by the sintered microfiber network (Figure II.6D), and the compacted bottom layer prevented the loss of catalyst

particles. In addition, the Cu MEFC media were stacked tightly during the time of packing to enhance axial heat transfer. Therefore, catalysts entrapped in MFEC structure are immobilized even under a high space velocity.

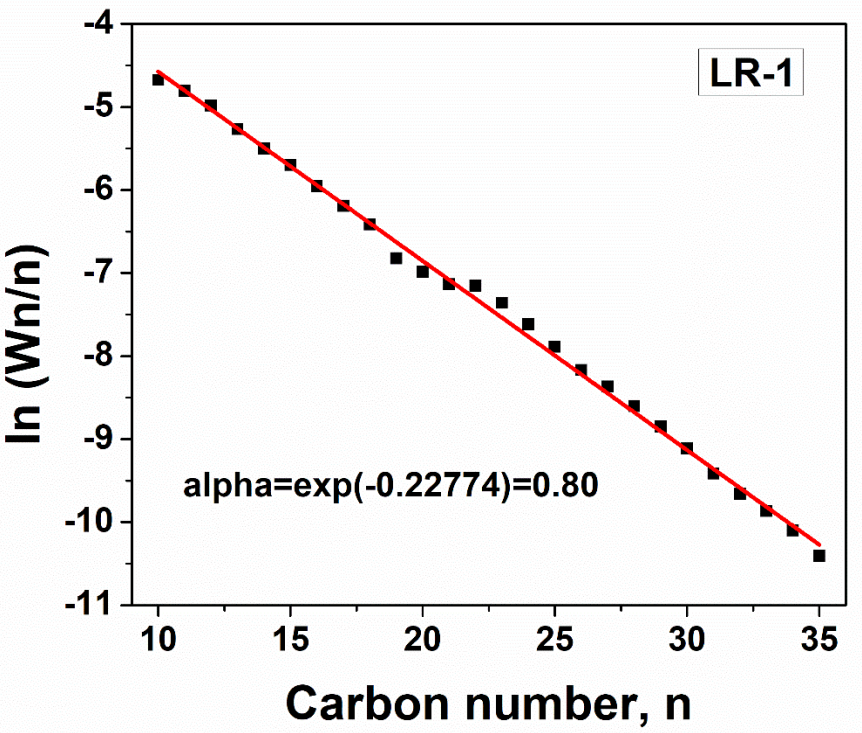

Figure II.7 Anderson-Schulz-Flory diagram of data from LR-1

The first experiment (LR-1 in Table II.2) was compared with SR-1 by keeping all the reaction conditions the same. The results show that both the apparent reaction rate constant and the catalyst productivity of LR-1 were lower than SR-1. This is mainly because the CO conversion in LR-1 (18.5 %) was much lower than the CO conversion in SR-1 (27.7 %). If the differences in CO conversion had been corrected, the reaction activity (apparent rate constant and catalyst productivity) of LR-1 would be higher than the reaction activity of SR-1. In LR-1, the product selectivities were similar to SR-1. Moreover, the α value in LR-1 was 0.80 (Figure II.7) which is also similar to the α value of SR-1 (0.81). In conclusion, copper microfibrous

entrapment enables the highly exothermic reaction to take place in a tubular reactor with a large reactor diameter without compromising the reaction activity or the product selectivity.

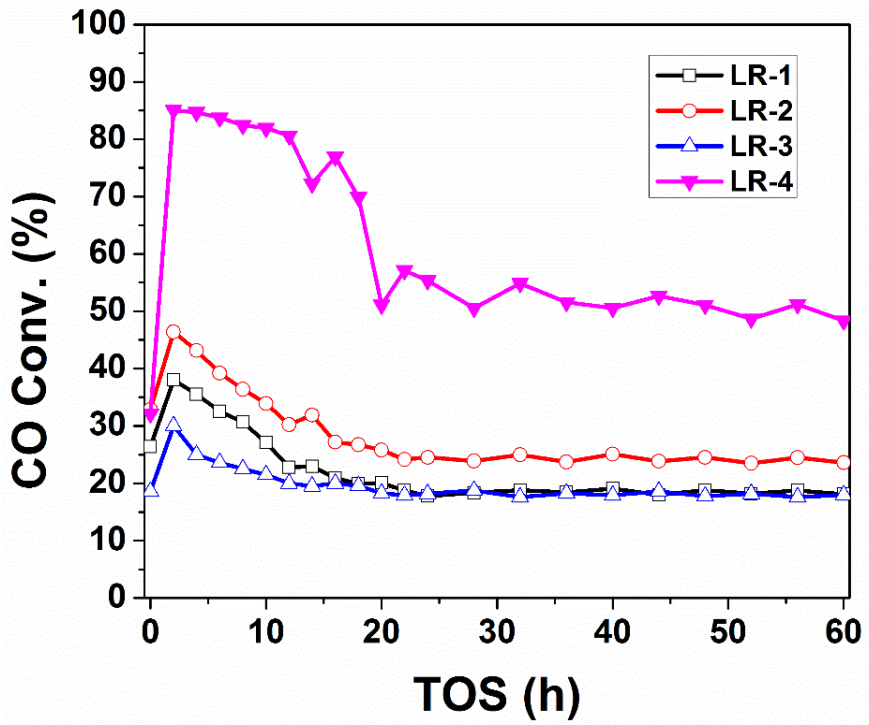

Figure II.8 CO conversion vs. time on stream for four experiments operated in the large reactor: LR-1 and LR-2 for Fe-FTS; LR-3 for Fe-FTS/Pt-MAS (empty dot for Cu MFEC structure); LR-4 for Fe-FTS (solid dot for packed bed)

To fairly compare the performance of MFEC with the catalysts tested in a small packed bed, the CO conversion should be kept at a similar level. Hence, more catalyst was loaded into the Cu MEFC structure, and the space velocity was also decreased. By holding other reaction conditions unchanged, the CO conversion in LR-2 was increased to 24.2 % (Figure II.8), which is comparable to the CO conversion (27.7 %) in SR-1. Compared with LR-1, the apparent reaction rate constant in LR-2 decreased to 108 mmol $(H_2 + CO)/g_{cat}/h$ and the productivity dropped to 0.14 $gC_5+/g_{cat}/h$. This does not mean the reaction activity was reduced since more catalyst was loaded and a lower flow rate of syngas was passed through the reactor. Meanwhile, the $C_5 – C_{20}$

selectivity was reduced to 22.8 C-%, and the selectivity of $C_1 – C_4$ and CO_2 slightly increased to 31.3 C-% and 40.3 C-%, respectively.

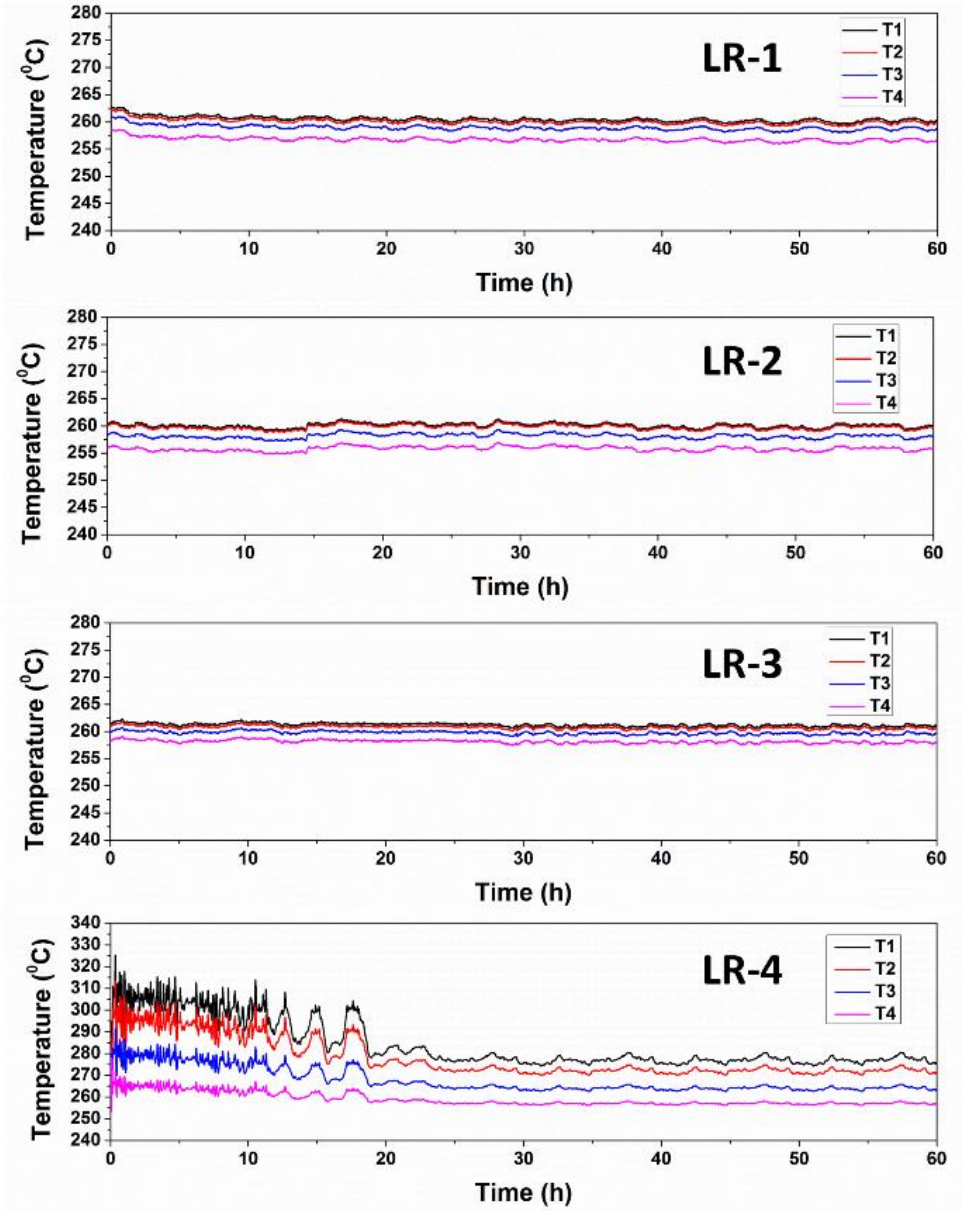

Figure II.9 Temperature profiles of four experiments in the large reactor: LR-1, LR-2, and LR-3 are Cu MFEC structures; LR-4 is a packed bed diluted with α-Al_2O_3 (From T_1 to T_4, the intervals between each point is 2.0 mm, 10.0 mm, and 5.0 mm, respectively. T_{wall} is the outside reactor temperature)

Under the same reaction conditions as LR-2, the Cu MFEC structure entrapped with hybrid catalyst Fe-FTS/Pt-MAS (LR-3 in Table II.2) was tested to compare the FTS performance of SR-4. As a result, both the apparent reaction rate constant and the catalyst productivity decreased when compared with SR-4. However, LR-3 had the highest $C_5 – C_{20}$ selectivity (39.0 C-%) and the lowest CO_2 selectivity (24.3 C-%). Meanwhile, the selectivity of $C_1 – C_4$ in LR-3 was similar to that in SR-4. Hence, the SR-4 has been scaled up to a large Cu MFEC reactor (34.00 mm I.D.) without apparently losing reaction activity or desired product selectivity.

It must be pointed out that under the same reaction conditions, CO conversion in LR-1 was lower than in SR-1 due to the impact of the Cu MFEC structure. The Cu MFEC structure can transfer the reaction heat out of the reactor and avoid temperature overshoot and the formation of hot spots. This implies that LR-1 operated at a lower temperature than SR-1, which led to a lower CO conversion. For comparison purposes, a packed bed was loaded (LR-4 in Table II.2) by using α-Al_2O_3 to dilute the bed to the same degree as LR-1 with all other reaction conditions unchanged. It turns out that the CO conversion in LR-4 (50.4 %) was much higher than in LR-1 (18.5 %), but with a lower $C_5 – C_{20}$ selectivity and higher CO_2 selectivity. This is mainly caused by the very poor heat transfer ability of a packed bed, which led to serious temperature overshooting and increased the CO conversion. As shown in Figure II.9, the maximum temperature difference between T1 and T4 for LR-4 reached around 54 ºC. While the largest temperature differences for all the Cu MFEC structures were less than 5 ºC. In addition, it took a long time for the packed bed to reach steady state. Figure II.8 shows that the time required to reach steady state was around 24 hours for all Cu MFEC structures, and more than 40 hours for the same size packed bed to reach the target CO conversion with 5 % variation. Therefore, the

Cu MFEC structure possesses many obvious advantages compared with the traditional packed bed.

II.3.2 Product Distribution

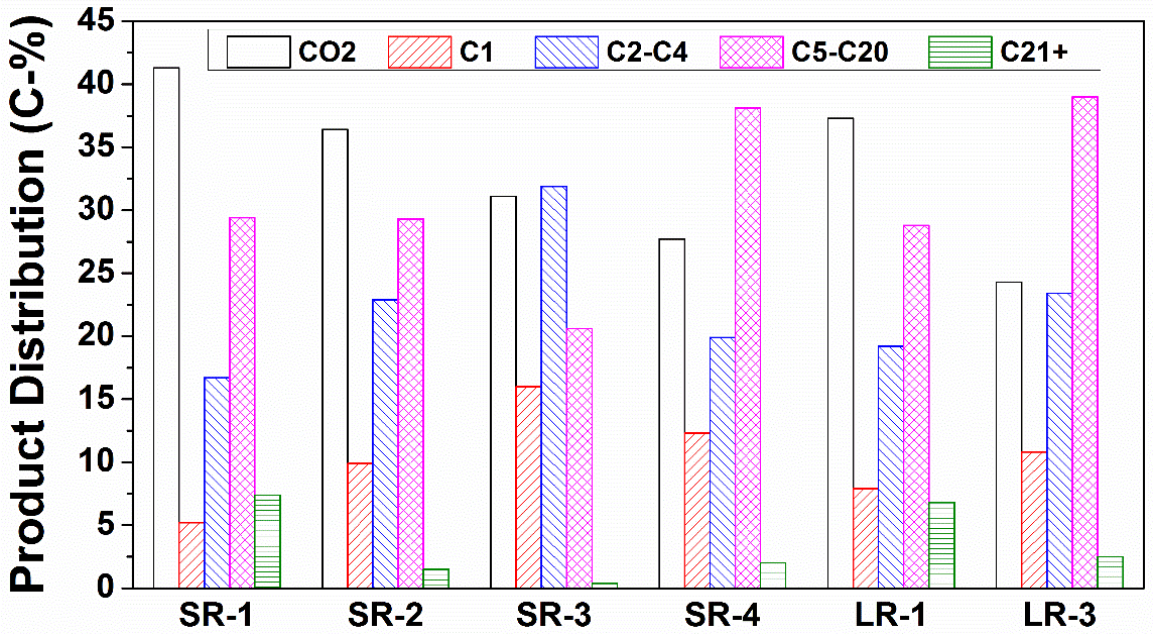

Figure II.10 Product distribution of the experiments operated both in the small reactor (SR-1 to SR-4) and in the large reactor (LR-1 and LR-3): SR-1 for Fe-FTS; SR-2 for Fe-FTS/ZSM-5; SR-3 for Fe-FTS/MAS; SR-4 for Fe-FTS/Pt-MAS; LR-1 for Fe-FTS with Cu MFEC structure; LR-3 for Fe-FTS/Pt-MAS with Cu MFEC structure

The product distributions of six major experiments are listed in Figure II.10. As shown in Figure II.10, the hybrid catalyst Fe-FTS/ZSM-5 significantly reduced C_{21}+ selectivity and increased the selectivities to lighter hydrocarbons including CH_4 and C_2 – C_4. This is attributed to the deep hydrocracking activity of ZSM-5. As hybrid catalyst Fe-FTS/ZSM-5 did, hybrid catalyst Fe-FTS/MAS further increased the selectivities of light hydrocarbons (CH_4 and C_2 – C_4) and greatly reduced the liquid products (C_5 – C_{20}) selectivity and wax (C_{21}+) selectivity. This is mainly because MAS has a larger pore size (3.5 nm) than ZSM-5 (0.56 nm), so long chain hydrocarbons

can access the internal surface of MAS, which results in over hydrocracking. Hybrid catalyst Fe-FTS/Pt-MAS with bifunctional catalyst Pt-MAS increased the production of liquid products by suppressing the formation of C_1, $C_2 – C_4$ and CO_2. This bifunctional catalyst (Pt-MAS) consists of the noble metal Pt which is responsible for hydrogenation/dehydrogenation reactions and the support MAS, whose acid sites are responsible for activation of C-C and C-H bonds via a carbocationic mechanism. A proper balance between acid sites strength and hydrogenation or dehydrogenation activity could lead to moderate cracking and maximize the formation of liquid products [96,98].

LR-1 was carried out in the presence of a thermally conductive copper microfibrous network at the same experimental conditions used for SR-1. Figure II.10 shows that LR-1 had a similar product distribution pattern with SR-1. This confirmed that MFEC could successfully remove the heat generated inside the 34.0 mm I.D reactor and provide as uniform a temperature profile as a packed bed reactor of 9.5 mm I.D. (SR-1) did. Similarly, LR-3 was compared to SR-4. Results shown in Figure II.10 suggest that they have a similar product distribution pattern except for the selectivity of $C_2 – C_4$ in the MFEC reactor was slightly higher than in the packed bed reactor in SR-4, but the liquid product ($C_5 – C_{20}$) selectivity was at a similar level. In short, the MFEC approach enabled FTS and bifunctional hydrocracking to take place simultaneously in a single reactor and provide efficient thermal management for both reactions in a fixed bed reactor with a large reactor diameter.

II.3.3 Olefin Selectivity

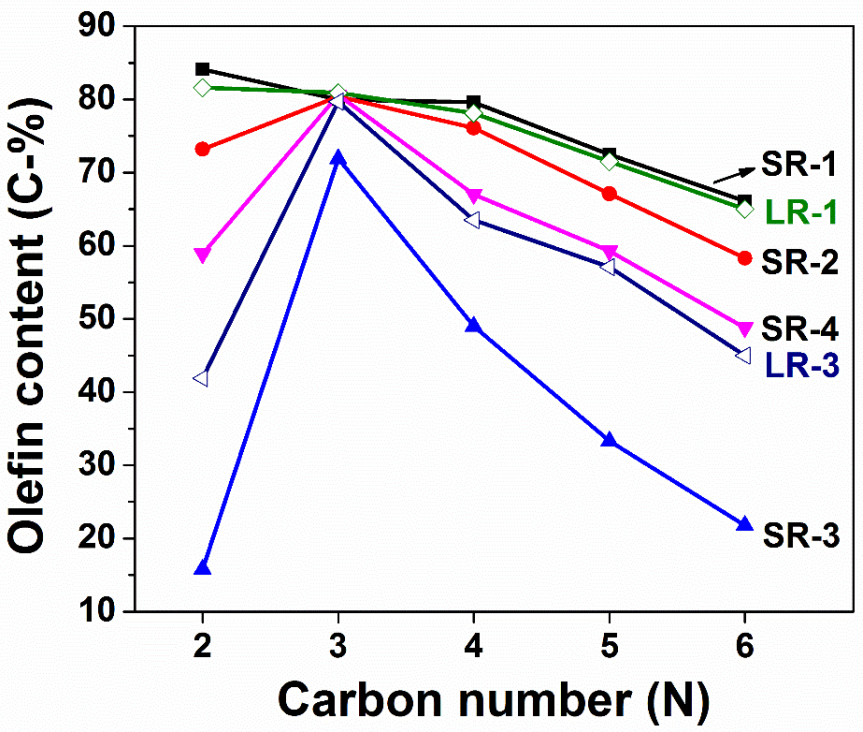

Figure II.11 Olefin content of light hydrocarbons for experiments operated in the small reactor (SR-1 to SR-4, solid dot) and in the large reactor (LR-1 and LR-3, empty dot): SR-1 for Fe-FTS; SR-2 for Fe-FTS/ZSM-5; SR-3 for Fe-FTS/MAS; SR-4 for Fe-FTS/Pt-MAS; LR-1 for Fe-FTS with Cu MFEC structure; LR-3 for Fe-FTS/Pt-MAS with Cu MFEC structure

The olefin content in carbon number fractions for gas phase products is shown in Figure II.11. It is shown that SR-1 demonstrated a very high olefin yield because of the relatively low tendency of secondary reactions for alkali-promoted iron-based catalysts. Moreover, the olefin content of SR-1 gradually declined with chain length, which is a typical phenomenon for Fe-based catalysts [12,99,100]. LR-1 demonstrated a similar olefin content to SR-1, which is further evidence to prove the MFEC approach is very successful for FTS in larger diameter reactors. Compared with plain FTS catalyst in SR-1, the hybrid catalysts (SR-2, SR-3, and SR-4) demonstrated lower olefin content. This is because the hydrocracking catalysts provided active protons to terminate the

active olefin components. The olefin content of SR-4 is higher than that of SR-3, due to the dehydrogenation effect of noble metal Pt. The LR-3 is an MFEC counterpart of SR-4. The result in Figure II.11 shows that the olefin content of LR-3 was slightly lower than SR-4. As mentioned above, the space velocity of LR-3 was decreased to increase the CO conversion to a comparable level with SR-4. Therefore, the lower olefin content in LR-3 is probably caused by the lower space velocity of LR-3, which is also consistent with the literature observations [12,101].

II.4 Conclusion

The Cu MFEC structure was evaluated for FTS using a highly active and stable iron-based Fischer-Tropsch synthesis catalyst (Fe-FTS) and various highly active hybrid FTS catalysts. At a CO conversion of 27.7 %, the apparent reaction rate constant of Fe-FTS reached 167 mmol (H_2 + CO)/g_{cat}/h. The catalyst productivity of Fe-FTS was 0.30 gC_5+/g_{cat}/h, which are comparable to those of the most active unsupported Fe-based catalyst. The hybrid catalyst of Fe-FTS and a bifunctional hydrocracking catalyst, i.e., Pt-MAS demonstrated FTS and hydrocracking activities simultaneously. Compared with Fe-FTS, the hybrid catalyst demonstrated a low CO_2 selectivity of 27.7 C-% and high $C_5 – C_{20}$ selectivity of 38.1 C-%. In addition, the MFEC approach enabled FTS to be carried out in a larger tubular reactor (34.0 mm I.D.) without comprising the production rate or selectivity to the desired product. The maximum temperature difference along the radial direction was less than 5 ºC for all the MFEC structures, while the temperature difference for the packed bed tested under the same conditions was around 54 ºC. Moreover, a steady state for the Cu MFEC structure can be reached rapidly compared with a packed bed of the same size. In conclusion, the Cu MFEC approach provides superior thermal management for FTS reaction, and it enables FTS process intensification. When combined with the hybrid

catalyst approach, Cu MFEC approach may provide a unique opportunity to utilize Gas-to-Liquids economically even at small scales.

Chapter III: Microfiber-assisted Direct Synthesis of DME from Syngas

Abstract

The synthesis of dimethyl ether (DME) is an important process to convert syngas into a high value-added chemical with broad applications, such as a diesel fuel alternative, a reaction intermediate for gasoline and diesel fuels formation, an environmentally friendly refrigerant, etc. There are mainly two approaches to synthesize DME from syngas: the two-step indirect synthesis and the one-step direct synthesis. The indirect synthesis process was carried out in two consecutive reaction steps: methanol synthesis and methanol dehydration. The methanol synthesis reaction is subject to an equilibrium limitation. Typically, it requires high pressures and high temperatures to achieve decent per pass conversions and production rates. However, the one-step direct synthesis process could overcome the reaction equilibrium by combining these two reactions to continuously consume the formed methanol in methanol dehydration and push the reaction forward. The problem is that both methanol synthesis (ΔH^0 = -90.8 kJ/mol) and methanol dehydration (ΔH^0 = -23.6 kJ/mol) are highly exothermic reactions. To achieve high conversion and high selectivity in a single reactor, new means of enhancing intra-bed heat transfer are required. In this investigation, a novel catalyst structure, copper microfibrous entrapped catalyst (Cu MFEC) structure, has been applied to handle the added thermal load. In a tubular reactor (34.0 mm I.D.), the direct syngas-to-DME (STD) reaction was carried out by packing with the Cu MFEC structure. The results showed a high per pass conversion (68.8 %) and high DME selectivity (66.6 C%). Meanwhile, the reactor packed with Cu MFEC structure exhibited a radial temperature deviation of 7.5 ºC and maintained a stable temperature profile throughout the entire reaction process. In contrast, the comparable packed bed showed a radial

temperature gradient of 35.5 ºC and a low DME selectivity (50.4 C%). The influences of the H_2:CO ratio, WHSV, and reaction temperature were also investigated. As a result, H_2:CO = 1:1 is the optimized ratio, and WHSV equal to 2.84 h^{-1} could reach a high DME productivity. The optimized reaction temperature is 275 ºC, which offers the highest DME productivity (1.96 $g/g_{catalyst}/h$). This is the first time the Cu MFEC structure has been successfully used to assist the thermal management in the one-step direct STD process.

Keywords: Methanol Synthesis, Methanol Dehydration, Dimethyl Ether (DME), Syngas-to-DME (STD), Microfibrous Entrapped Catalysts (MFEC), Process Intensification (PI)

III.1 Introduction

The accelerating depletion of petroleum and the increasing demand for liquid fuels have drawn tremendous attention to synthetic fuel (synfuel). Typically, synfuel is catalytically converted from syngas that is a mixture of hydrogen and carbon monoxide. Syngas can be produced from natural gas reforming, coal gasification, and biomass gasification. There are two well-known approaches to produce synfuel from syngas: (1) Fischer-Tropsch Synthesis (FTS) and (2) syngas to methanol then methanol to dimethyl ether (DME); in the second approach, the methanol can also be converted to gasoline or diesel [8,11,19,22]. FTS process mainly produces linear paraffins and olefins including liquefied petroleum gas (LPG), gasoline, diesel, and waxes. FTS yields a broad product spectrum, and it requires complex subsequent processes to separate the initial products and upgrade them to meet liquid fuel specifications. For example, the LPG fraction need be sent to a polymerization unit to upgrade the light olefins into gasoline and diesel. The gasoline fraction needs to go through the refining units to increase its octane number. The heavy waxes must be cracked into middle distillates. Contrastingly, the syngas-to-methanol based approach is

simple because it has a narrow product distribution. For instance, syngas-to-DME (STD) process could reach 80 % of DME selectivity [102], and the rest of the products are all in the gas phase except water (under atmospheric pressure and room temperature). Although DME is in gas phase, it can form a liquid phase when pressurized above 0.5 MPa and easily separate from other gas phase products. Therefore, the STD process received considerable attention.

The broad range of applications of DME has made the STD process even more popular [103,104]. As a potential diesel fuel alternative, DME has high cetane value, low auto-ignition temperature, and less toxic emissions. Due to its simple structure (DME only has C-H and C-O bonds; no C-C bonds), DME combustion produces less CO and other partially-combusted emissions. In addition, unlike other ethers, DME does not form explosive peroxides. Hence, it is safe to store and transport. Moreover, DME can be used as an environmentally friendly refrigerant because it does not have the ozone depletion effect. Furthermore, DME is an important reaction intermediate for the famous industrial processes of methanol-to-gasoline (MTG) and methanol-to-olefins (MTO) [8,11,22,105]. The MTG process consists of two reaction steps: methanol dehydration to DME and DME conversion to gasoline. The MTO process is like the MTG: methanol dehydration to form DME is first, then DME is converted to light olefins. These light olefins can be used to continue to synthesize diesel fuels by utilizing the Mobil-Olefins-to-Gasoline-and-Distillate process, or they can be used as raw materials to synthesize polymers. In short, DME is important in the modern chemical industry both as a product and as a reaction intermediate.

DME synthesis can be categorized into two approaches: the two-step indirect synthesis and the single-step direct synthesis [8,102,106,107]. The indirect synthesis process was carried out in two consecutive reaction steps. The indirect synthesis process was carried out in two consecutive

reaction steps. The first reaction step is syngas conversion on metal oxide catalysts, such as $CuO/ZnO/Al_2O_3$ to form methanol through CO hydrogenation (Eq.III.1). The second reaction is that methanol dehydration to produce DME over solid acid catalysts (Eq.III.2), such as γ-Al_2O_3 and zeolites. The first reaction is subject to an equilibrium limitation [8,23], and it is favored at low temperatures (240 – 300 ºC) and high pressures (50 – 200 atm). However, low temperature operation restricts the catalyst activity and volumetric productivity. To solve this issue, a one-step process has been developed. In the 1970s, Haldor-Topsoe [22] successfully combined these two reaction processes, methanol synthesis and methanol dehydration, together into one reaction step using mixed catalysts or bi-functional catalysts. This method consumes methanol for DME synthesis, which breaks the reaction equilibrium of methanol synthesis and greatly moves the reaction forward. It turns out that the one-step reaction can reach high CO conversion (more than 80 %) even at a low reaction pressure. The Water-Gas-Shift (WGS) reaction (Eq.III.3) occurs as a side reaction, which is an unavoidable reaction that always occurs with the methanol synthesis reaction. The overall reaction is listed in Eq.III.4 by combining the above three reactions (Eq.III.1 – Eq.III.3).

Methanol Synthesis: $CO + 2H_2 \leftrightarrow CH_3OH$ $\Delta H^0 = -90.8$ kJ/mol (Eq.III.1)

Methanol Dehydration: $2CH_3OH \leftrightarrow CH_3OCH_3 + H_2O$ $\Delta H^0 = -23.6$ kJ/mol (Eq.III.2)

Water-Gas-Shift Reaction: $CO + H_2O \leftrightarrow CO_2 + H_2$ $\Delta H^0 = -41.1$ kJ/mol (Eq.III.3)

Overall Reaction: $3CO + 3H_2 \rightarrow CH_3OCH_3 + CO_2$ $\Delta H^0_{net} = -246.3$ kJ/mol (Eq.III.4)

As we can see from Eq.III.1 to Eq.III.3, all three reactions are highly exothermic. If we combined these three reactions, the total net reaction enthalpy reaches -246.3 kJ/mol. This means

that a tremendous amount of heat will be generated during the STD reaction process. In addition, the product selectivity and catalyst activity and lifetime are highly depended on the reaction temperature. Therefore, thermal management is a key issue for the STD process to avoid temperature overshoot and reaction runaway. Conventionally, fixed-bed is a commonly used reactor system due to its simplicity and low cost. However, for the highly exothermic reactions like STD, the poor heat transfer performance of fixed-bed generated various problems. The main problem is the thermodynamic limitation and rapid catalyst deactivation. In industry, a common solution is to increase syngas recycle rate to increase heat convection. This results in a low CO conversion as well as high capital expenditure (CAPEX) and operating expense (OPEX). To address this issue, fluidized-bed reactors and slurry reactors draw people's attention. They have their advantages and disadvantages. For instance, a fluidized-bed reactor has excellent heat transfer ability and can easily remove the reaction heat from the reactor and maintain a stable reaction temperature. However, it requires catalysts with good mechanical strength and complicated downstream recovery processes [13,108,109]. The slurry reactor has been known as a potential reactor system for industrial scale DME production owing to the high thermal conductivity of the well-mixed liquid phase. Meanwhile, syngas must be transferred to a liquid phase solvent first, then to catalyst particles mixed in the liquid solvent. This causes severe limitations in mass transfer and leads to decreases in the reaction rate. Moreover, catalyst attrition and product separation is another serious issue, especially for small size catalyst particles [103,110,111].

To deal with these issues, our group developed a novel reactor system called microfibrous entrapped catalyst (MFEC) structure which is now commercially available at IntraMicron Inc. MFEC is a catalyst structure that consists of a highly porous network made of micron-sized

metal fibers with high thermal conductivity and small catalyst particles entrapped inside [68–71,112]. MFEC reactor system is based on fixed-bed operation. Hence, it has many advantages of fixed-bed, such as simple operation, low CAPEX & OPEX, easy catalyst separation, scalable to small or modular designs, etc. However, MFEC reactor system is different from fixed-bed system because it overcomes many disadvantages of fixed-bed. For instance, MFEC structure significantly reduces pressure drop compared with traditional fixed-bed because of its high void volume (70 - 80 %). Since small particles are used, intra-particle heat transfer and mass transfer are greatly enhanced in MFEC structure, and an uniform particle distribution is achieved. Furthermore, MFEC structure can be used for pre-manufactured catalyst particles, which greatly extends its application to many heterogeneous reactions. Previous efforts show that the MFEC structure can be widely used in various fields. For example, Yang et al. used the MFEC structure to increase external mass transfer in desulfurization [74,75]. Zhu et al. demonstrated the electrical conductivity of microfibrous metal structure in fuel cell [76,77]. Gu et al. investigated the pressure drop of the MFEC filter [78]. Sheng et al. simulated and measured the thermal properties of MFEC structure and carried out the highly exothermic reaction of Fischer-Tropsch Synthesis (FTS) in copper MFEC structure [49,54,79]. According to Sheng et al.'s investigation, the radial thermal conductivity of Cu MFEC was 56 times that of a traditional packed bed with a similar packing property (~ 20 vol% of catalyst). Meanwhile, the inside wall heat transfer coefficient was 10 times more. With Cu MFEC structure, the FTS run showed a stable temperature profile, and the maximum temperature deviation was 6.4 ºC. In contrast, the comparable traditional fixed-bed had a maximum temperature deviation of 460 ºC and completely ignited the reaction. Based on that, Cheng et al. applied Cu MFEC structure in a process intensified reaction of FTS and hydrocracking to handle the added thermal load. It turns out that Cu MFEC structure is highly

effective in maintaining a stable reaction temperature. Therefore, Cu MFEC structure is a promising alternative to the traditional fixed-bed system for highly exothermic reactions.

Based on these previous achievements in the application of MFEC structure, a Cu MFEC structure was employed in the STD process to address the added thermal load from the process intensification of methanol synthesis and methanol dehydration reactions into one-step. As mentioned above, both methanol synthesis (ΔH^0 = -90.8 kJ/mol) and methanol dehydration (ΔH^0 = -23.6 kJ/mol) reactions are highly exothermic reactions, like FTS (ΔH^0 = -165.0 kJ/mol) and hydrocracking. Therefore, we expect Cu MFEC structure will also work on the STD process quite efficiently. A physically mixed catalyst, methanol synthesis catalyst mixed with methanol dehydration catalyst, was entrapped in Cu MFEC structure to produce DME from syngas. The experiments were carried out in a large tubular reactor (34.0 mm I.D.) packed with small catalyst particles (80 – 140 mesh). There was a four-point thermocouple in the radial direction to directly record the radial temperature distribution profiles during the reaction. Using these profiles, the actual inside wall heat transfer coefficient can be calculated and compared with the simulated value. This reactor system was based on the fixed-bed system, but due to the high voidage of MFEC structure, it doesn't experience the severe pressure drops usually encountered in small particle packed beds. The natural of Cu MFEC structure also assures a significant enhancement in intra-bed heat transfer that helps maintain a stable reaction temperature. The experimental results showed that, under similar reaction conditions, the Cu MFEC bed demonstrated an extremely low radial temperature gradient (7.5 ºC). It also ended up with a high DME selectivity under a high CO conversion. However, the comparable packed bed experienced temperature overshoot (35.5 ºC), produced more methane and other side products (C_2 – C_4), and deactivated

catalysts quickly. This is the first time that Cu MFEC structure has been applied to the STG process.

III.2 Experiment

III.2.1 Catalysts Preparation

In the STD process, two kinds of catalysts have been used, and both are commercially available. HiFuel@R120 was used as the methanol synthesis catalyst and was directly purchased from Alfa Aesar; this catalyst was crushed and sieved to 80 – 140 mesh. The methanol dehydration catalyst was γ-Al_2O_3 (Alfa Aesar, #43832). Before use, the γ-Al_2O_3 pellets were crushed and screened to 80 – 140 mesh then calcined at 500 ºC for 10 hours. After that, the calcined γ-Al_2O_3 particles were physically mixed with the same size HiFuel@R120 particles in a mass-based ratio of 2:1.

III.2.2 Cu MFEC Fabrication

A wet-lay paper-making technique was used to fabricate Cu microfibrous media. The detailed process can be found in the literature [53,79,113]. Typically, raw Cu microfibers and cellulose fibers were mixed in a blender with a large amount of water. The resulting mixtures were cast into a paper-making die. A preformed Cu microfibrous sheet was formed by quickly removing the water. A two-sided sheet was prepared by overlaying two pieces of performed sheets fabricated from different diameters of raw Cu microfibers. Usually, the top layer was made from 12 μm Cu microfibers, and the bottom layer was from 6 μm Cu microfibers (IntraMicron, Auburn, AL, USA). After that, the preformed two-sided sheet was dried, then the dried sheet was pre-oxidized in flowing air at 500 ºC for 30 min to remove the cellulose. Afterward, the pre-oxidized sheet was sintered in flowing hydrogen at 700 ºC for 60 min to form the conjunctions between Cu

microfibers. These conjunctions composed a sinter-locked network through the Cu microfibrous medium, which greatly enhanced its heat transfer performance. The resulting Cu microfibrous medium has a fluffy top layer and compact bottom layer, which is owing to the different diameters of raw Cu microfibers. This kind of two-sided design enable catalyst particles with certain sizes can be easily loaded into the top layer, and the bottom layer used to prevent the loaded particles from leaking out.

III.2.3 Characterization

The morphologies of Cu MFEC structure before and after catalyst loading were characterized on a JEOL JSM-7000F scanning electron microscope (SEM). Quantachrom Autosorb-iQ was used to record N_2 adsorption/desorption isotherms at -196 ºC. Before the measurement, samples were degassed at 200 ºC with N_2 flow overnight. The total surface areas were calculated via the Brunauer-Emmett-Teller (BET) equation.

III.2.4 Packing Reactors

There were two types of tubular reactors used: 9.0 mm I.D. small reactor and 34.0 mm I.D. large reactor. The small reactor was only used with traditional packing material, while the large reactor was used both with traditional packing material and an MFEC structure. As Figure III.1 shows, the bottom zone was packed with Raschig rings. The middle zone was the active zone and packed with mixed catalysts in a mass ratio of Hifuel@R120: calcined γ-Al_2O_3 = 2:1. The top zone was a pre-heating zone packed with Cu microfibrous media that did not contain catalysts.

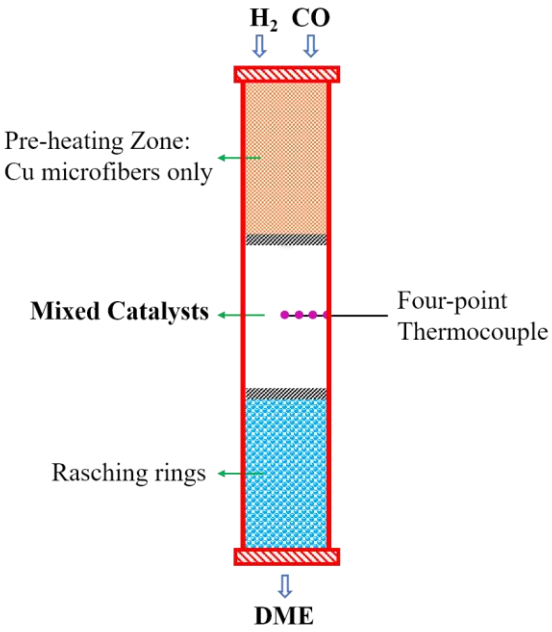

Figure III.1 The scheme of the DME reactor system

To prepare the Cu MFEC structure, circular disks with a diameter of 36.0 mm were punched from the sintered Cu microfibrous media. Then, the catalyst particles (80 – 140 mesh) were entrapped into the punched disks to form Cu MFEC. After that, the Cu MFEC was packed into the large reactor, piece by piece. It must be noted that the disk size (36.0 mm) was 6 % larger than the inside diameter of the large reactor (34.0 mm); this provides a tremendous number of contact points between the Cu microfibers and the reactor inside wall. Previous experience has shown that this could significantly increase the inside wall heat transfer coefficient. A comparable packed bed (34.0 mm I.D.) was diluted to the same packing density as the Cu MFEC structure by utilizing glass beads (80 – 140 mesh).

III.2.5 Reaction Apparatus

Figure III.2 shows the schematic of the reaction apparatus. There is a pre-heater installed before the reactor used to mix and pre-heat the inlet gases. A pressure transmitter was set right after the

pre-heater and followed up with the major reactor. A back-pressure regulator was installed after the reactor to control the system pressure. The outlet stream went through a hot trap (150 ºC) then a chiller to cool down the fluid. Between the hot trap and the chiller, there is bypass directly connected with an online gas chromatograph (GC, Agilent 6890) to take samples. A cold trap (2 ºC) followed the chiller to collect liquid products. The online GC was equipped with a packed column (Hayesep-DB 100/120). A thermal conductivity detector (TCD) was used to measure the concentrations of H_2, N_2, CO, CO_2, DME, and $C_1 - C_4$ using nitrogen as the internal standard. In the same GC, a flame ionization detector (FID) armed with a capillary column (DB-5) was used offline to analyze the liquid products.

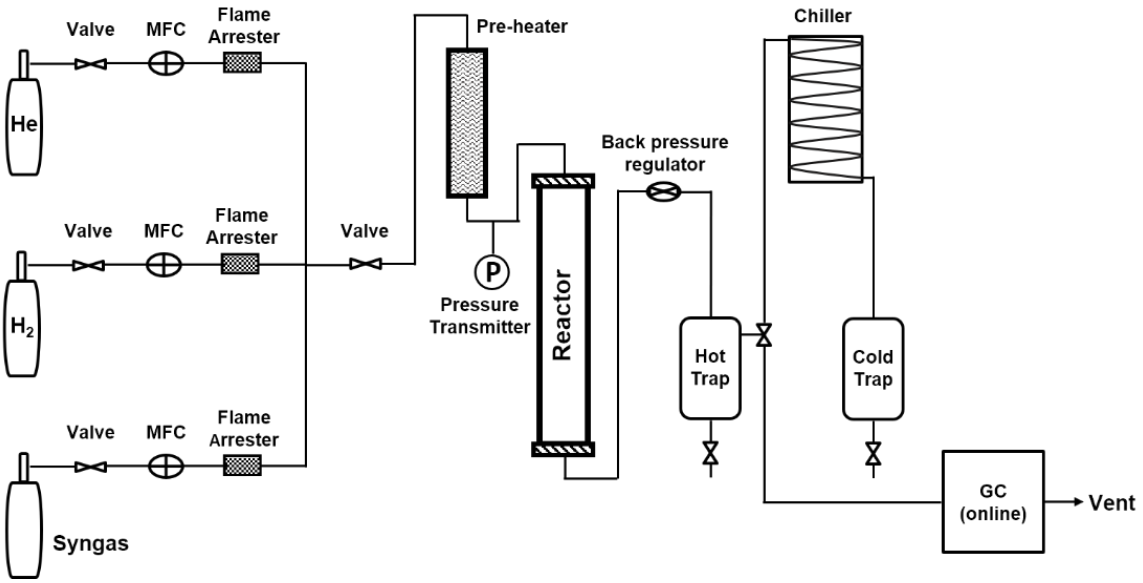

Figure III.2 The schematic of STD reaction apparatus

III.2.6 STD Reaction Operation

The mixed catalysts were pre-activated in situ under flowing ultra-high purity hydrogen (Airgas, HY UHP300) following a temperature program. For the temperature program, the flow was first heated to 130 ºC and hold for 2 hours. Then, the temperature was slowly increased to 280 ºC for

another 10 hours. Lastly, the temperature was gradually increased to 380 ºC for 4 hours. After the temperature program, the catalysts were cooled to 260 ºC, and hydrogen was switched to syngas to initiate STD reactions. A typical experiment was carried out at 30 atm using a syngas with an H_2/CO ratio of 1:1 to slowly build the pressure. The syngas mixture was directly purchased from Airgas with 2.0 vol% nitrogen as the internal standard. There were two reactors used: 9.0 mm I.D. small reactor (SR) and 34.0 mm I.D. large reactor (LR). The small reactor only used as packed beds (PB), but the large reactor used as both packed beds and the Cu MFEC structure (MFEC). In this paper, all experiments have been named as X@Y-#; X denotes the reactor size (SR or LR), Y stands for the reactor type (PB or MFEC), and # represents the experimental number. For instance, if the small reactor was operated as a packed bed, it will be named SR@PB-#. If the large reactor has been packed with the Cu MFEC structure, then it will be named LR@MFEC-#.

III.3 Results and Discussion

III.3.1 Catalysts Characterization

Table III.1 Nitrogen sorption data

Sample	BET Surface Area (m^2/g)	Pore Volume (cm^3/g)
HiFuel@R120	78	0.20
Calcined γ-Al_2O_3	233	0.77
Mixed Catalyst *	130	0.39

* For mixed catalyst, the BET surface area, and pore volume were calculated the two mixed components based on a mass ratio of HiFuel@R120:Calcined γ-Al_2O_3 = 2:1.

In this investigation, a commercial catalyst HiFuel@R120 has been used as the methanol synthesis catalyst and a calcined γ-Al_2O_3 as the methanol dehydration catalyst. The catalyst for

the one-step STD reaction was a physical mixing of HiFuel@R120 and γ-Al_2O_3 in a 2:1 mass ratio. HiFuel@R120 is a well know methanol reforming catalyst that was developed by Johnson Matthey. This is a CuO/ZnO/Al_2O_3 based catalyst; its detailed compositions can be found in the literature [114]. The BET surface areas of HiFuel@R120 and γ-Al_2O_3 were measured by N_2 adsorption (Figure III.3). As we can see from Table III.1, HiFuel@R120 has a relatively low surface area (78 m^2/g) and pore volume (0.20 cm^3/g). This is mainly due to its composition nature: 64.1 wt% CuO, 24.4 wt% ZnO, and 9.7 wt% Al_2O_3. The calcined γ-Al_2O_3 has a relatively high surface area (233 m^2/g) and pore volume (0.77 cm^3/g); a theoretical BET surface area and pore volume of the mixed catalyst were calculated by taking an average value of HiFuel@R120 and calcined γ-Al_2O_3 based on the mixed ratio (Table III.1). The mixed catalyst showed an average BET surface area of 130 m^2/g and pore volume of 0.39 cm^3/g.

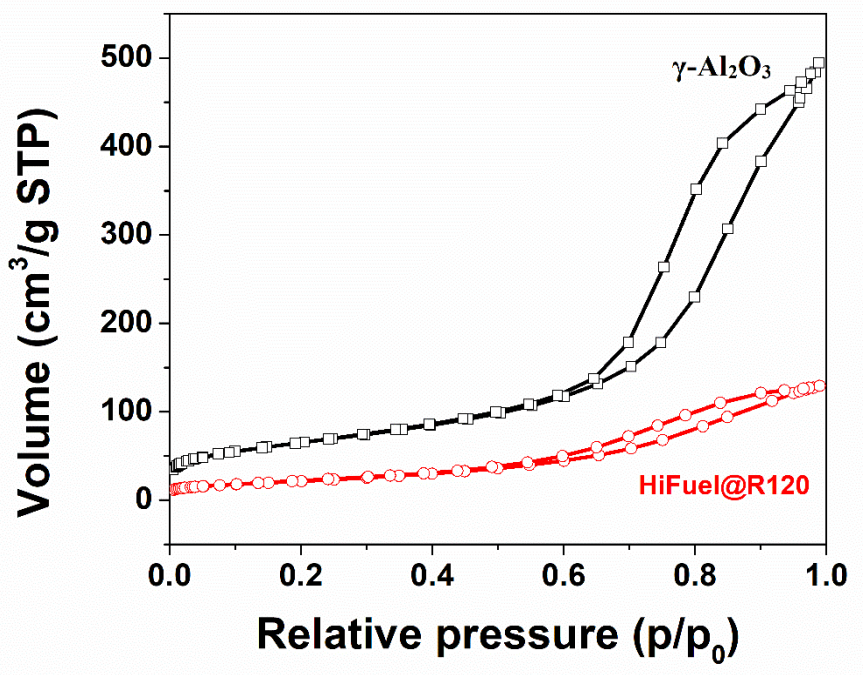

Figure III.3 N_2 adsorption/desorption isotherms of HiFuel@R120 and calcined γ-Al_2O_3

III.3.2 Reaction Activity and Selectivity

III.3.2.1 H_2:CO Ratio

Table III.2 STD reaction data with different H_2:CO ratio in a small reactor (9.0 mm I.D.)

Experiment	SR@PB-1	SR@PB-2	SR@PB-3
H_2:CO Ratio	1:1	2:1	3:1
GHSV / h^{-1}	1000	1500	2000
CO Conv. (%)	79.0	83.3	87.2
H_2 Conv. (%)	75.5	48.9	32.8
Carbon balance*, C%			
CO	21.0	16.7	12.8
CH_3OH	0.0	0.0	0.0
DME	51.4	56.3	60.8
CO_2	26.9	25.2	24.4
CH_4	0.2	0.9	1.2
C_2H_6	0.2	0.2	0.1
C_3H_8	0.2	0.2	0.2
C_4H_{10}	0.1	0.5	0.5
$C_5 – C_{10}$	0.0	0.0	0.0

* The carbon balance data were based on carbon atoms, not the product selectivity

Three experiments were designed to determine the optimized H_2:CO ratio. In a small packed bed (9.0 mm I.D.), 4.0 g of mixed catalysts (HiFuel@R120:γ-Al_2O_3 = 2:1 in mass) were packed without dilution. The H_2:CO ratio was adjusted by increasing H_2 flow rate and keeping CO flow rate constant. As can be seen in Table 2, SR@PB-1 used a syngas with an H_2:CO = 1:1; the H_2:CO ratio in SR@PB-2 and SR@PB-3 were 2:1 and 3:1, respectively. All of these reactions were operated using the same pressure (30 atm) and reaction temperature (260 ºC). Table III.2

shows that the CO conversion slowly increased from 79.0 % to 87.2 % as the H_2:CO ratio increased from 1:1 to 3:1. Meanwhile, the DME selectivity also slowly increased as the H_2:CO ratio increased. However, the H_2 conversion sharply decreased from 75.5 % to 32.8 % as the H_2:CO ratio increased. For example, when the H_2:CO ratio was 2:1, the H_2 conversion was around 50 % which means there was only half of H_2 was reacted. When H_2:CO ratio increased to 3:1, the H_2 conversion was around 1/3 which means there was only 1/3 of H_2 consumed. Therefore, we could estimate the actual reacted H_2:CO ratio was around 1:1.

In the STD process, the major reactions were Eq.III.5 and Eq.III.6:

$$CO + H_2 = CH_3OH \qquad \text{(Eq.III.5)}$$

$$2\,CH_3OH = CH_3OCH_3 + H_2O \qquad \text{(Eq.III.6)}$$

This is based on the fact that the selectivity of CH_3OH was zero (Table III.2); this means all the produced CH_3OH was consumed in methanol dehydration. Hence, the net reaction of these two major reactions was:

$$2\,CO + 4\,H_2 = CH_3OCH_3 + H_2O \qquad \text{(Eq.III.7)}$$

As we mentioned above, the WGS reaction is an inevitable side reaction:

$$CO + H_2O = CO_2 + H_2 \qquad \text{(Eq.III.8)}$$

According to the product distribution in Table III.2, other side reactions occurred as listed in Eq.III.9 – Eq.III.12:

$$CO + 3\,H_2 = CH_4 + H_2O \qquad \text{(Eq.III.9)}$$

$$2\,CO + 5\,H_2 = C_2H_6 + 2\,H_2O \qquad \text{(Eq.III.10)}$$

$$3\,CO + 7\,H_2 = C_3H_8 + 3\,H_2O \qquad \text{(Eq.III.11)}$$

$$4\,CO + 9\,H_2 = C_4H_{10} + 4\,H_2O \qquad \text{(Eq.III.12)}$$

Since the selectivities of all the products were determined by GC, we could perform mass balance calculations for CO, H_2, and H_2O to determine the overall reaction equation. For SR@PB-1, assume 100 mol of CO and 100 mol of H_2 were added into the reactor; 79.0 mol of CO was reacted, and 21.0 mol of CO was unreacted. As shown in Table III.3, the total amount of reacted and produced H_2 were 104.6 mol and 26.9 mol, respectively. Hence, the net reacted H_2 was 77.7 mol, but the actual reacted H_2 that was calculated from H_2 conversion was 75.5 mol. Apparently, there are errors between the actual reacted H_2 and calculated value. This is because H_2 molecular weight is low, and its TCD signal is not strong. This resulted in a relatively small correction factor, and its error is relatively larger than other heavy compounds. The reacted H_2O (26.9 mol) was slightly higher than the produced H_2O (26.4 mol), resulting in a negative value of net produced H_2O (-0.5 mol); this also contains errors. In short, the net produced H_2O was around zero. If all the minor reactions (from Eq.III.9 to Eq.III.12) were neglected, the net reaction should be Eq.III.13 since there was no water accumulated.

$$3\,CO + 3\,H_2 = CH_3OCH_3 + CO_2 \qquad \text{(Eq.III.13)}$$

$$3\,CO + 3.22\,H_2 = 1.04\,CH_3OCH_3 + 0.93\,CO_2 + 0.11\,H_2O \qquad \text{(Eq.III.14)}$$

$$3\,CO + 3.42\,H_2 = 1.07\,CH_3OCH_3 + 0.86\,CO_2 + 0.21\,H_2O \qquad \text{(Eq.III.15)}$$

Table III.3 A complete mass balance calculation for all the reactions in the STD process

Experiment		SR@PB-1	SR@PB-2	SR@PB-3
CO Balance [a]	Reacted CO	79.0	83.3	87.2
	Unreacted CO	21.0	16.7	12.8
H_2 Balance [b]	Reacted H_2	104.6	117.4	127.0
	Produced H_2	26.9	25.2	24.4
	Net Reacted H_2	77.7	92.2	102.6
	Actual Reacted H_2	75.5	97.8	98.4
H_2O Balance [c]	Produced H_2O	26.4	30.0	32.4
	Reacted H_2O	26.9	25.2	24.4
	Net Produced H_2O	-0.5	4.8	8.0

[a] The reacted CO was calculated from CO conversion that was directly determined by GC, and the unreacted CO was calculated by subtracting the reacted CO from 100;

[b] The reacted H_2 was calculated from all the reactions that consume H_2 (Eq.III.7, Eq.III.9 – Eq.III.12), the produced H_2 was calculated from the WGS reaction (Eq.III.8), the net reacted H_2 was calculated by subtracting the produced H_2 from the reacted H_2, and the actual reacted H_2 was calculated from H_2 conversion which directly measured by GC;

[c] The produced H_2O was calculated from all the reactions that generated H_2O (Eq.III.7, Eq.III.9 – Eq.III.12), the reacted H_2O was calculated from WGS reaction (Eq.III.8), and the net produced H_2O was calculated by subtracting the reacted H_2O from the produced H_2O.0

The above reaction data proved that the theoretical reaction ratio of H_2:CO should be 1:1 when the feeding stream of H_2:CO ratio is 1:1. When the feeding stream of H_2:CO ratio was increased to 2:1 or 3:1, we could still carry a similar calculation. For instance, assume 100 mol of CO and 200 mol of H_2 were put into SR@PB-2, and 100 mol of CO and 300 mol of H_2 were added into SR@PB-3. The results in Table 3 showed that the net reacted H_2 matched with the actual reacted H_2 by ignoring minor errors in both SR@PB-2 and SR@PB-3. However, there was a small amount of H_2O accumulated in both reaction processes, and the accumulated H_2O mass was slightly increased from 4.8 mol to 8.0 mol as the H_2:CO ratio increased from 2:1 to 3:1. Similarly, if all the minor reactions (from Eq.III.9 to Eq.III.12) were neglected, the net reaction should be Eq.III.14 and Eq.III.15 for SR@PB-2 and SR@PB-3 respectively.

The above calculation shows that the theoretical H_2:CO ratio is around 1.1:1 when the feeding stream of H_2:CO ratio is 2:1 or 3:1, which is approaching to the 1:1 ratio. According to the literature [115,116], the H_2:CO ratio near 1:1 results in optimal DME productivity and materials utilization. We could conclude that the process intensified STD process is suitable for syngas from biomass or coal gasification, which usually have a lower H_2:CO ratio (0.6 –1.0). This is mainly because of the WGS reaction, since this reaction could consume CO and produce H_2. By doing that, the H_2:CO ratio has been adjusted.

III.3.2.2 GHSV

Table III.4 STD reaction data with a different syngas flow rate in a small reactor (9.0 mm I.D.)

Experiment [a]	SR@PB-1	SR@PB-4	SR@PB-5	SR@PB-6
GHSV (h^{-1})	1000	1500	2000	2500
WHSV (h^{-1})	1.42	2.13	2.84	3.55
CO Conv. (%)	79.0	78.3	68.9	54.6
H_2 Conv. (%)	75.5	75.0	62.1	43.8
Product Selectivity (C%)				
CH_3OH	0.0	0.0	0.0	0.0
DME	65.0	65.4	65.1	65.2
CO_2	34.0	33.7	34.2	34.1
CH_4	0.2	0.2	0.1	0.1
$C_2 – C_4$	0.8	0.7	0.6	0.6
$C_5 – C_{10}$	0.0	0.0	0.0	0.0
DME Productivity ($g/g_{catalyst}/h$) [b]	1.07	1.61	1.88	1.86

[a] All the experiments in Table III.4 were operated at 260 ºC, 30 atm, and H_2:CO = 1:1.

[b] The DME productivity was calculated from the equation of DME productivity = [WHSV x (CO concentration) x (CO conversion) x (DME selectivity) x (Molecular weight of DME)]/(Standard molar volume), and the catalyst weight was based on Hifuel@R120.

The experimental results in Table III.4 demonstrated a constant H_2:CO = 1:1, but a changing GHSV through adjusting the syngas flow rate. As the GHSV increased from 1000 – 2000 h^{-1}, DME productivity increased from 1.07 to 1.88 $g/g_{catalyst}/h$. However, further increased the GHSV to 2500 h^{-1} led to a decrease in DME productivity. Hence, GHSV = 2000 h^{-1} or WHSV = 2.84 h^{-1} is an optimized flow rate that offers the highest DME productivity. Considering SR@PB-5 has a high single pass conversion (68.9 %), high DME selectivity (65.1 C%), and high DME productivity (1.88 $g/g_{catalyst}/h$), which made the STD process in a benefit position in synfuel production.

III.3.2.3 Reaction Temperature

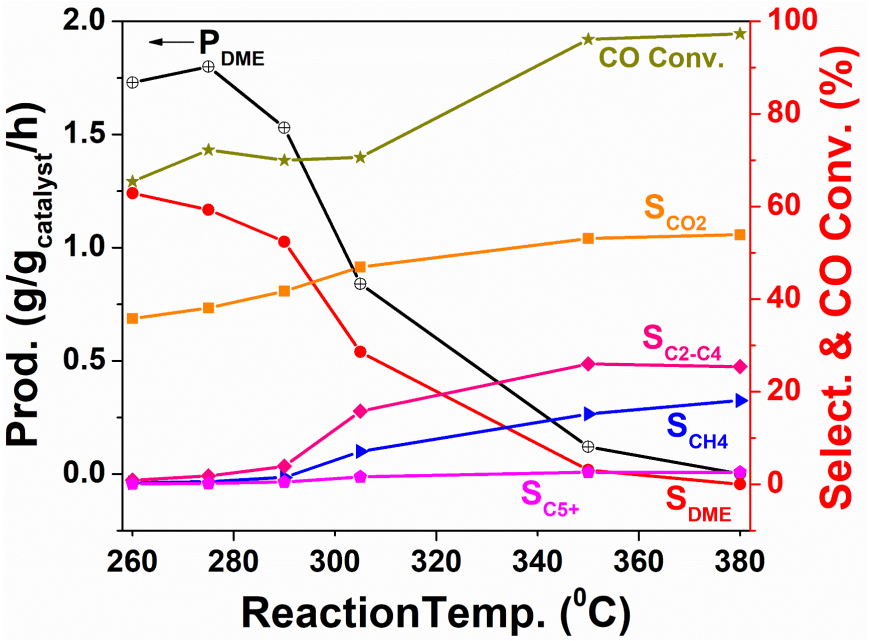

Figure III.4 The product selectivity and DME productivity change with the reaction temperature*

* All the experiments in Figure III.4 were carried out at 30 atm, WHSV = 2.84 h^{-1}, and H_2:CO = 1:1. 1.5 g of mixed catalyst (HiFuel@R120:γ-Al_2O_3 = 2:1 in mass, 80 – 140 mesh) diluted with the same size glass beads (33.1 vol% of the mixed catalyst) were packed into a small reactor (9.0 mm I.D.).

Considering packed bed has poor thermal management ability and might experience temperature overshoot, or formation of hotspots even for a small reactor. Hence, a small packed bed (9.0 mm

I.D.) was diluted with glass beads to reduce its exothermicity. Then, the diluted small packed bed was used to determine the effects of reaction temperature. As can be seen from Figure III.4, the CO conversion increased as the reaction temperature rose from 260 ºC to 275 ºC. Meanwhile, the DME productivity also increased. However, when the reaction temperature further increased to 290 ºC, both the CO conversion and DME productivity slightly dropped. In the meantime, the selectivity of undesired side products (CH_4 and $C_2 – C_4$) increased. If continue rose the reaction temperature, the DME selectivity and productivity significantly decreased. Eventually, the methanation reaction and other side reactions start to become the major reactions when the reaction temperature reached 350 ºC or higher. Therefore, maintaining an appropriate reaction temperature is important for decent DME selectivity and productivity. Based on the above experimental results, 275 ºC is an appropriate reaction temperature for the STD process, because it offers the highest DME productivity.

III.3.2.4 Reactor Size & Type

The above results show that a high single pass conversion and high DME productivity was attained when operated at 275 ºC with a WHSV = 2.84 h^{-1} in the small reactor (9.0 mm I.D.). By keeping the same reaction conditions (reaction temperature and WHSV), a large reactor (34.0 mm I.D.) was used to scale-up the STD process. As Table III.5 shows, the CO conversion of LR@PB (70.1 %) was slightly lower than the CO conversion of SR@PB-7 (72.2 %). Also, the DME selectivity of LR@PB (50.4 C%) was lower than the DME selectivity of SR@PB-7 (59.3 C%). This is because the large packed bed has poor heat transfer ability, which led to significant temperature overshoot. The highest temperature overshoot in the radial direct was 35.5 ºC when operated at 275 ºC (Table III.5). However, a comparable reactor was packed with Cu MFEC structure and all other reaction conditions were kept unchanged (LR@MFEC). It resulted in a

high DME selectivity (66.6 %) and high DME productivity (1.96 $g/g_{catalyst}/h$). When compared with LR@PB, the CO conversion in LR@MFEC was slightly decreased. This is because the LR@MFEC reactor maintained a stable reaction temperature, and the highest temperature deviation was 7.5 ºC. Hence, the real reaction temperature inside the LR@MFEC reactor was much lower than the real reaction temperature inside the LR@PB reactor. A high reaction temperature could increase the CO conversion.

Table III.5 STD reaction data with different reactor size and type

Experiment *	SR@PB-7	LR@PB	LR@MFEC
Reactor Type	PB	PB	Cu MFEC
Reactor I.D. (mm)	9.0	34.0	34.0
T deviation (ºC)	6.1	35.5	7.5
CO Conv. (%)	72.2	70.1	68.8
H_2 Conv. (%)	65.1	63.3	60.6
Product Select. (C%)			
CH_3OH	0.0	0.0	0.0
DME	59.3	50.4	66.6
CO_2	38.1	43.3	32.9
CH_4	0.6	1.6	0.1
$C_2 – C_4$	1.8	4.1	0.4
$C_5 – C_{10}$	0.2	0.6	0.0
DME Productivity ($g/g_{catalyst}/h$)	1.80	1.51	1.96

* All the experiments in Table III.5 were carried out at 275 ºC, WHSV = 2.84 h^{-1}, 30 atm, and H_2:CO = 1:1. SR@PB-7 was packed with 1.5 g of mixed catalyst (HiFuel@R120:γ-Al_2O_3 = 2:1 in mass, 80 – 140 mesh) in a small reactor (9.0 mm I.D.), and diluted with the same size glass beads (33.1 vol% of the mixed catalyst); LR@PB was packed with 21 g of the same mixed catalyst into a 34.0 mm I.D. reactor, and kept a similar volume percentage of the mixed catalyst (33.4 vol%) as in SR@PB-7; LR@MFEC was packed with the same amount of mixed catalyst (21 g) as in LR@PB but packed with Cu MFEC structure, and kept the same volume percentage (33.4 vol% of the mixed catalyst and 10.9 vol% of Cu fibers).

As we mentioned before, the temperature overshoot increased the selectivity of undesired side products, such as CH_4 and $C_2 – C_4$. Without an efficient way to transfer out the reaction heat in time, eventually the major product will be undesired side products $C_1 – C_4$. Hence, the reaction temperature of STD must be carefully controlled in order to receive a high DME selectivity and productivity. With the assistance of Cu MFEC structure, we achieved a high DME selectivity (66.6 %) and productivity (1.96 $g/g_{catalyst}/h$) under a high per pass conversion (68.8 %). This was due to the high inside wall heat transfer coefficient of Cu MFEC structure, which greatly enhanced the intra-bed heat transfer and maintained a stable reaction temperature. Based on the above reaction data, we can draw a conclusion that Cu MFEC structure has been successfully used to scale-up the STD process. It was estimated that Cu MFEC structure could enable the direct STD process to operate at a tubular reactor diameter of 6" without compromising DME selectivity and productivity.

III.3.3 Temperature Profile

The radial temperature profiles were recorded for all the experiments that were carried out in the large reactor (34.0 mm I.D.), through a 4-point thermocouple in the radial direction. As shown in Figure III.5, LR@PB demonstrated a sharp rise in temperature when the reaction started. After reaching a certain point, the temperature profile stays relative stable, but the average reaction temperature inside the reactor was much higher than the set temperature (275 ºC). The highest temperature deviation was 35.5 ºC which is at centerline. However, the experiment packed with Cu MFEC structure (LR@MFEC) showed a stable temperature profile throughout the entire reaction processes. The highest temperature deviation was 7.5 ºC (Table III.5), which is much lower than in the traditional packed bed (LR@PB). This is mainly because of the Cu MFEC structure that can highly efficiently transfer the generated heat out of the reactor and maintain a

stable reaction temperature inside the reactor. Moreover, a longer bed life can be expected for the reactor equipped with Cu MFEC structure since a higher temperature will accelerate coke formation and deactivate the mixed catalysts. It must be noted that the scale-up data are based on a 34.0 mm I.D. tubular reactor, which is an acceptable lab scale reactor, but a larger diameter reactor (6" I.D.) could be used according to our estimation. As the reactor size increases, the thermal effects become more significant. When the temperature reaches a certain point, eventually the reaction will experience thermal runaway and produce mostly undesired side products. Therefore, Cu MFEC structure provides a highly efficient way to handle the highly exothermic process intensified STD process.

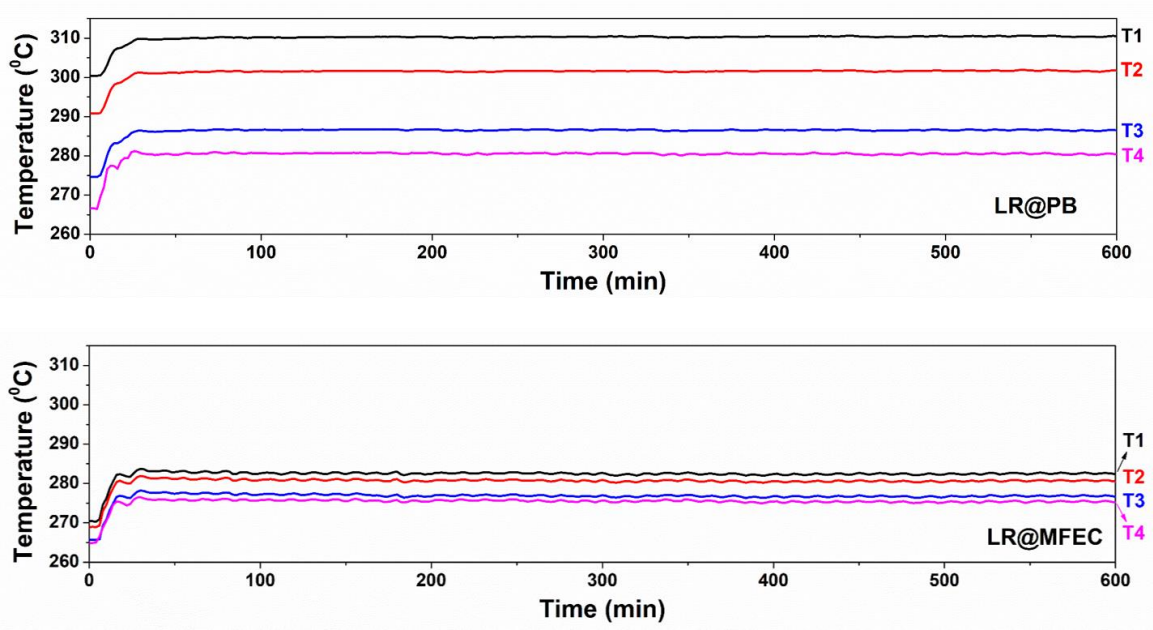

Figure III.5 Radial temperature profiles in the large reactor: T1 to T4 are temperature points started from centerline to the inside wall temperature, and the interval between each point is 10.0 mm, 5.0 mm, and 2.0 mm, respectively

III.4 Conclusion

The process intensified STD process has been carried out in two reactors of different size: a small reactor (9.0 mm I.D.) and a large reactor (34.0 mm I.D.). The small reactor was used to determine the influences of H_2:CO, GHSV/WHSV, and reaction temperature. The results showed that an optimized H_2:CO is 1:1, and a high CO conversion (68.9 %) and high DME productivity (1.88 $g/g_{catalyst}/h$) were achieved when GHSV equal to 2000 h^{-1} (WHSV = 2.84 h^{-1}) was used. A higher reaction temperature would end up with a lower DME selectivity and productivity, and 275 ºC is an optimized reaction temperature. The large reactor was used to scale-up the direct STD process; it turns out the packed bed experienced a high temperature overshoot (35.5 ºC) and led to a low DME selectivity (50.4 C%). However, when Cu MFEC structure was used to carry out the scale-up experiments, it showed a low temperature deviation (7.5 ºC) and a high DME selectivity (66.6 C%). This significant difference in temperature control between Cu MFEC structure and the traditional packed bed was only shown on a lab acceptable level (34.0 mm I.D. tubular reactor); the difference could go much higher if a larger diameter tube (ca. 6" I.D.) was used. As the temperature overshoot become more significant, eventually the side reactions will become dominate reactions, and the STD reaction will completely runaway and no DME was produced. Also, the highest DME productivity (1.96 $g/g_{catalyst}/h$) was achieved with the assistance of Cu MFEC structure. In conclusion, the one-step STD process has been successfully scaled-up by using the Cu MFEC structure in enhancing heat transfer and resulting in high reaction activity and productivity.

Chapter IV: Process Intensified Direct Production of Gasoline from Syngas

Abstract

Syngas-to-Gasoline (STG) is an important process to convert syngas into gasoline at a high yield and a high selectivity. Conventional STG process is operated in three consecutive, separate and highly exothermic steps: methanol synthesis from syngas, methanol dehydration to dimethyl ether, and dimethyl ether conversion to gasoline. Each step requires its reactor systems, product separation systems, recycle loops, etc. Among these steps, methanol synthesis has high costs because it is operated under equilibrium limitation, and requires high pressures and high temperatures to achieve decent per pass conversions and production rates. This paper, as a process intensification endeavor to overcome the equilibrium limitation of methanol synthesis and significantly reduce capital and operational expenditures (CAPEX and OPEX), examines the opportunity to integrate these three reaction steps into a single reaction vessel. A single tubular reactor with 3 reaction zones has been built and tested at lab scales. This single vessel STG (SV-STG) demonstrated a high gasoline selectivity of 74.8 wt% at a single pass CO conversion of 78.3 % in a small tubular reactor (9.0 mm I.D.); these values are comparable to those obtained in traditional STG processes. Moreover, Cu Microfibrous Entrapped Catalysts (Cu MFEC) structure with high effective radial thermal conductivity has been successfully tested for SV-STG at a larger tubular reactor (41.mm I.D.). The SV-STG filled with Cu MFEC structure demonstrated improved production rate and gasoline selectivity. It exhibited a maximum radial temperature gradient of less than 5 ºC, while the comparable packed beds showed a maximum radial temperature gradient around 40 ºC. It was estimated that Cu MFEC could enable the SV-STG to operate at a tubular diameter of 4 – 5 inches without comprising gasoline selectivity. SV-

STG combined with Cu MFEC structure has a great potential to intensify and simplify STG process, significantly reduce CAPEX and OPEX, and enhance scalability and modularity.

Keywords: Syngas-to-Gasoline (STG), Methanol-to-Gasoline (MTG), Methanol Synthesis, Dimethyl Ether (DME), Fischer-Tropsch Synthesis (FTS), Microfibrous Entrapped Catalysts (MFEC), Process Intensification (PI)

IV.1 Introduction

The increasing demands for liquid fuels have drawn significant research attention to synthetic fuels. Currently, two well-known approaches to synthesize liquid fuels from syngas have been developed [8,11,19,22,23]. One is Fischer-Tropsch synthesis (FTS); the other one is Syngas-to-Gasoline (STG) based on methanol synthesis and methanol-to-gasoline (MTG) process. FTS process produces a broad spectrum of high value-added products including LPG, gasoline, diesel, and waxes. Typically, it requires complex and expensive subsequent processes to upgrade the products to meet liquid fuel specifications. For instance, the LPG fraction will be sent to a polymerization unit to upgrade the $C_3 – C_4$ olefins into gasoline and diesel. The gasoline fraction will be sent to refining units to increase its octane number. The heavy wax products will be hydrocracked or thermally cracked into middle distillates.

STG approach is a multiple step process [8,10,11,19,22] for gasoline production. It typically consists of three steps: methanol production from syngas, dimethyl ether production via methanol dehydration, and gasoline production from DME on zeolite-based catalysts. The reaction mechanism is complicated and has been discussed elsewhere [30,32,117]; a simplified reaction path is given in Eq.IV.1 – Eq.IV.8. Compared with the FTS process, STG process has a very narrow product distribution, and its product spectrum is limited to a maximum carbon

number of around C_{10}. Typical STG gasoline has an octane number over 90, which means it can be directly used as automobile fuels without further treatments. However, STG process is subject to an equilibrium limitation of the first reaction (syngas-to-methanol) [8,23]. This reaction is favored at low temperatures (240 – 300 ºC) and high pressures (50 – 200 atm), but low temperature operation limits the catalyst activity and volumetric production rate, which is similar ammonia synthesis. To solve this issue, some innovative processes have been developed. For example, Haldor-Topsoe [22] successfully combined the first two processes, methanol synthesis and methanol dehydration processes, together into one reaction unit. This innovation consumes methanol, the sole product of the methanol synthesis, for DME synthesis and greatly increased the syngas conversion even at low system pressure. The Water-Gas-Shift (WGS) reaction (Eq.IV.3) occurs as a side reaction. If combined the first three reactions (Eq.IV.1 – Eq.IV.3) together, the overall reaction is in Eq.IV.4 and the H_2:CO ratio is 1:1. According to the literature [115,116], this ratio results in optimal DME productivity and materials utilization. This means the combined process for syngas-to-DME is suitable for syngas from biomass or coal (low H_2:CO ratio) due to their high WGS activity. In the TIGAS (Topsoe Improved Gasoline Synthesis) process, STG process consists of two consecutive steps: syngas to DME and DME to gasoline.

Methanol Synthesis: $CO + 2H_2 \leftrightarrow CH_3OH$ (Eq.IV.1)

Methanol Dehydration: $2CH_3OH \leftrightarrow DME + H_2O$ (Eq.IV.2)

Water-Gas-Shift Reaction: $CO + H_2O \leftrightarrow CO_2 + H_2$ (Eq.IV.3)

Overall Reaction of Syngas-to-DME: $3CO + 3H_2 \rightarrow DME + CO_2$ (Eq.IV.4)

DME to Gasoline: $DME \rightarrow$ Light Olefins $+ H_2O$ (Eq.IV.5)

$$\text{Light Olefins} + \text{DME} \rightarrow \text{Heavy Olefins} + H_2O \quad \text{(Eq.IV.6)}$$

$$\text{Heavy Olefins} \rightarrow \text{Aromatics} + \text{Paraffins} \quad \text{(Eq.IV.7)}$$

$$\text{Aromatics} + \text{DME} \rightarrow \text{Higher Aromatics} + H_2O \quad \text{(Eq.IV.8)}$$

Based on those previous achievements, researchers want to further integrate these two reaction processes into one single process: syngas directly to gasoline. For instance, both Fujimoto et al. [118] and Chang et al. [119] try to directly synthesize gasoline from syngas by using a mixed catalyst composed of a methanol synthesis catalyst and an MTG catalyst. Nevertheless, the major products are C_1 – C_4 paraffins, which is different from the STG process with multiple steps. There were many other similar attempts [8,120–122], but they all reached a similar result that C_1 – C_4 paraffins dominated the products. This disappointing result is due to the lack of knowledge of STG's reaction nature. MTG cannot be operated together with methanol synthesis. MTG requires light olefins as essential intermediates to synthesize long-chain hydrocarbons and aromatics (Eq.IV.5 – Eq.IV.8). Methanol synthesis catalyst, which has the function of hydrogeneration (Eq.IV.1) [26,30,32,117,123–125], hydrogenate these intermediates into short chain paraffins and interrupt the chain growth for MTG. Moreover, the reaction of syngas to methanol (Eq.IV.1) operates around 240 – 300 ºC, and the MTG process (Eq.IV.5 – Eq.IV.8) requires a reaction temperature around 360 – 400 ºC [8,11,105,126]. Hence, these two reactions have distinguished working temperature ranges, and a single temperature cannot make both of them working properly. As a result, these two catalytic reactions must be carried out separately.

In this study, an STG reactor with 3 zones was employed to directly convert syngas-to-gasoline. The first zone (Zone-1) is a mixed catalyst zone (methanol synthesis catalyst mixed with methanol dehydration catalyst) to produce DME from syngas. The third zone (Zone-3) is a

zeolite zone packed with ZSM-5 to convert the DME to gasoline. The second zone (Zone-2) is a relatively inert zone packed with γ-Al_2O_3 mainly used to separate Zone-1 from Zone-3 since those two zones have different working temperatures. In addition, Zone-2 can prevent the back diffusion of gas mixtures from Zone-3 to Zone-1 since light olefins produced from Zone-3 must be separated from hydrogen activation in Zone-1. Furthermore, γ-Al_2O_3 packed in Zone-2 as a methanol dehydration catalyst enables the maximum conversion of methanol synthesized in Zone-1 to DME. As shown below, this carefully designed multi-zone reactor system can solve the issues that are encountered in the conventional STG process with a mixed bed strategy.

The SV-STG reactor system has been further integrated with a thermal conductivity catalyst structure called Microfibrous Entrapped Catalyst (MFEC) for efficient thermal management. The MFEC structure was developed by our group and is a catalyst network supported by micron-sized metal fibers with high thermal conductivity [53,69,74,75,79,127–129]. By supporting small catalyst particles in a high voidage matrix of microfibers, the catalyst is suitable for fixed bed applications without experiencing severe pressure drops or bed channeling encountered in small particle packed beds. Previous efforts on this unique catalyst structure have shown significant enhancement in intra-bed heat transfer and mass transfer. Especially for the FTS process, Cu MFEC structure can efficiently transfer the reaction heat out of the reactor and maintain a stable reaction temperature [52,79,127] and improved FTS product selectivity, process stability and maneuverability, and process safety. It must be noted that both methanol synthesis (ΔH = -90.8 kJ/mol) and MTG (ΔH = -55.7 kJ/mol) process, like FTS, are highly exothermic reactions. Therefore, Cu MFEC structure will also improve the STG process performance.

IV.2 Experimental

IV.2.1 Fabrication of Cu MFEC

A conventional paper-making technique was utilized to prepare Cu microfiber sheets. The detailed process can be found in many literature [53,79,113]. Typically, micro-sized raw Cu fibers and cellulose fibers were mixed and blended with a large amount of water. The resulting mixture was then cast into a paper-making machine. By removing the water, preformed Cu microfiber sheets were formed. A two-sided microfiber sheet can be prepared by overlaying two pieces of performed sheets fabricated from different diameters of raw Cu fibers. The top layer was made from 12 μm Cu fibers, and the bottom layer was from 6 μm Cu fibers (IntraMicron, Auburn, AL, USA). Then, the preformed two-sided sheet was dried, and a self-supporting sheet was formed. After that, the dried sheet was pre-oxidized in flowing air at 500 ºC for 30 min to remove the bulk of cellulose. Subsequently, the pre-oxidized sheet was sintered in flowing hydrogen at 700 ºC for 60 min to form the fiber-fiber junctions. These junctions composed a sinter-locked network through the microfiber media, which significantly enhanced its heat transfer performance. The top layer of the media was fluffy, and the bottom layer was compact since they were made by different sizes of raw fibers. The last step was loading catalyst particles into this porous Cu microfiber media. Because of the two-sided design, catalyst particles with certain sizes can be easily loaded into the top layer of the microfiber media without leaking or moving out from the bottom layer.

IV.2.2 Catalyst Preparation

For STG process, three kinds of catalysts have been used, and they are all commercially available. One is the methanol synthesis catalyst named HiFuel@R120 which was directly

purchased from Alfa Aesar; this catalyst was crushed and sieved to 80 – 140 mesh. Another one is γ-Al_2O_3 (Alfa Aesar, #43832) used as the methanol dehydration catalysts. Before use, the γ-Al_2O_3 particles were crushed and screened to 80 – 140 mesh then calcined at 500 ºC for 10 hours. The third kind of catalyst is ZSM-5 extruded (ACS Materials, CAS #308081-08-5, Si/Al=38:1); this was used as the MTG catalyst. The ZSM-5 extruded was first crushed and separated into 80 – 140 mesh then activated at 540 ºC for 3 hours before use.

IV.2.3 Catalyst Characterization

The surface morphologies of Cu MFEC structure before and after catalyst loading were characterized on a JEOL JSM-7000F scanning electron microscope (SEM).

IV.2.4 Reactor Packing

The experiments in this paper were operated in two tubular reactors: 9.0 mm I.D. small reactor and 41.0 mm I.D. large reactor. Both reactors have been designed as multi-zone reactors. Figure IV.1 showed that it starts with the pre-heating zone, which is packed with Cu microfibers only without any catalysts, to preheat the reactants to a certain temperature. The major reaction zones have been separated into three zones. In both Zone-1 and Zone-3 six-point thermocouples were used to detect the temperature inside the reactor. In each zone, separate temperature controllers and heating tapes were used to control and maintain the outside wall temperature. Typically, Zone-1 was packed with mixed catalyst (Hifuel@R120 : calcined γ-Al_2O_3 = 2:1 in mass ratio), and Zone-2 and Zone-3 were packed with calcined γ-Al_2O_3 and calcined ZSM-5 respectively. The small reactor (9.0 mm I.D.) was packed without any dilution. If there was any missing zone due to the experimental design, catalysts supposed to be packed in this zone were replaced by the same size glass beads.

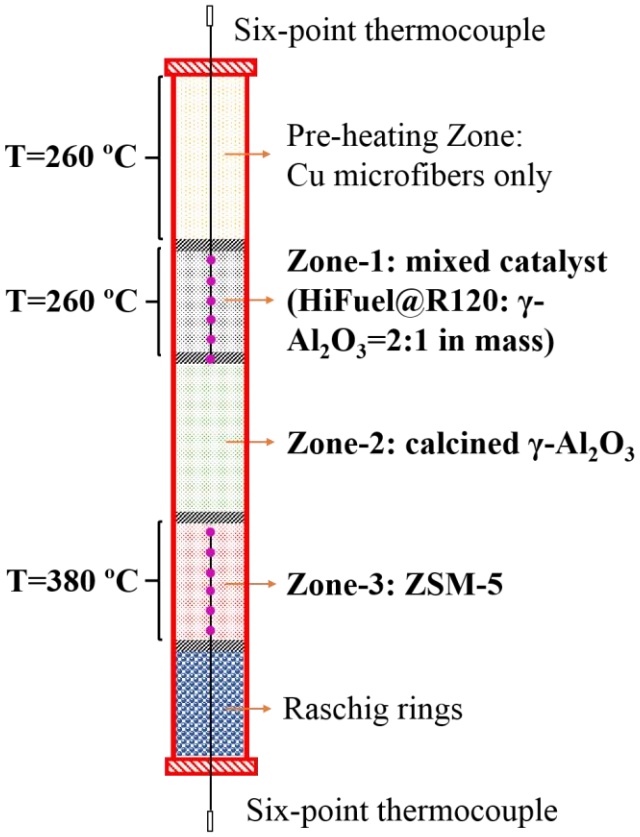

Figure IV.1 The scheme of the multi-zone reactor system

The Cu MFEC was only used in the large reactor (41.0 mm I.D.). First, circular disks with a diameter of 43.5 mm were punched from the sintered Cu microfiber sheets. Also, a small hole was punched in the middle of each disk to insert a 1/16 inch six-point thermocouple. Second, the catalyst particles (80 – 140 mesh) were entrapped into the punched disks to form Cu MFEC, and then the Cu MFEC was packed into the large reactor, piece by piece. It must be noted that the disk size (43.5 mm) was 6 % larger than the inside diameter of the large reactor (41.0 mm), which offers tremendous contact points between the Cu microfiber media and the inside reactor wall. Based on our experience, this will greatly increase the inside wall heat transfer coefficient compared with that of the traditional packed bed. To make a fair comparison, the comparable

packed bed was diluted to the same packing density as the Cu MFEC bed by using glass beads (80 – 140 mesh).

IV.2.5 Reaction Apparatus and Operations

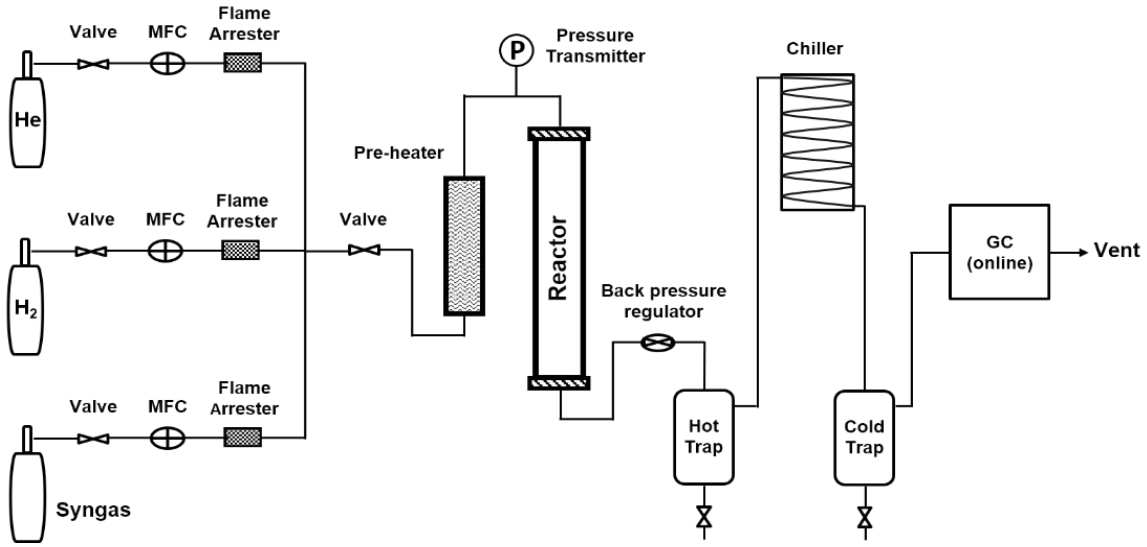

Figure IV.2 The schematic of STG reaction apparatus

The schematic of the reaction apparatus is shown in Figure IV.2. The inlet gases were mixed and pre-heated in the pre-heater to reach the operating temperature before flowing into the reactor. A pressure transmitter was set right after the pre-heater and followed up with the major reactor. A back-pressure regulator was installed after the reactor to adjust the operating pressure. Then, the outlet stream went sequentially through a hot trap (150 ºC) and a cold trap (2 ºC) to collect heavy hydrocarbons and liquid products, respectively. The vent gas products were analyzed on an online gas chromatograph (GC, Agilent 6890) equipped with a packed column (Hayesep-DB 100/120). A thermal conductivity detector (TCD) was used to determine the concentrations of H_2, N_2, CO, CO_2, and $C_1 – C_6$ by using nitrogen as the internal standard. In the same GC, a flame ionization detector (FID) connected with a capillary column (DB-5) was used offline to analyze the liquid products. First, the collected liquid hydrocarbons were separated from water then

diluted with carbon disulfide (Alfa Aesar, ACS grade, >99.9 wt%) before shooting into the FID detector. Before starting the SV-STG operation, the catalysts in all three zones were pre-reduced in situ at 130 ºC for 2 hours with flowing ultra-high purity hydrogen (Airgas, HY UHP300) then the temperature was slowly increased to 280 ºC for another 10 hours followed by gradually increasing the temperature to 320 ºC for 4 hours. After that, the catalysts in the first two zones (Zone-1 & Zone-2) were cooled to 260 ºC, and the catalysts in the third zone (Zone-3) were heated to 380 ºC to initiate the SV-STG reactions. All the experiments in this paper were carried out at 3.0 MPa using a syngas with an H_2/CO ratio of 1:1. This syngas was directly purchased from Airgas with 2.0 vol% nitrogen as the internal standard.

IV.3 Results and Discussion

IV.3.1 Reaction Activity and Selectivity

IV.3.1.1 SV-STG in Small Reactor (9.0 mm I.D.)

To prove our previous statement that the multi-zone reactor system can solve all the issues met in a single reactor of the STG process, we carefully designed control experiments in the small packed bed reactor. For PB-1, only the first two zones (Zone-1 & Zone-2) were packed with the corresponding catalysts; Zone-3 was packed with a certain amount of glass beads instead of ZSM-5 particles to reach the same bed length (5 inches). PB-2 was packed in the opposite way of PB-1, which means only Zone-3 was packed with catalyst particles, and the first two zones were packed with glass beads instead of the corresponding catalysts. Then, in PB-3, all three zones were packed with the corresponding catalyst particles, and the reactor packing properties are shown in (Table IV.1).

Table IV.1 SV-STG Reactor packing configurations

Reactor packing	Reaction zones [a]	Volume Percentage (%)			Catalyst loading (g)	Bed length (inches)
		Catalyst	Cu fiber	Voidage		
PB [b] (9.0 mm I.D.)	Zone-1	packed without dilution			4.0	3.0
	Zone-2	packed without dilution			2.4	3.0
	Zone-3	packed without dilution			4.5	5.0
MFEC [c] (41.0 mm I.D.)	Zone-1	21.9	13.5	64.6	24.0	4.0
	Zone-2	29.2	8.9	61.9	14.4	3.0
	Zone-3	19.6	12.3	68.1	27.0	7.5
PB [d] (41.0 mm I.D.)	Zone-1	20.6	0.0	79.4	24.0	4.0
	Zone-2	29.2	0.0	70.8	14.4	3.0
	Zone-3	19.0	0.0	81.0	27.0	7.5

[a] Zone-1: mixed HiFuel@R120 with calcined γ-Al_2O_3 in 2:1 mass ratio; Zone-2: calcined γ-Al_2O_3 (500 ºC for 10 h); Zone-3: calcined ZSM-5 extruded (540 ºC for 3 h); all the catalyst particles were in 80 – 140 mesh.

[b] For the small packed bed reactor (9.0 mm I.D.), there were no dilutions in all three zones.

[c] For the MFEC bed, the second zone was only 3 inches. To better separate Zone-3 from Zone-1, an additional 4 inches Raschig rings were added.

[d] For the large packed bed (41.0 mm I.D.), it was diluted with glass beads, so the voidage is the volume percentage of glass beads and the actual voidage together.

The experimental results in PB-1 (Table IV.2) show that all the methanol produced from syngas was converted to DME. In addition, there were negligible amounts of other hydrocarbons formed when the ZSM-5 zone was taken out. The reason is that the catalysts in the first two zones were only aimed to synthesize DME. However, if ZSM-5 was used alone (PB-2 in Table IV.2) there was almost no reaction activity in the syngas, which means ZSM-5 cannot active H_2 or CO. Considering this, if a reactor system can prevent the light olefins formed on ZSM-5 from contacting the active hydrogen species produced on methanol synthesis catalyst, we could integrate the entire STG process into a single reactor. Therefore, a multi-zone reactor system has been proposed like PB-3 to operate the entire STG process in a single vessel. A relatively inert

zone (Zone-2) has been added between the DME formation zone (Zone-1) and the ZSM-5 zone (Zone-3). By doing this, the direct contact between Zone-1 and Zone-3 can be prevented. In addition, the back diffusion of light olefins from Zone-3 to Zone-1 can also be greatly reduced since Zone-2 is relatively long (3 inches) compared with the reactor size (9.0 mm I.D.). Moreover, Zone-1 and Zone-3 can be operated at different temperatures after they have been separated by a certain distance. The experimental results in PB-3 show a very high gasoline selectivity (74.8 wt%) under a high CO conversion (78.3 %); these values are similar to the traditional STG process with two or three steps. Hence, with this multi-zone reactor system design, a single vessel STG could be achieved under a high CO conversion and a high gasoline selectivity.

IV.3.1.2 SV-STG in Large Reactor (41.0 mm I.D.)

A microfibrous Entrapped Catalyst (MFEC) structure was developed by our group, which is a highly efficient heat transfer media. Figure IV.3A shows a picture of sintered Cu microfiber medium with two layers; the top layer has a very fluffy structure (Figure IV.3D). The medium was punched to a certain size (Figure IV.3B) then catalyst particles were easily migrated into the top layer of the punched medium by utilizing a shaker; this resulted in an acceptable dispersion. After that, the punched medium was pressed, and Cu MFEC structure was formed (Figure IV.3C). The loaded catalyst particles were entrapped and immobilized by the top layer of microfiber network (Figure IV.3E), and the compact bottom layer prevented the loss of catalyst particles. It has already been proven that Cu MFEC structure works well to scale-up FTS in a 4 inches diameter tube. The Cu MFEC structure can transfer out the heat generated in the FTS process and maintain a stable reaction temperature. In addition, Cu microfiber media is inert during the FTS process. Furthermore, Cu MFEC structure is stable during the FTS catalyst

regeneration process to burn off coke formed on the catalyst. All these benefits drove us to apply Cu MFEC structure to the SV-STG process.

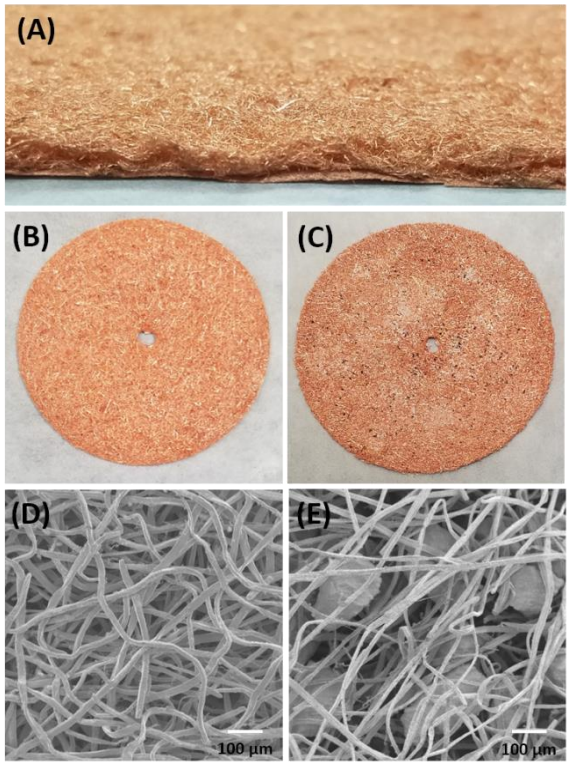

Figure IV.3 Images of Cu MFEC structure: (A) Picture of sintered Cu microfiber medium; (B) Picture of punched Cu microfiber medium before catalyst loading; (C) Picture of Cu MFEC after catalyst loading; (D) SEM image of Cu microfiber medium before catalyst loading; (E) SEM image of Cu MFEC after catalyst loading

As shown in Table IV.1, a large tubular reactor (41.0 mm I.D.) was equipped with the Cu MFEC structure. This is the first time that an MFEC structure has been applied to STG or MTG related process. By maintaining the multi-zone reactor packing pattern, the 41.0 mm I.D. tubular reactor contains six-fold more catalyst than the small packed bed (9.0 mm I.D.) for all three zones. The MFEC-1 demonstrated 46.0 C% gasoline selectivity with 65.3 % CO conversion. Both the CO conversion and the gasoline selectivity are very high compared to the FTS process, although they were slightly lower than in PB-3. This may be due to the differences in packing

density and bed voidage. PB-3 was packed without any dilution, so it was more condensed per unit volume than MFEC-1. In addition, the Cu MFEC structure transferred the reaction heat more efficiently than the packed bed. As a result, the reaction temperature in PB-3 was higher than in MFEC-1, or there were more hot spots formed in PB-3 than in MFEC-1. Apparently, higher temperature leads to higher CO conversion. Also, the linear velocity in MFEC-1 was slower than in PB-3 due to the different dilution ratio under the same WHSV. The residence time in MFEC-1 was also longer than in PB-3. ZSM-5 has strong acidity; it can be used as a hydrocracking catalyst; therefore, the long residence time might lead to some secondary reactions, that consume the primary products, such as hydrocracking the long chain hydrocarbons to short chain hydrocarbons. This is one possible reason why the gasoline selectivity dropped, and the selectivity of C_2 – C_4 increased in MFEC-1 compared to PB-3. Another reason that caused a lower gasoline selectivity in MFEC-1 than in PB-3 is the CO_2 selectivity increased to 36.0 C% in MFEC-1 due to the lower real reaction temperature in MFEC-1 than in PB-3, as mentioned above. In summary, for the first time, Cu MFEC structure has been successfully used to scale-up the SV-STG process without apparent loss of reaction activity or gasoline cut selectivity.

On the other hand, the comparable packed bed (PB-4) showed a much higher CO conversion (79.6 %) than MFEC-1 (CO conversion 65.3 %), but its gasoline selectivity was lower. The main reason is that the large packed bed experienced thermal overshoot, so the real reaction temperature inside the reactor was much higher than the set temperature. Figure IV. 4 shows the central line temperature profiles in Zone-1. The Cu MFEC bed (MFEC-1) demonstrated a stable temperature profile throughout the reaction process, and the highest temperature overshoot was within 5 ºC. However, PB-4 showed a sharp rise in temperature when the reaction started then

reached a relatively stable temperature profile. The highest temperature overshoot was around 40 ºC which is much higher than in the Cu MFEC bed. In short, Cu MFEC structure can highly efficiently transfer the reaction heat out of the reactor and maintain a stable reaction temperature. By doing this, a higher gasoline selectivity is received. Moreover, a longer bed life can be expected since a higher temperature will accelerate coke formation and deactivate the catalysts. It must be noted that this data is based on a 41.0 mm I.D. tubular reactor which is an acceptable bench scale reactor, but a larger diameter reactor could be used (ca. 4 – 5" I.D.). As the reactor size increased, the thermal effects become more significant. When the temperature reaches a certain point, the reaction can experience thermal runaway and produce mostly methane. Therefore, Cu MFEC structure provides a very efficient way to deal with the highly exothermic process of SV-STG.

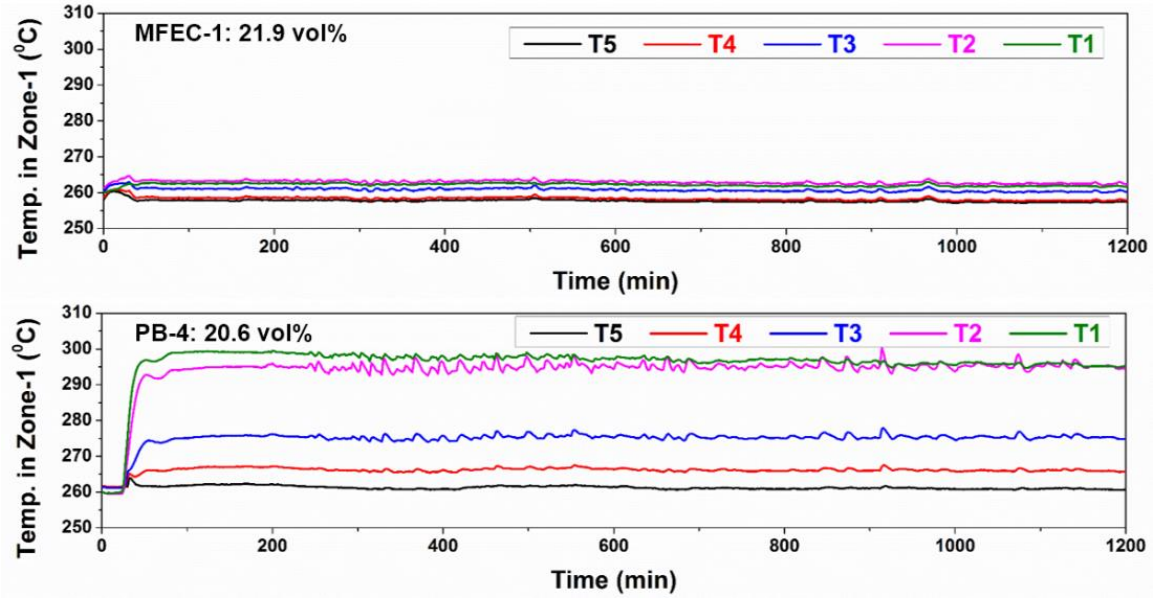

Figure IV.4 Axial direction central line temperature profiles in Zone-1: T1 to T5 started from the top to the bottom, and the interval between each temperature point is 1"

Table IV.2 Performance of both packed bed and Cu MFEC bed [a]

Reactor Type	**PB-1**	**PB-2**	**PB-3**	**PB-4**	**MFEC-1**	**MFEC-2**	**MFEC-3**	**MFEC-4** [b]
Reactor I.D.	9.0 mm	9.0 mm	9.0 mm	41.0 mm	41.0 mm	41.0 mm	41.0 mm	41.0 mm
Reaction Zone [c]	Zone-1 & Zone-2	Zone-3	all three Zones	all three Zones	all three Zones	all three Zones	all three Zones	all three Zones
WHSV (h^{-1}) [d]	0.92	0.92	0.92	0.92	0.92	0.46	0.32	0.46
CO Conv. (%)	75.8	1.2	78.3	79.6	65.3	80.7	85.8	77.6
H_2 Conv. (%)	84.8	1.8	51.1	63.4	41.3	50.5	55.7	67.3
Product Selectivity, C%								
CH_3OH	0.0	0.0	0.0	0.0	0.0	0.0	0.0	0.0
DME	62.4	0.0	0.0	0.0	0.0	0.0	0.0	0.0
CO_2	35.5	26.6	33.0	37.2	36.0	37.5	43.1	35.8
CH_4	0.6	21.3	1.3	1.0	1.2	1.8	3.5	0.7
$C_2 – C_4$	1.5	52.1	13.7	20.6	16.8	19.4	24.9	18.7
$C_5 – C_{10}$	0.0	0.0	52.0	41.2	46.0	41.3	28.5	44.8
Hydrocarbon Selectivity, wt%								
$C_1 – C_4$	100.0	100.0	25.2	38.5	31.5	38.1	58.8	32.9
$C_5 – C_{10}$	0.0	0.0	74.8	61.5	68.5	61.9	41.2	67.1

[a] All the reactions were operated at P = 30 atm, and used H_2:CO = 1:1.

[b] Zone-3 in MFEC-4 is the half length of Zone-3 in MFEC-2 with the same volume loading of the catalyst.

[c] All three reaction zones were heated using separate heating tapes, and their operating temperatures were controlled by different temperature controllers.Zone-1 and Zone-2 were set at 260 ºC, and Zone-3 was set at 380 ºC.

[d] The WHSV values were calculated based on Zone-1.

The CO conversion in MFEC-1 was not very high, so the gas flow rate was decreased to increase the CO conversion. As we can see from MFEC-2 and MFEC-3 in Table IV.2, the CO conversion increased from 80.7 % to 85.8 % as the gas flow rate decreased. Meanwhile, gasoline selectivity dropped as the CO conversion increased. This indicates that there are some secondary reactions, which can consume the gasoline range products and decreased its selectivity as the residence time increases. As mentioned above, ZSM-5 is packed in Zone-3 and is used to convert

DME to gasoline, but it also has strong acidity allowing it to also act as the hydrocracking catalyst to further consume the synthesized gasoline range products. To prove this, a control experiment, MFEC-4, was designed. The Zone-3 in MFEC-4 is half the length of Zone-3 in MFEC-2 with the same volume loading of catalysts; all other reaction conditions as the same.MFEC-4 maintained a similar CO conversion (77.6 %) to MFEC-2 (80.7 %) but brought the gasoline selectivity to 44.8 C%, which is close to the selectivity in MFEC-1 (46.0 C%). This is because the residence time of Zone-3 in MFEC-4 is the same as the residence time of Zone-3 in MFEC-1. Hence, the residence time of Zone-3 is a crucial point for the gasoline selectivity. This also supports our hypothesis that gasoline is an intermediate product on ZSM-5. In order words, gasoline selectivity can be maximized with an appropriate residence time; a short residence time results in a low yield, and a long residence time results in further consumption of the gasoline products.

IV.3.2 SV-STG Liquid Products

As can be seen from Figure IV.5, the liquid phase products of the SV-STG process show a completely different GC-FID pattern than the liquid phase products from a typical Cobalt-based FTS process. The majority of products of SV-STG are carbon C_{10} or below, but the Co-based FTS showed some obvious signals until carbon C_{23}. Also, products sharing the same carbon number showed different retention times for SV-STG and Co-based FTS. This represents that they are different compounds even though they have the same carbon number. To identify the liquid products of the SV-STG process, another gas chromatograph (GC) was connected to a high-resolution time-of-flight (TOF) mass spectrometer (MS) and used as offline. The GC is an Agilent 6890N with a Rxi-5SilMS capillary column (Restek, #13623-124), and it is equipped with a G2614A auto injector purchased from Agilent Technologies (Santa Clara, CA). The MS is

a Waters GCT Premier benchtop orthogonal acceleration time-of-flight (oa-TOF) mass spectrometer. Helium was used as the carrier gas with a constant pressure of 45 kPa. The temperature program consisted of an initial temperature of 40 ºC for 4 min then the temperature was ramped to 280 ºC at a rate of 5 ºC/min and held at 280 ºC for 11 min. The internal calibrant was heptacosafluorotributylamine (m/z 118.9919, Sigma Chemical Co.), and the data was compared against the NIST MS search 2.0 program. The detailed liquid product compositions of SV-STG are listed in Figure IV. 6; it shows that most of the SV-STG liquid products were aromatic compounds, which is quite different from the Co-based FTS that mainly contained paraffins. However, the liquid products from the SV-STG process were similar to the liquid products received from traditional STG process with multiple steps. This indicated that SV-STG does not change the reaction mechanism or the reaction pathway of STG, it only process intensified traditional STG process into a single vessel. According to the literature [9,11,130], traditional STG process produces gasoline with a high octane number (RON more than 90). Based on these facts, we can expect that gasoline produced from SV-STG process also will have high octane number.

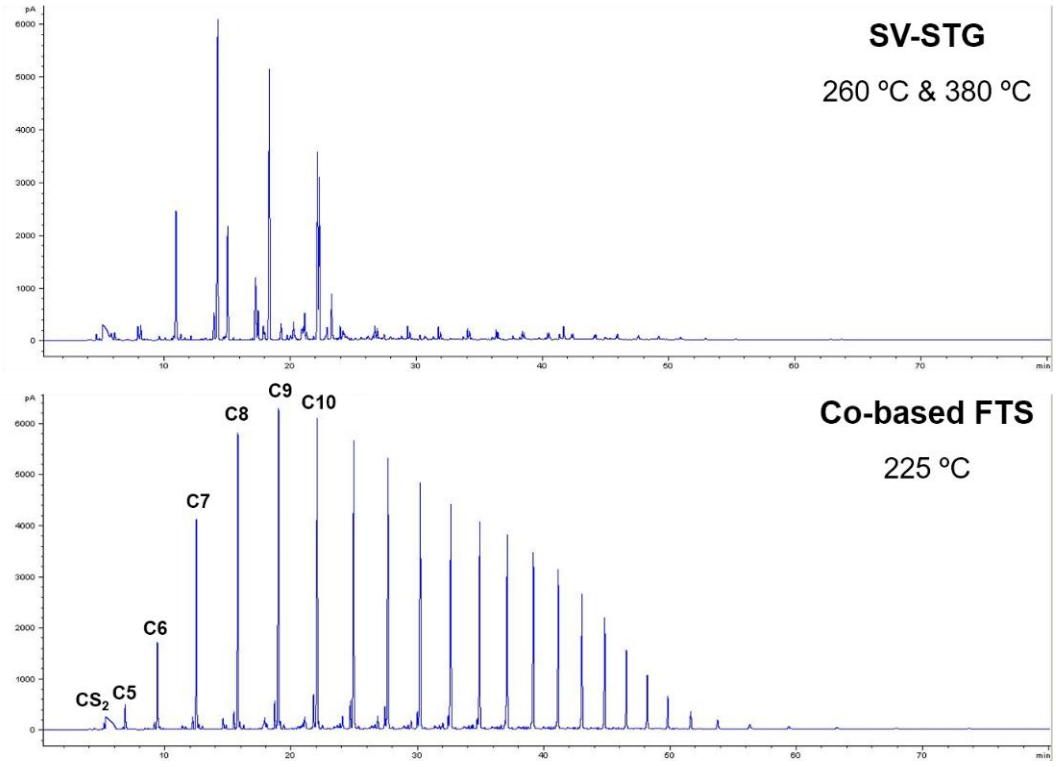

Figure IV.5 Comparing the GC-FID signal of SV-STG liquid products with Co-based FTS liquid products

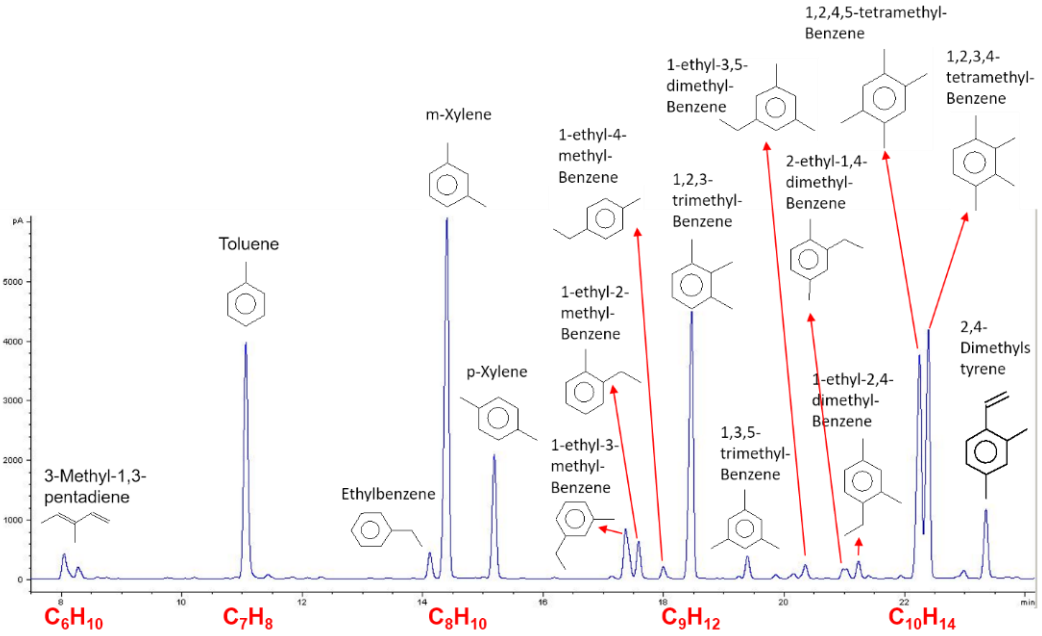

Figure IV.6 SV-STG liquid phase product identifications

IV.3.3 Process Intensification

A schematic flow sheet of traditional fixed bed STG process is shown in Figure IV.7, which is combined methanol synthesis from syngas with fixed bed MTG process [130,131]. Typically, purified syngas is employed for the methanol synthesis reaction, and it is compressed to 50 – 200 atm pressure. This high pressure is desired to shift the reaction equilibrium towards methanol formation. The highly exothermic nature of the methanol formation reaction inhibits the reaction equilibrium, and that is why the reaction usually operated under high pressure. The product stream is cooled down, and the gas phase compounds are separated with compressed methanol. The unreacted syngas is recycled back to the reactor. The liquid products must be carefully depressurized, and unwanted fuel gases were eliminated. The leftover liquid product is crude methanol which contains around 17 wt% water. The depressurized crude methanol is pumped to a heat exchanger to vaporize it then fed into a fixed bed reactor for methanol dehydration. In this reactor, methanol is partially dehydrated to an equilibrium mixture of methanol, DME and water. The effluent is split into four parallel streams and mixed with the heated recycle gas then fed into four parallel ZSM-5 reactors. These reactors contain ZSM-5 catalysts to convert DME and methanol to hydrocarbons and water. There is a total of five reactors in train: four reactors are operated in conversion mode, while one reactor is regenerating. This multiple reactor design is used to minimize pressure drop and to maintain constant product selectivity. The final effluent is cooled and separated into three phases: gas, liquid hydrocarbons, and liquid water. Most of the gas is recycled back to the ZSM-5 reactors to remove reaction heat. Typically, a gas recycle molar ratio of 9:1 is required to limit the reaction temperature rise to 68 ºC [125]. This high molar recycle ratio requires a medium pressure (c.a. 20 atm) to compress methanol and enable sufficient methanol to be converted.

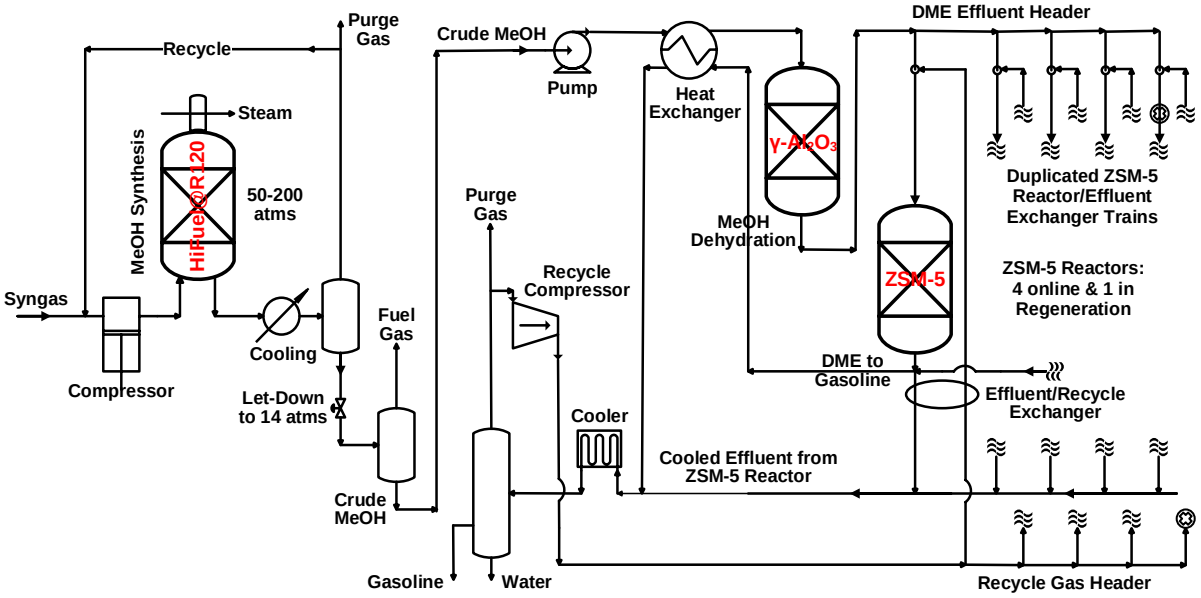

Figure IV.7 Flow sheet of traditional fixed bed STG process

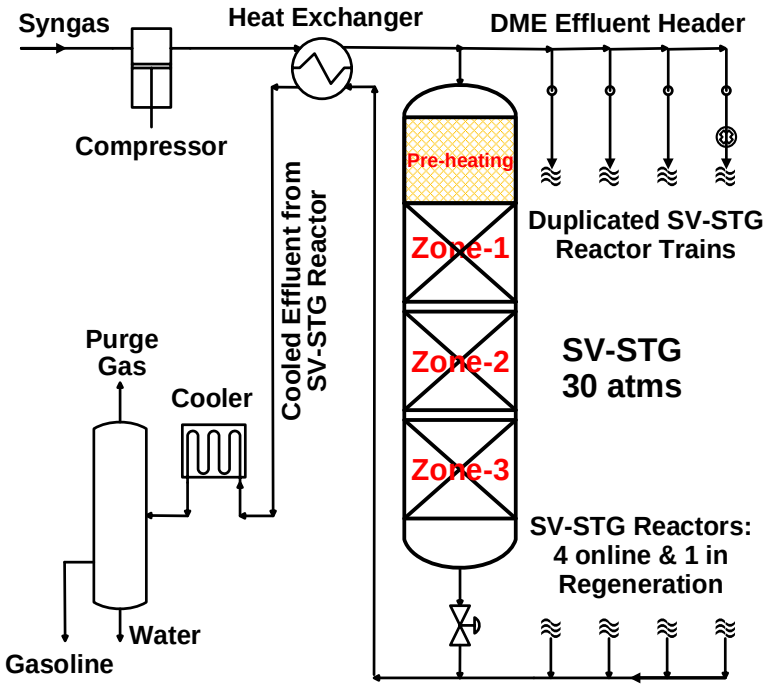

Figure IV.8 Flow sheet of the SV-STG process

The flow sheet of the SV-STG process is much simpler than traditional STG process. As shown in Figure IV.8, purified syngas is preheated before being fed into the single vessel reactor. The preheating heat is mainly recuperated from the reaction, which saves a lot of energy requirement. Then, the preheated syngas is fed to a single vessel with multiple reaction zones under a medium pressure of 30 atm. The effluent is passed through a heat exchanger to given heat to the fresh syngas before it is sent to a cooler. After being cooled, the final products are separated into three phases like the traditional STG process. However, unlike the traditional STG process, no gas recycle is required for SV-STG due to the high CO per pass conversion. As already stated, the main function for gas recycle is to efficiently remove reaction heat and compensate the low per pass conversion [31,125,130]. For the SV-STG process, Cu MFEC structure can achieve the same purpose of highly efficient transfer of the reaction heat. Another reason to run the gas recycle is to enhance oligomerization of light olefins to ensure that the gasoline products have a high aromatic concentration. As mentioned above, the gasoline products derived from the SV-STG process are highly aromatic. Therefore, it is also unnecessary to run the gas recycle in SV-STG process. Obviously, both recycle processes in traditional STG require a tremendous amount of energy and need the corresponding facilities to separate those recycle gases. More important, SV-STG used one step to directly convert syngas to gasoline. This is greatly process intensified when compared with traditional fixed bed STG process, which contains three steps and each step requires independent reactor systems and corresponding facilities. For these reasons, the SV-STG process greatly reduced CAPEX and OPEX when compared to traditional STG process.

Table IV.3 Comparison of SV-STG with the traditional STG process [4,38–41,53,127]

Process	Traditional STG	SV-STG
Reaction steps & reactors	3 steps with separate reactors	1 step in a single vessel
Recycle loops [a]	2	0
Operation pressure	200 – 300 atm (MeOH synthesis) 20 – 30 atm (MeOH dehydration & ZSM-5 reactor)	20 – 30 atm
Intra-bed conductivities	0.1 – 0.2 W/m-K	9 – 65 W/m-K
Approximate inside-wall heat transfer coefficients	35 W/m^2-K	3000 W/m^2-K
Temperature control	Poor	Excellent
Reactor diameter	Limited size	Larger
Volumetric productivity	Low	High
Pressure drop	Severe	Low
Catalyst particle size	3000 – 5000 μm	60 – 250 μm
Regenerability	Regenerable	Regenerable
CAPEX & OPEX	High	Significantly reduced
Scalability & modularity	High	Great increased

Furthermore, SV-STG has a few other advantages (in Table IV.3) compared with traditional STG. For instance, the first step of traditional STG process is methanol synthesis, which operates at extremely high pressure (50 – 200 atm) since reaction equilibrium is limited by pressure and temperature. The following two steps are also operated under medium pressure (20 – 30 atm). However, the whole process of SV-STG is operated at medium pressure (20 – 30 atm), which further reduces CAPEX and OPEX. Also, the intra-bed conductivity and inside-wall heat transfer coefficient in SV-STG are higher than in traditional STG. As a result, the SV-STG process maintains a stable reaction temperature, but the traditional fixed bed usually has poor temperature control. Due to excellent temperature control, SV-STG can use a larger diameter

tube than traditional STG; this increases its volumetric productivity. However, typically fixed bed system has a limited reactor size, not only because of temperature control but also pressure drop. This is one reason traditional STG process prefer to use large catalyst particles and small reactor tubes, to avoid severe pressure drop. Copper MFEC structure can significantly reduce pressure drop, which allows it to use small catalyst particles. The small particles can also reduce internal mass transfer limitations and increase reaction activity. It is worth noting that Cu MFEC structure in SV-STG reactor does not affect regeneration. It has been demonstrated successes in regenerating hydrocracking catalysts in FTS process, by passing through a gas composed of N_2 and a low percentage of O_2 to burn off coke formed on the catalysts without destroying the Cu MFEC structure. Although the Cu MFEC media are partially oxidized, they will also be reduced during the pre-reduction process to activate the catalysts. Therefore, the flow sheet of SV-STG (Figure IV.8) is also designed in a five reactors train, just like the traditional STG process: four on operations and one in regeneration. In short, SV-STG equipped with Cu MFEC structure greatly process intensified traditional STG process and significantly reduced CAPEX and OPEX as well as enhanced scalability and modularity.

IV.4 Conclusion

A simple SV-STG reactor has been designed for the process intensification of STG process by integrating three separate STG steps into one single reaction vessel. This SV-STG reactor consists of three consecutive zones: Zone-1 was used for methanol synthesis and methanol dehydration to DME, Zone-2 was mainly used for separation of Zone-1 and Zone-3, and Zone-3 was used to convert DME to gasoline. This simplified design separated hydrogen activation in Zone-1 from olefin formation and oligomerization in Zone-3, and prevented the most important reaction intermediates of light olefins to be hydrogenated to short chain paraffins. The SV-STG

process demonstrated a high gasoline selectivity of 74.8 wt% and a single pass conversion of 78.3 % in a small tubular reactor (9.0 mm I.D.). In addition, SV-STG has been successfully scaled to a larger reactor tube (41.mm I.D.) using Cu MFEC structure at improved the reaction activity and gasoline selectivity. The Cu MFEC structure also rendered excellent temperature control. The maximum temperature difference in the radial direction was less than 5 ºC for the MFEC structure, while the temperature difference for the comparable packed bed was around 40 ºC. This significant difference in temperature control between Cu MFEC structure and packed bed was only shown on a 41.0 mm I.D. tubular reactor (lab acceptable level); this difference could go much higher if a larger diameter tube (ca. 6.0" I.D.) was used. Furthermore, Cu MFEC structure assisted SV-STG process has an extremely simple flow sheet compared with the traditional fixed bed STG process. For SV-STG equipped with Cu MFEC structure, there was only one step for gasoline production from syngas and no need for gas recycle. Due to the integration between methanol synthesis and DME synthesis, SV-SGT gets ride of the high-temperature and high-pressure operations required for methanol synthesis step in conventional STG and drastically reduced both CAPEX and OPEX of the STG process. In contrast, the traditional STG process requires three steps for gasoline production and two gas recycle loops along with the relative recycle gas separation systems and recompression systems. In conclusion, the SV-STG approach, especially with the assistance of Cu MFEC structure in heat and mass transfer, has the right potential to simplify and intensify the STG process and reduce the CAPEX and OPEX for the production of gasoline from syngas.

Chapter V: Proposed Future Work

V.1 Steam Jacket Reactor

Table V.1 Overall Heat Transfer Coefficients of Various Fluids (Liquids and Gasses)

Conditions of heat transfer	Overall heat transfer coefficient, W/(m^2·K)
Gases in free convection	5 – 37
Water in free convection	100 – 1200
Oil in free convection	50 – 350
Gases flow in tubes and between tubes	10 – 350
Water flowing in tubes	500 – 1200
Oil flowing in tubes	300 – 1700
Boiling water	2000 – 100000
Condensation of water vapor	4000 – 140000
Cu MFEC	1000 – 3000

The Cu MFEC structure works well to transfer the reaction heat to the reactor wall, but the reactor wall has only been cooled using static air and flowing air. As we can see from Table V.1, the overall heat transfer coefficient of Cu MFEC structure can reach 3000 W/(m^2·K), but the static air only has a heat transfer coefficient of 5 – 37 W/(m^2·K), even for the flowing air it is only 10 – 350 W/(m^2·K). Hence, the outside wall heat transfer coefficient is too low and greatly limits the heat transfer out of the reactor. In a word, we spent a great deal of effort to solve the inside wall heat transfer issue, but now we are limited by the outside wall heat transfer coefficient. The outside wall heat transfer issue should be relatively simple to solve because all that needs to be done is remove the heat quickly from the reactor wall. Therefore, we are planning to build a steam jacket reactor, which uses steam condensation to remove the heat from the reactor wall.

V.2 Extend Operation Time of SV-STG

V.2.1 Adjust Operation Conditions

Under typical MTG reaction conditions, ZSM-5 catalyst undergoes slow deactivation. This mainly results from the coke formation during the reaction. According to the literature [11,132], the MTG bed ages through a band-aging mechanism. The MTG reaction on ZSM-5 occurs over a relatively small band or zone in the fixed bed system. As the ZSM-5 catalyst deactivates, the reaction band travels slowly down to the reactor. As the band nears the end of the ZSM-5 bed, the output product becomes more olefinic and less aromatic. At a certain point, methanol breakthrough occurs which means the end of the bed cycle and the bed must be regenerated. The residence time in ZSM-5 zone has to be a certain range to maximize the selectivity of gasoline cut. This is because, as we mentioned in Chapter III, gasoline is an intermediate product on ZSM-5. If the residence time is too short, it results in a low yield; if residence time is too long, it results in further consumption of the gasoline products. To extend the bed life, more ZSM-5 catalyst will be added. At the same time, the operating conditions will be adjusted to remain a constant residence time and maintain the rate of gasoline production. At first, a higher flow rate was applied. As the band-aging progresses, the active bed becomes shorter, and the flow rate has to be slowed down to maintain a relatively constant residence time. By doing this, a commercial MTG process could extend ZSM-5 catalyst lifetime to around 20 days from a typical lifetime of 7 days [125]. Compared with the traditional MTG process, the SV-STG process is just integrated multiple reactor systems in a single vessel, but the reaction nature does not change. Therefore, we expect that this kind of strategy will also work on the SV-STG process.

As we mentioned above, ZSM-5 undergoes slow deactivation in MTG process. When we discuss catalyst deactivation, we usually mean coke formation. However, upon closer inspection, there are two kinds of species that cause deactivation [133]. One reason for deactivation is, as mentioned previously, coke formation; this is a graphitic species deposition. This usually happens at the inside pores of zeolites. Another cause of deactivation is that molecules that are too large, or that have high proton affinity to diffuse through the microporous channels block access to the active sites of catalyst. This often occurs on the outside surface of zeolites. In short, there is internal and external deactivation. The factors that influence catalyst deactivation include catalyst topology, acid strength, acid site density, pore size, and crystal size. ZSM-5 belongs to MFI group and literature reports that for catalysts with MFI topology, those large external molecules are the major contributors to catalyst deactivation [133]. The influence of catalyst acid strength and acid site density, catalyst pore size, and catalyst crystal size will be discussed in V.1.2. Also, the reaction temperature has a big influence in catalyst deactivation. Schulz [134] reported that the severe deactivation for ZSM-5 catalyst was caused by alkylated benzene molecules which mainly as ethyltrimethylbenzene and isopropyldimethylbenzene. They applied temperature program desorption tests to the used catalyst. The result showed that these benzene molecules dealkylated at temperatures above 350 ºC; this led to desorption of alkenes and lighter polymethylated benzenes, which freed catalyst from any carbon deposition. Therefore, Schulz suggests that the equilibrium of benzene alkylation and dealkylation happens around 350 ºC. Others designed experiments that showed that higher reaction temperature led to longer catalyst lifetimes and less remaining benzene compounds inside and outside of the catalyst. Under Schulz's reaction conditions, the test temperature increased from 290 ºC to 380 ºC, and the corresponding lifetimes of ZSM-5 increased from 0.5 h to 400 h. However, further increasing the

test temperature to 480 ºC led to a slight decrease in lifetime. Hence, increasing the reaction temperature to a certain value may also extend the catalyst lifetime.

V.2.2 Post Modification of ZSM-5

There is a common agreement that the higher acid strength and the higher acid site density, the more rapidly zeolite deactivation occurs in the MTG process[135–137]. In addition, zeolites with large crystal size deactivated faster than those with smaller crystal size [138]. This is because only the outer part of the zeolite crystal is active in the MTG reaction. Moreover, the literature shows that increasing the pore size of a zeolite and introducing mesoporosity into the zeolite structure can increase its capacity for coke formation and increase its lifetime [133,139–144]. In summary, there are four main approaches to extend zeolite lifetime: 1) reduce the acid strength; 2) reduce acid site density; 3) decrease zeolite crystal size; 4) increase zeolite pore size or introduce mesoporosity into its structure. Many methods were used to reach these results, including steam treatment and alkaline modification.

V.2.2.1 Steam Treatment

Steam treatment is a simple and common method to post modify zeolites. It can adjust zeolites' acidity and pore structure. There are many successful examples that steam treatment of ZSM-5 increased its stability by reducing the number of acid sites. For instance, Zhao et al. [137] used steam treatment of a commercial ZSM-5 at a temperature of 400 – 500 ºC to investigate its changes in acidity and pore structure and its stability in the reaction of ethanol dehydration. The experiment was carried out in a fixed bed reactor. The loaded ZSM-5 zeolites were slowly heated to a certain temperature (400 ºC, 450 ºC, 500 ºC, and 550 ºC) in a flow of pure nitrogen. Then, a pure steam flow (WHSV=13.8 h^{-1}) was passed through these samples under these specific

temperatures for 6 hours. After that, the samples were cooled to room temperature under the protection of flowing nitrogen. All the samples were denoted as HTx, where x represents the steam treatment temperature.

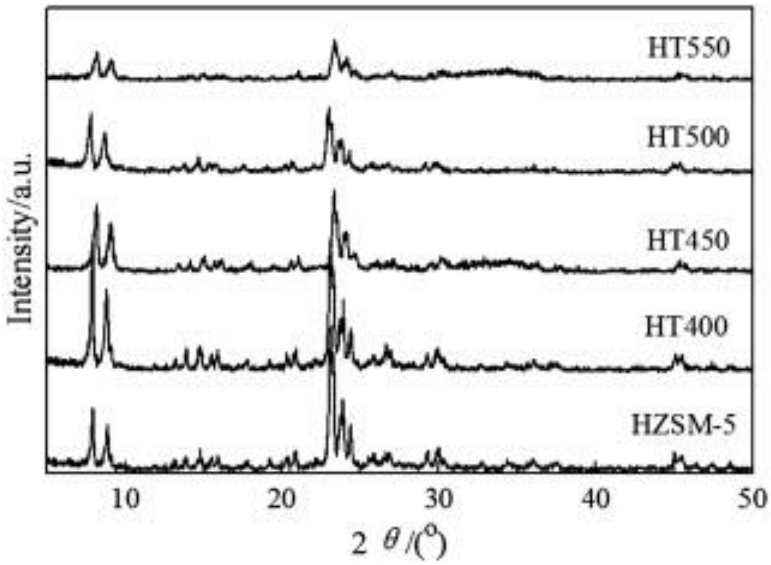

Figure V. 1 XRD patterns of the samples [137]

Table V.2 Properties of the parent and the steam treated HZSM-5 Zeolites [137]

Sample	Hydrothermal treatment T (°C)	SiO_2/Al_2O_3	Relative crystallinity (%)
HZSM-5	No treatment	25.5	100
HT400	400	28.5	98.6
HT450	450	29.4	82.4
HT500	500	28.5	76.7
HT550	550	28.9	57.3

Zhao et al. reported that steam treatment of ZSM-5 does not change zeolite structure. As shown in Figure V.1, all the samples exhibit a typical MFI structure, which means the steam treatment under high temperature did not destroy the zeolite structure. However, it did decrease the crystallinity. Table V.2 shows that the relative crystallinity decreased as the treatment

temperature increased. Also, the Si/Al ratio increased slightly after steam treatment. This is caused by dealumination effects during the steam treatment. Moreover, according to the N_2 adsorption/desorption results, a hysteresis loop appeared on these steam treated samples in the relative pressure of 0.45 – 1.00 (Figure V.2), which indicates the formation of mesopores in the zeolite structure. Zhao et al. claimed that those new mesopores might be generated from the structural rearrangement and secondary pore formation. Furthermore, Table V.3 shows that the total surface areas (S_{BET}), microporous areas (S_{micro}), and microporous volume (V_{micro}) decreased with the increased steam treatment temperature. This is also resultant from the newly generated mesoporous structure. However, when the treatment temperature was increased to 550 ºC, both S_{micro} and V_{micro} decreased dramatically. This is because the treatment temperature was too high and led to the partial destruction of the zeolite framework.

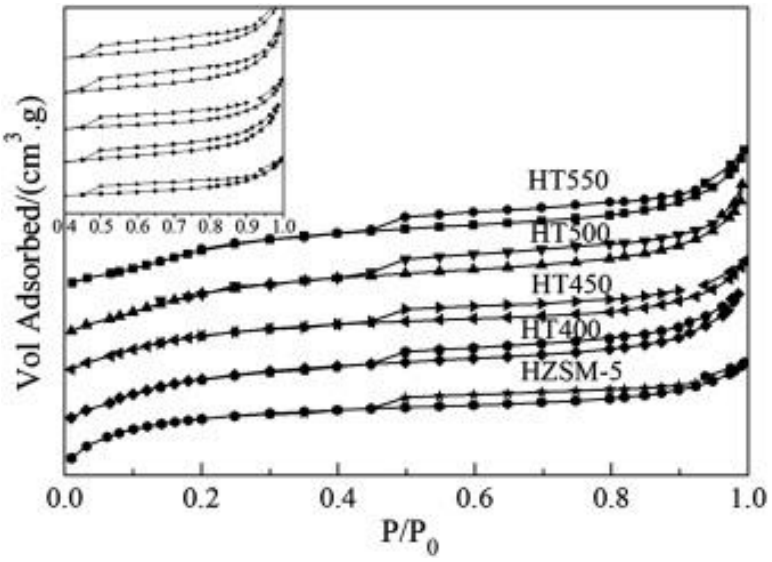

Figure V. 2 N_2 adsorption and desorption isotherms for the parent ZSM-5 and the steam treated ZSM-5 [137]

Table V.3 Textural properties of the parent and steam treated HZSM-5 zeolites [137]

Sample	Surface area (m^2/g^{-1})			Pore volume (cm^3/g^{-1})			rp/(nm)
	S_{BET}[a]	S_{micro}[b]	S_{ext}	V_{total}[c]	V_{micro}[b]	V_{meso}	
HZSM-5	326.5	242.4	84.1	0.181	0.112	0.069	2.22
HT400	328.6	210.1	118.5	0.198	0.096	0.102	2.41
HT450	297.9	189.4	108.5	0.178	0.087	0.091	2.39
HT500	319.0	177.0	142.0	0.207	0.081	0.126	2.59
HT550	288.6	155.5	133.1	0.188	0.067	0.121	2.61

[a] BET method

[b] Volume adsorbed at $P/P_0 = 0.99$

[c] t-plot method

The NH_3-TPD patterns were shown in Figure V.3. The lower temperature desorption peaks (100 – 300 ºC) belong to weak acid sites, and higher temperature peaks (350 – 500 ºC) belong to strong acid sites. The characterization results showed that the peak intensities of both the weak and strong acid sites decreased after steam treatment. Also, the steam treated samples demonstrated a lower desorption temperature in the high temperature region. These factors indicate that the steam treatment decreased the ZSM-5 acidity, especially for those strong acid sites.

The authors also demonstrated a stability test by comparisons the performance of HT500 with the parent ZSM-5 in the reaction of ethanol dehydration to ethylene. As Figure V.4 shows, the parent HZSM-5 started with high ethanol conversion, then dropped dramatically after around 20 hours of reaction. However, the steam treated HT500 remained active for more than 350 hours even under higher reaction temperature (275 ºC) than the parent HZSM-5 (250 ºC). The

steam treatment greatly extended ZSM-5 lifetime by reducing its acid strength to slow the coke formation and generating mesoporous structure to increase its capacity for coke accumulation.

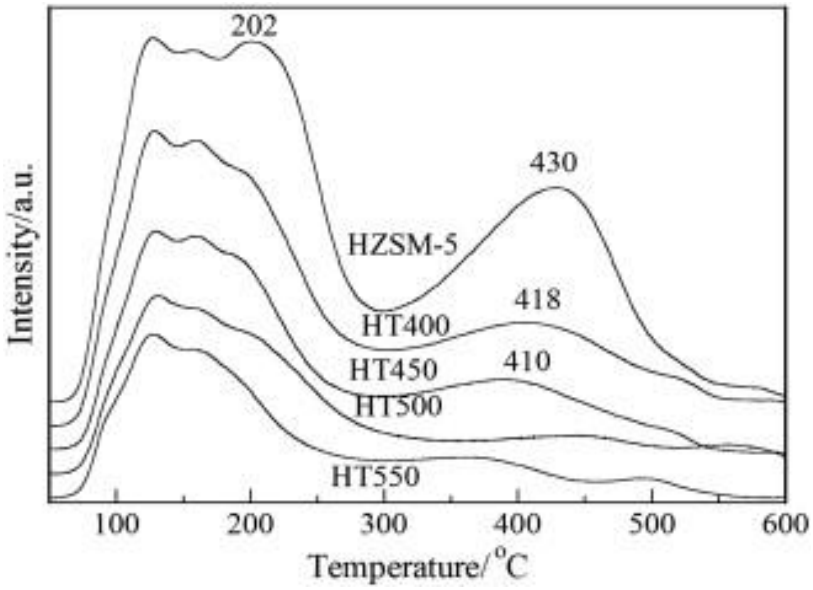

Figure V. 3 NH_3-TPD profiles of the parent and treated HZSM-5 catalyst [137]

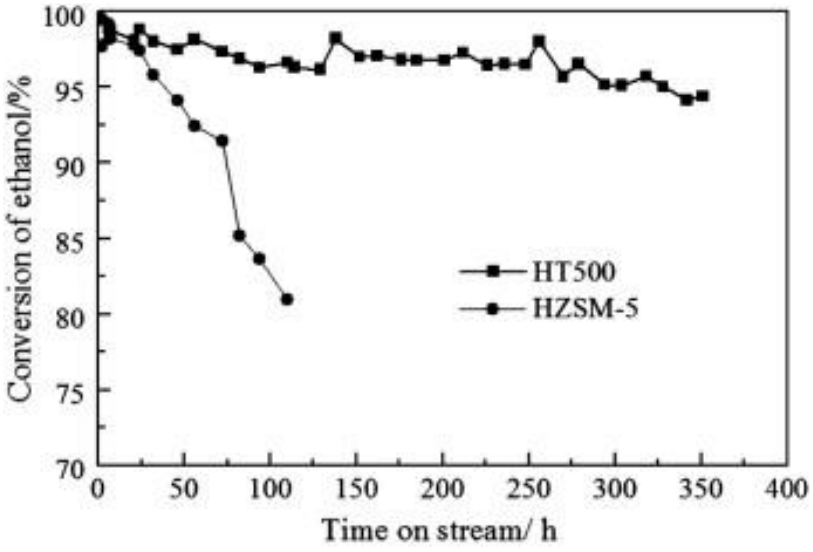

Figure V. 4 The stability test of HT500 and parent HZSM-5 (reaction condition: HZSM-5, T = 250 °C; HT500, T = 275 °C, WHSV = 2.37 h^{-1}, 20 vol% ethanol) [137]

In short, steam treatment of zeolites under appropriate conditions could adjust zeolite acidity, especially by reducing the strength of strong acid sites. This could lead to slow coke formation rates which in turn increases zeolite stability. In addition, steam treatment could also create some mesoporous structure in zeolites, which increase resistance to coke deposition. Therefore, we plan to do a steam treatment for ZSM-5 (T=500 ºC for 6 hours) to extend its lifetime in the SV-STG process.

V.2.2.2 Alkaline Modification

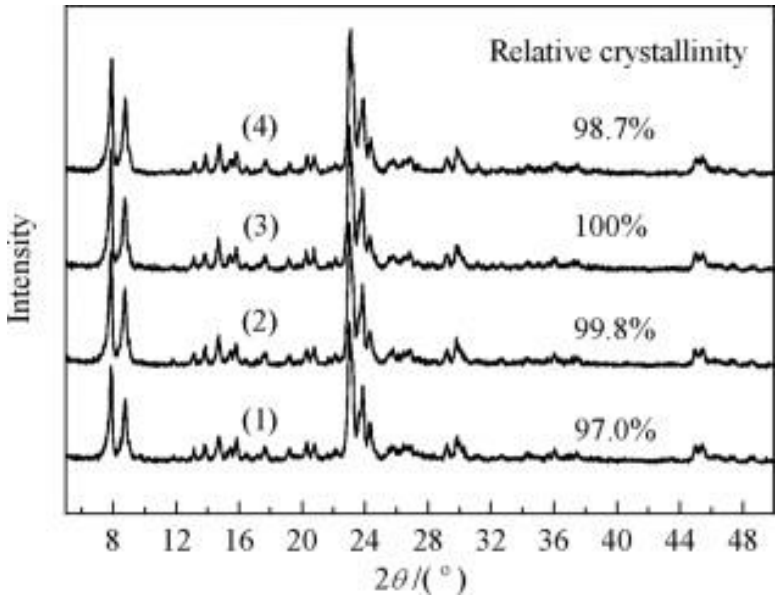

Figure V. 5 XRD patterns of HZSM-5 with different TPAOH treatment time. (1) nHZ; (2) T24; (3) T48; (4) T72 [145]

Alkaline modification of zeolites means treating the zeolites in an alkaline medium, which helps to clear the zeolite channels and obtain mesoporous zeolites. Traditional, inorganic alkali like NaOH was used to treat zeolites. Usually, these alkalis are strong, and they sometimes easily destroy the zeolite structure, but there are some successful examples. For instance, Bjørgen et al. [146] reported treatment of HZSM-5 with NaOH solution, which improved catalyst lifetime by 3.3

fold (quantified as the total conversion capacity) and enhanced selectivity towards the desired gasoline products. These results were achieved by modifying acidity, improving crystallinity, and introducing a mesoporous structure. Groen et al. [147,148] demonstrated the formation of accessible intra-crystalline mesopores after a controlled desilication of HZSM-5 by NaOH solution. Currently, organic alkalines are getting popular to do post modification of zeolites due to its controllable alkalinity which leads to mild modification without severe destroy zeolite structure. Tetrapropylammonium hydroxide (TPAOH) is one of the common organic alkalines used to modify ZSM-5.

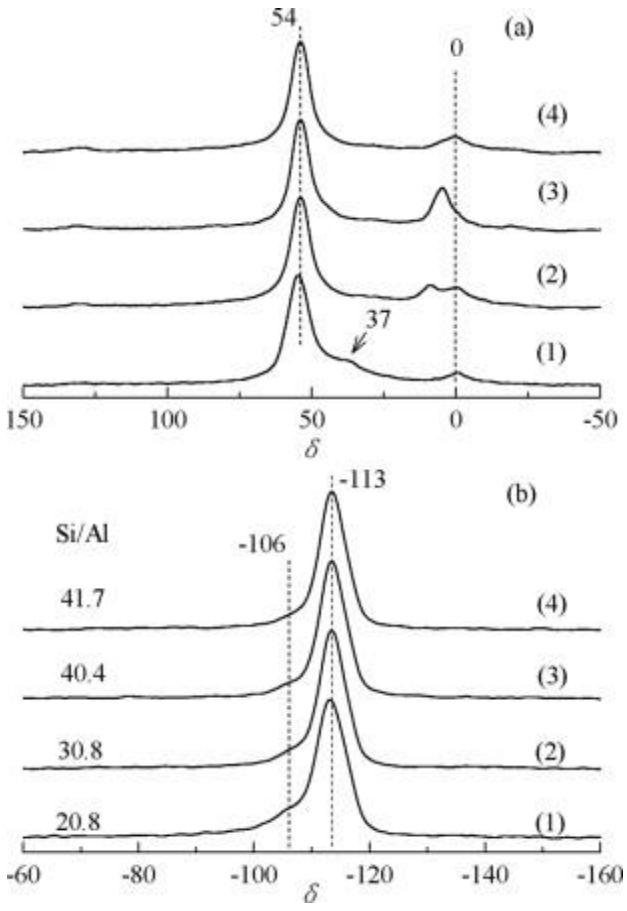

Figure V. 6 (a) ^{27}Al and (b) ^{29}Si MAS NMR spectra of HZSM-5 with different TPAOH treatment time: (1) HZ; (2) T24-HZ; (3) T48-HZ; (4) T72-HZ [145]

Guo et al. [145] reported a post-modification of nanocrystalline ZSM-5 using TPAOH, which greatly increased catalyst stability. First, nanocrystalline NaZSM-5 powder was treated with TAPOH solution at 170 ºC for a certain period (24, 48, and 72 hours) in an autoclave. After washing with deionized water and drying, the treated samples were calcinated. Then, NH_4NO_3 solution was used to do ion exchange, followed by washing, drying, and calcination. The obtained samples are nanocrystalline HZSM-5 and denoted as Tx-HZ (x represents the treatment time). As shown in Figure V.5, all the samples have a similar XRD pattern, which means the TPAOH treatment did not affect the crystal structure. Instead, the peak intensity slightly increased as the treatment time increased. This indicates that the relative crystallinity increased after TPAOH treatment, which Guo et al. considered as the secondary crystallization of amorphous species or non-framework silicon and aluminum on the zeolite surface. Guo et al. also showed MAS NMR data to support this claim. Figure V.6a is the ^{27}Al MAS NMR spectra of the ZSM-5 samples. There are two major peaks: δ=54 represents tetrahedrally coordinated framework aluminum; δ=0 arises from the six-coordinated non-framework aluminum. For the parent sample HZ, δ=37 has a signal that is attributed to five-coordinated framework aluminum. We can clearly see that the signal of five-coordinated framework aluminum significantly decreased after treatment with TPAOH. At the same time, the signal for non-framework aluminum greatly increased, which indicated the TPAOH treatment could remove aluminum from the ZSM-5 lattice. As treatment time increased, the δ=0 signal continues to increase, but the signal for T72-HZ sample decreased compared to T48-HZ sample. This indicates that after 48 hours of treatment the dealumination started to drop and recrystallization begin to take occur. The corresponding Si/Al ratio (Figure V.6b) could also support this concept. After 24 hours of treatment, the Si/Al ratio increased from 20.8 to 30.8 as a result of framework dealumination.

When treatment time increased to 48 hours, the Si/Al ratio continue increased to 40.4, which means dealumination continued to occur. However, if the treatment time increased to 72 hours, the Si/Al ratio only slightly increased to 41.7. This is because the secondary crystallization started to recrystallize these non-framework aluminum species.

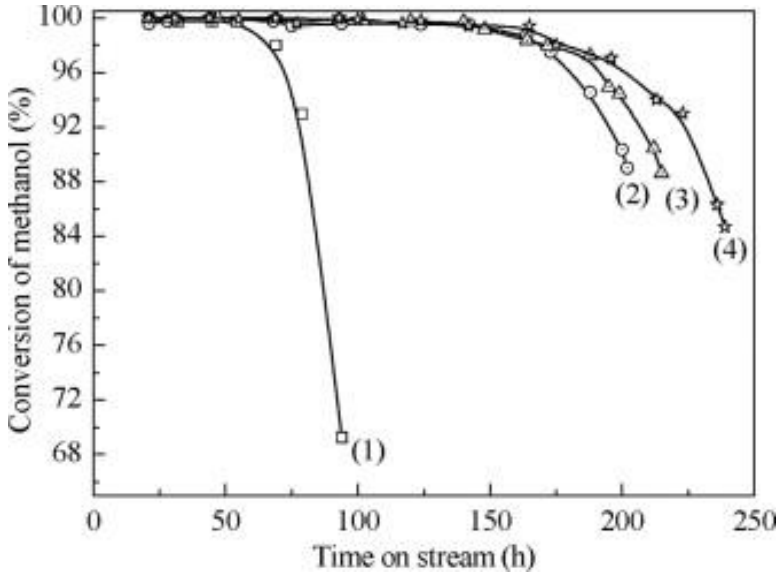

Figure V. 7 Conversion of methanol to hydrocarbons as a function of time on stream. (1) nHZ; (2) T24; (3) T48; (4) T72 [145]

Guo et al. applied these TPAOH treated ZSM-5 samples to the MTG reaction and compared with the performance of untreated parent ZSM-5. As shown in Figure V.7, the parent ZSM-5 sample displayed a high methanol conversion (above 98%), but it only lasted for 70 hours before quickly deactivating. Compared with the parent ZSM-5, T24-HZ maintained a high methanol conversion (above 98%) for 170 hours, and its deactivation process is slower than the parent ZSM-5. As the TPAOH treatment time increased, catalyst lifetime continued to increase. Therefore, TPAOH treatment could significantly increase ZSM-5 lifetime in the MTG reaction.

V.2.3 Direct Synthesis of Mesoporous ZSM-5

The above methods are posted modification of ZSM-5 to generate a mesoporous structure that could extend its lifetime in MTG related reactions. There are methods to directly synthesize mesoporous ZSM-5 which could also lead to a longer lifetime. Rownaghi et al. [140] reported a novel method to directly synthesize uniform mesoporous ZSM-5 single crystals by using TPAOH as a structure directing agent to generate mesopores. Figure V.8 shows that the mesoporous ZSM-5 has a similar XRD pattern to the conventional ZSM-5 and both of them are well matched to MFI structure. However, the crystal morphology is quite different between the mesoporous ZSM-5 and the conventional ZSM-5 (Figure V.9). Figure V.9a shows mesoporous ZSM-5 are micro-rectangular crystals composed of small nanocrystals. In contrast, conventional ZSM-5 has a typical shape of micron size ZSM-5 crystals (Figure V.9d). The N_2 adsorption/desorption isotherms clearly show that mesoporous ZSM-5 exhibited a type-IV isotherm, which is often associated with mesoporous materials. On the other hand, the conventional ZSM-5 displayed a type-I isotherm, which is a typical microporous material. The mesoporous ZSM-5 exhibited a high total pore volume of 0.46 cm^3/g^{-1} ($p/p_0 = 0.995$), which is more than double the total pore volume of the conventional ZSM-5 (0.20 cm^3/g^{-1}). This is mainly what contributed to the mesoporous structure. The authors claimed that the mesoporous structure plays a crucial role in catalyst stability. The novel mesoporous ZSM-5 exhibited improved stability in MTG reaction by increasing external surface area, which resulted in a faster diffusion of the hydrocarbon products in the ZSM-5 channels and a slower coke formation rate.

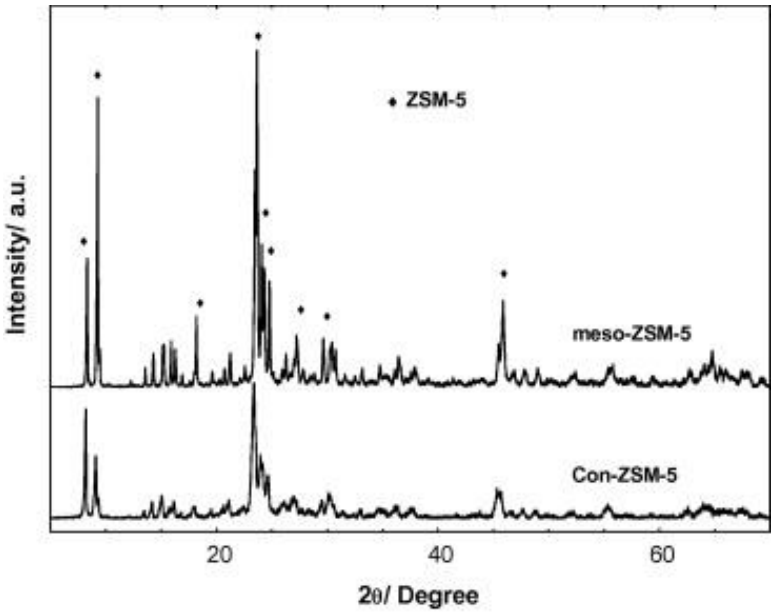

Figure V. 8 XRD patterns of mesoporous ZSM-5 single crystals and conventional ZSM-5 [140]

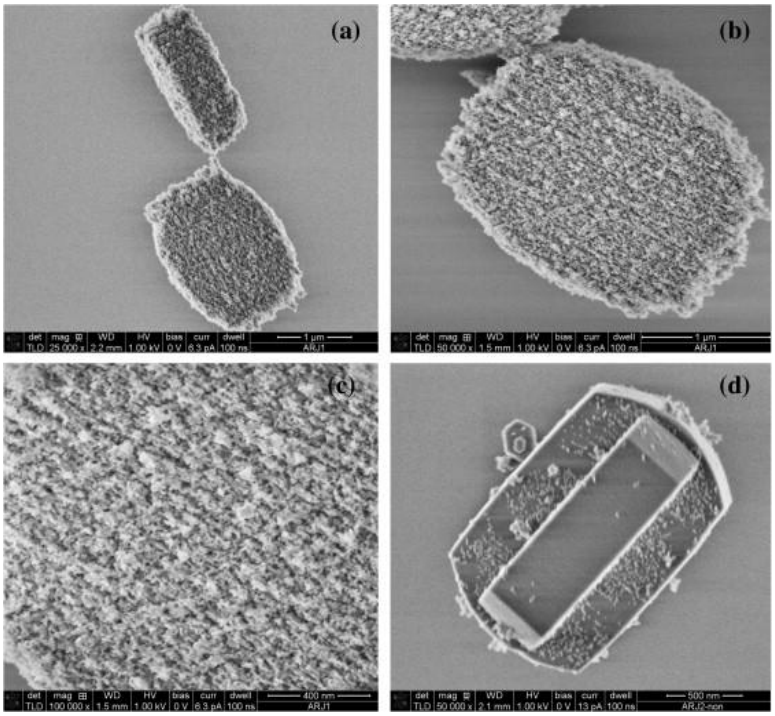

Figure V. 9 (a–c) SEM images of mesoporous ZSM-5 single crystals (three different magnifications), and (d) conventional ZSM-5 crystals [140]

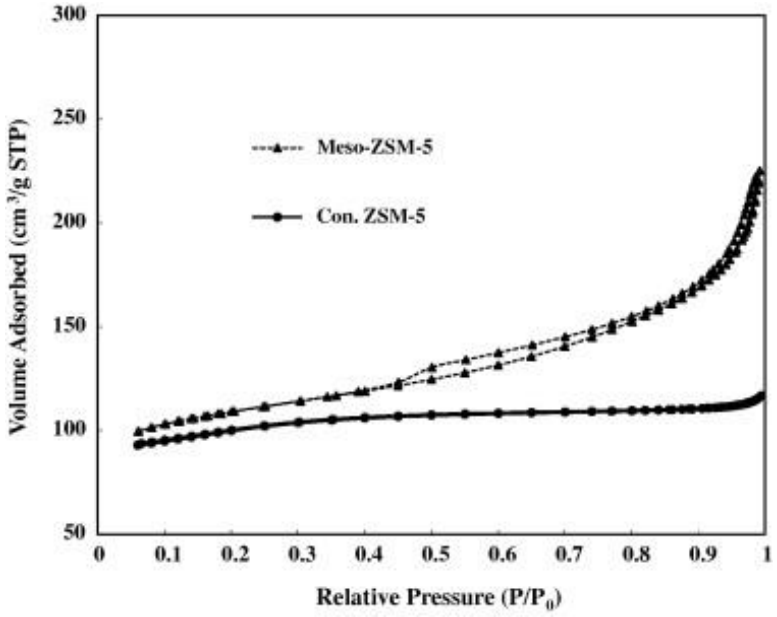

Figure V. 10 N_2 adsorption/desorption isotherms of mesoporous ZSM-5 and conventional ZSM-5 [140]

V.2.4 Catalyst Regeneration

The above methods are all used to extend zeolite lifetime, but the catalyst will be deactivated and need to be regenerated eventually. According to literature, there are mainly three forms of deactivation. First, the deposition of carbonaceous residues or coke on zeolite surface and inside zeolite channels. Second, water produced in the MTG process could slowly cause an irreversible destruction effect to the zeolite structure. Third, the high temperature involved in the regeneration process may affect the zeolite structure. From the above, we know that the zeolite used in the MTG process has a limited lifetime even with catalyst regeneration because an irreversible destruction of the catalyst happens during the reaction process.

There are two common methods to regenerate the deactivated zeolites: solvent wash and burning off the coke. Solvent wash means using an organic solvent, such as acetone, to dissolve the coke. This method required a large amount of solvent, so it is relatively expensive. Another

drawback is that it can only partially remove the coke. Hence, people tend to use another method: directly burning off the coke in air. This method is usually conducted at high temperatures (400 – 500 ºC) and must be in an oxidative environment. In the traditional STG process, typically there are five zeolite reactors totally: four zeolite reactors are in operation, and one is always in regeneration. As we mentioned above, the zeolite in the MTG process is easily deactivated by coke deposition, which is one the most important reasons why the traditional STG process uses separate reactor systems for each reaction step. In short, coke burning is not a problem for the traditional STG process.

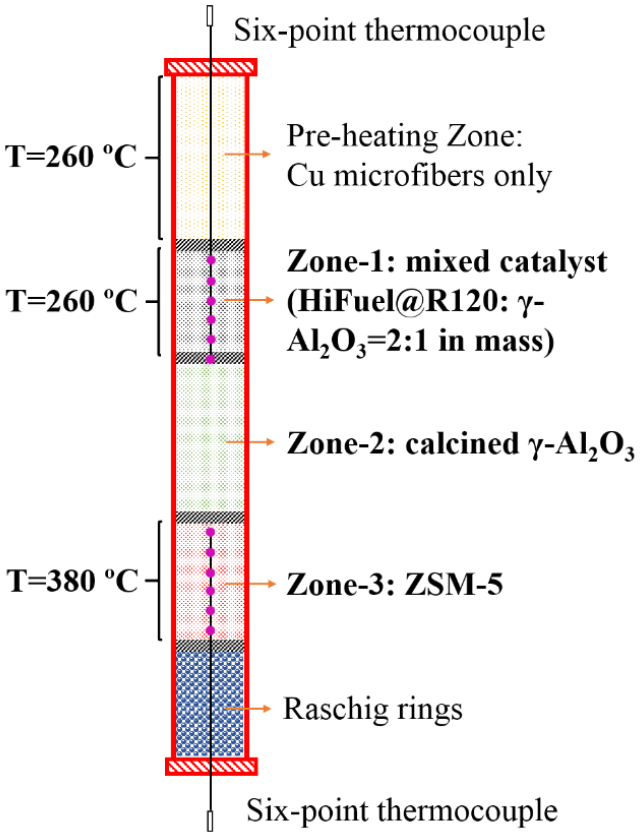

Figure V. 11 The scheme of SV-STG

However, for the SV-STG process, there are at least two issues that need to be addressed. First, whether the ZSM-5 regeneration process will affect other catalysts inside the reactor?

Second, does the Cu MFEC structure remain stable during the regeneration process? In the SV-STG, there are three different reaction zones, and each zone has different catalysts (Figure V.11). The first zone was loaded with a mixed catalyst including methanol reforming catalyst (HiFeul@R120) and γ-Al_2O_3, and the second zone loaded with γ-Al_2O_3. When flowing air through the system under high temperature (400 – 500 ºC), will the other two kinds of catalysts be stable? Based on our understanding, it will not cause side effects on the other catalysts. First, γ-Al_2O_3 in Zone-2 is stable under the regeneration conditions. Second, we can control the temperature of each specific zone. We can stop heating Zone-1 when Zone-3 has been heated to 400 – 500 ºC. Although the temperature of Zone-1 might still be higher than the room temperature, HiFuel@R120 is composed of CuO/Zn_2O_3/Al_2O_3, hence it should be stable. Even if it has been oxidized, it has to go through the pre-reduction process before a new reaction cycle is started.

Another issue is that the SV-STG system used Cu MFEC structure to increase reactor size and better manage the generated reaction heat. Cu MFEC is sintered Cu microfibers entrapped with catalyst particles. Under a typical zeolite regeneration condition (400 – 500 ºC with flowing air), Cu metal will be oxidized. However, this regeneration process has been demonstrated successfully in the regeneration of hydrocracking catalysts in the FTS process. The Cu MFEC structure is not harmed by passing through a gas composed of N_2 and a low percentage of O_2 (5%) to burn off coke formed on the catalysts. Although the Cu MFEC media is partially oxidized, they will also be reduced during the pre-reduction process to activate the catalysts. Based on the above discussion, we expect that both the Cu MFEC structure and the other catalysts in the SV-STG system will be stable under the typical zeolite regeneration condition.

V.3 Economic Cost Calculation

The flow sheet of the SV-STG process is simpler than the traditional STG process. This could lead to a dramatic reduction in both CAPEX and OPEX, but we did not show any simulation data to support this claim. Therefore, we plan to use Aspen to build models and to calculate the economic cost for both the traditional STG process and the SV-STG process. By doing this, we can directly compare these two processes and show the benefits of the SV-STG.

V.4 Develop SV-STO

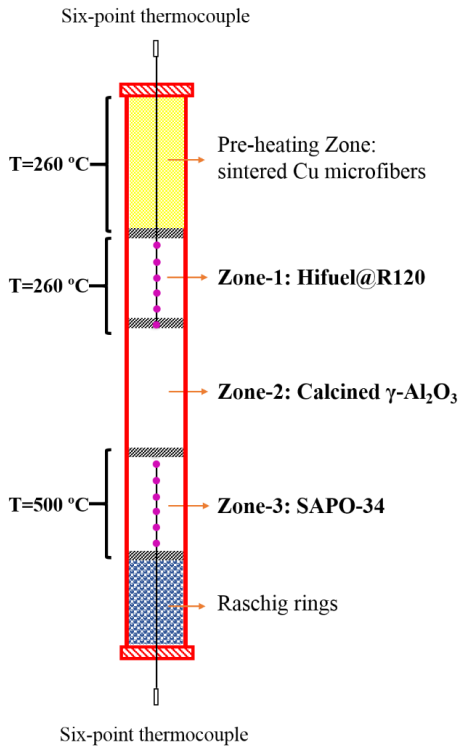

Figure V.12 The scheme of SV-STO

In the methanol-to-olefins (MTO) process, methanol is converted at very high temperatures (470 – 515 ºC), and consequently the heavy hydrocarbons formed under these conditions are cracked to give products comprised mainly of propene and butene. Typically, the olefins yield exceeded

90%. The process can be modified for high ethylene and propylene yield (about 60%). If we can integrate these processes into a single vessel just like the SV-STG process, we can start with syngas and directly produce olefins in a single vessel (SV-STO) with extremely high selectivity. The only difference between SV-STO and SV-STG is the catalyst used in Zone-3 and the reaction temperature in Zone-3. As we see in Figure V.12, we plan to load the MTO catalyst (SAPO-34) in Zone-3 and operate Zone-3 under a typical MTO reaction temperature (500 ºC). Since the SV-STG system has been operated successfully, we have reason to expect the SV-STO system will also be successful.

References

1 A. A. Adesina, *Appl. Catal. A Gen.*, 1996, **138**, 345–367.

2 C. H. Bartholomew, *Catal. Letters*, **7**, 303–315.

3 G. P. van der Laan, *Kinetics, Selectivity and Scale Up of the Fischer-Tropsch Synthesis*, 1999.

4 M. D. Andre Steynberg, *Fischer-Tropsch Technology by Andre Steynberg , Mark Dry (Editor)*, 2004.

5 A. Y. Khodakov, W. Chu and P. Fongarland, 2007, **107**, 1692–1744.

6 H. Schulz, *Appl. Catal. A Gen.*, 1999, **186**, 3–12.

7 A. N. Stranges, *Stud. Surf. Sci. Catal.*, 2007, **163**, 1–27.

8 A. Galadima and O. Muraza, *J. Nat. Gas Sci. Eng.*, 2015, **25**, 303–316.

9 F. J. Keil, *Microporous Mesoporous Mater.*, 1999, **29**, 49–66.

10 Exxon Mobil Research and Engineering, *Methanol to Gasoline (MTG) Production of Clean Gasoline from Coal*, 2009.

11 J. E. Penick, W. Lee, J. Maziuk and D. Corporation, *Development of the Methanol-to-Gasoline Process*, 1983.

12 G. P. van der Laan and A. A. C. M. Beenackers, *Catal. Rev. Sci. Eng.*, 1999, **41**, 255–318.

13 A. Y. Khodakov, W. Chu and P. Fongarland, *Am. Chem. Soc.*, 2007, **107**, 1692–1744.

14 E. de Smit and B. M. Weckhuysen, *Chem. Soc. Rev.*, 2008, **37**, 2758.

15 F. Ren, H. Li, D. Wang, J. Wang, W. Pan and J. Li, *ACS Div. Fuel Chem. Prepr.*, 2003, **48**, 921–922.

16 A. B. Stiles, F. Chen, J. B. Harrison, X. Hu, D. A. Storm and H. X. Yang, *Ind. Eng. Chem. Res.*, 1991, **30**, 811–821.

17 Z. Chu, H. Chen, Y. Yu, Q. Wang and D. Fang, *J. Mol. Catal. A Chem.*, 2013, **366**, 48–53.

18 B. Sabour, M. H. Peyrovi, T. Hamoule and M. Rashidzadeh, *J. Ind. Eng. Chem.*, 2014, **20**, 222–227.

19 S. S. Penner, *Coal Gasification: Direct Applications and Syntheses of Chemicals and Fuels*, 1987.

20 H. Kölbel and K. D. Tillmetz, *J. Catal.*, 1974, **34**, 307–316.

21 M. E. Dry, *Appl. Catal. A Gen.*, 1996, **138**, 319–344.

22 L. V. MacDougall, *Catal. Today*, 1991, **8**, 337–369.

23 S. S. Penner, *Energy*, 1987, **12**, 689–728.

24 R. A. van Santen, A. J. Markvoort, I. A. W. Filot, M. M. Ghouri and E. J. M. Hensen, *Phys. Chem. Chem. Phys.*, 2013, **15**, 17038–17063.

25 A. Jones and B. D. McNicol, *J. Catal.*, 1977, **47**, 384–388.

26 K. C. Waugh, *Catal. Today*, 1992, **15**, 51–75.

27 J. A. Rabo, A. P. Risch and M. L. Poutsma, *J. Catal.*, 1978, **53**, 295–311.

28 M. Poutsma, *J. Catal.*, 1978, **52**, 157–168.

29 G. Henrici-Olivé and S. Olivé, *Angew. Chemie Int. Ed. English*, 1976, **15**, 136–141.

30 J. F. Haw, W. Song, D. M. Marcus and J. B. Nicholas, *Acc. Chem. Res.*, 2003, **36**, 317–326.

31 M. Stöcker, *Microporous Mesoporous Mater.*, 1999, **29**, 3–48.

32 E. G. Derouane, eds. F. R. Ribeiro, A. E. Rodrigues, L. D. Rollmann and C. Naccache, Springer Netherlands, Dordrecht, 1984, pp. 515–528.

33 J. P. van den Berg, J. P. Wolthuizen and J. H. C. van Hooff, *5th International Conference on Zeolites*, (*LVC Rees, Ed*), 1980, 649.

34 M. B. Sayed, R. A. Kydd and R. P. Cooney, *J. Catal.*, 1984, **88**, 137–149.

35 T. Mole and J. A. Whiteside, *J. Catal.*, 1982, **75**, 284–290.

36 T. Mole, *J. Catal.*, 1983, **84**, 423–434.

37 J. J. Spivey, G. F. Froment, W. J. H. Dehertog, and A. J. Marchi, *Zeolite Catalysis in the Conversion of Methanol into Olefins*, 1992.

38 S. Saeidi, M. K. Nikoo, A. Mirvakili, S. Bahrani, S. Amin, N. Aishah and M. R. Rahimpour, *Rev. Chem. Eng.*, 2015, **31**, 209–238.

39 R. Guettel, U. Kunz and T. Turek, *Chem. Eng. Technol.*, 2008, **31**, 746–754.

40 B. H. Davis, *Top. Catal.*, 2005, **32**, 143–168.

41 S. T. Sie and R. Krishna, *Appl. Catal. A Gen.*, 1999, **186**, 55–70.

42 R. M. De Deugd, F. Kapteijn and J. A. Moulijn, *Top. Catal.*, 2003, **26**, 29–39.

43 M. Sheng, *Enhanced Heat Transfer Catalyst Structures for Fischer-Tropsch Synthesis*, 2011.

44 A. O. Odunsi, T. S. O'Donovan and D. A. Reay, *Appl. Therm. Eng.*, 2016, **93**, 1377–1393.

45 E. Durham, R. Xu, S. Zhang, M. R. Eden and C. B. Roberts, *Ind. Eng. Chem. Res.*, 2013, **52**, 3133–3136.

46 E. Durham, C. Stewart, D. Roe, R. Xu, S. Zhang and C. B. Roberts, *Ind. Eng. Chem. Res.*, 2014, **53**, 9695–9702.

47 R. Xu, S. Zhang and C. B. Roberts, *Ind. Eng. Chem. Res.*, 2013, **52**, 14514–14524.

48 R. M. De Deugd, F. Kapteijn and J. A. Moulijn, *Catal. Today*, 2003, **79**–**80**, 495–501.

49 M. Sheng, D. R. Cahela, H. Y. Yang, C. F. Gonzalez, W. R. Yantz, D. K. Harris and B. J. Tatarchuk, *Int. J. Heat Mass Transf.*, 2013, **56**, 10–19.

50 Q. Gu, P. Zhao, R. T. Henderson and B. J. Tatarchuk, *Ind. Eng. Chem. Res.*, 2016, **55**, 8025–8033.

51 S. Wahid, D. R. Cahela and B. J. Tatarchuk, *Ind. Eng. Chem. Res.*, 2013, **52**, 14472–14482.

52 X. Cheng, H. Yang and B. J. Tatarchuk, *Catal. Today*, 2016, **273**, 62–71.

53 M. Sheng, D. R. Cahela, H. Yang, C. F. Gonzalez, W. R. Yantz, D. K. Harris and B. J. Tatarchuk, *Int. J. Heat Mass Transf.*, 2013, **56**, 10–19.

54 M. Sheng, H. Yang, D. R. Cahela, W. R. Yantz, C. F. Gonzalez and B. J. Tatarchuk, *Appl. Catal. A Gen.*, 2012, **445**–**446**, 143–152.

55 E. F. Sousa-Aguiar, F. B. Noronha and A. Faro, Jr., *Catal. Sci. Technol.*, 2011, **1**, 698–713.

56 R. M. De Deugd, F. Kapteijn and J. a. Moulijn, *Top. Catal.*, 2003, **26**, 29–39.

57 D. J. Duvenhage and T. Shingles, *Catal. Today*, 2002, **71**, 301–305.

58 M. E. Dry, *Catal. Today*, 2002, **71**, 227–241.

59 R. L. Espinoza, a. P. Steynberg, B. Jager and a. C. Vosloo, *Appl. Catal. A Gen.*, 1999, **186**, 13–26.

60 W. Liu, J. Hu and Y. Wang, *Catal. Today*, 2009, **140**, 142–148.

61 A.-M. Hilmen, E. Bergene, O. a. Lindvåg, D. Schanke, S. Eri and a. Holmen, *Catal.*

Today, 2001, **69**, 227–232.

62 R. M. De Deugd, F. Kapteijn and J. a. Moulijn, *Catal. Today*, 2003, **79**–**80**, 495–501.

63 L. C. Almeida, F. J. Echave, O. Sanz, M. a. Centeno, G. Arzamendi, L. M. Gandía, E. F. Sousa-Aguiar, J. a. Odriozola and M. Montes, *Chem. Eng. J.*, 2011, **167**, 536–544.

64 J. C. Park, N. S. Roh, D. H. Chun, H. Jung and J. I. Yang, *Fuel Process. Technol.*, 2014, **119**, 60–66.

65 C. Maretto and R. Krishna, *Catal. Today*, 2001, **66**, 241–248.

66 E. Tronconi, G. Groppi, T. Boger and A. Heibel, *Chem. Eng. Sci.*, 2004, **59**, 4941–4949.

67 L. Giani, G. Groppi and E. Tronconi, *Ind. Eng. Chem. Res.*, 2005, **44**, 4993–5002.

68 D. K. Harris, D. R. Cahela and B. J. Tatarchuk, *Compos. - Part A Appl. Sci. Manuf.*, 2001, **32**, 1117–1126.

69 D. R. Cahela and B. J. Tatarchuk, *Catal. Today*, 2001, **69**, 33–39.

70 B. Tatarchuk, H. Yang, R. Kalluri and D. Cahela, *U.S. Patent 8420023B2*, 2013.

71 B. J. Tatarchuk, B. K. Chang, Y. Lu, L. Chen, E. Luna and D. Cahela, *U.S. Patent S7501012B2*, 2009.

72 H. Yang, B. J. Tatarchuk, T. J. Barron and P. S. Dimick, *U.S. Patent 9,614,263*, 2017.

73 H. Yang, P. S. Dimick, T. J. Barron and B. J. Tatarchuk, *U.S. Patent EP2872247A1*, 2015.

74 H. Yang, D. R. Cahela and B. J. Tatarchuk, *Chem. Eng. Sci.*, 2008, **63**, 2707–2716.

75 H. Yang, Y. Lu and B. J. Tatarchuk, *J. Power Sources*, 2007, **174**, 302–311.

76 W. H. Zhu, P. J. Durben and B. J. Tatarchuk, *J. Power Sources*, 2002, **111**, 221–231.

77 W. H. Zhu, M. E. Flanzer and B. J. Tatarchuk, *J. Power Sources*, 2002, **112**, 353–366.

78 Q. Gu, R. T. Henderson and B. J. Tatarchuk, *Eng. Appl. Comput. Fluid Mech.*, 2015, **9**, 567–576.

79 M. Sheng, H. Yang, D. R. Cahela and B. J. Tatarchuk, *J. Catal.*, 2011, **281**, 254–262.

80 H. Schulz, *Catal. Today*, 2011, **178**, 151–156.

81 S. Zhang, R. Xu, E. Durham and C. B. Roberts, *AIChE J.*, 2014, **60**, 2573–2583.

82 Y. Yoneyama, J. He, Y. Morii, S. Azuma and N. Tsubaki, *Catal. Today*, 2005, **104**, 37–40.

83 C. Kibby, K. Jothimurugesan, T. Das, H. S. Lacheen, T. Rea and R. J. Saxton, *Catal. Today*, 2013, **215**, 131–141.

84 S. Sartipi, M. Makkee, F. Kapteijn and J. Gascon, *Catal. Sci. Technol.*, 2014, **4**, 893.

85 K. Keyvanloo, M. K. Mardkhe, T. M. Alam, C. H. Bartholomew, B. F. Woodfield and W. C. Hecker, *ACS Catal.*, 2014, **4**, 1071–1077.

86 C. L. Kibby, K. Jothimurugesan, T. K. Das, R. J. Saxton and A. W. Burton, 2011.

87 K. Keyvanloo, J. B. Horton, W. C. Hecker and M. D. Argyle, *Catal. Sci. Technol.*, 2014, **4**, 4289–4300.

88 Y. Zhang, X. Shi, J. M. Kim, D. Wu, Y. Sun and S. Peng, *Catal. Today*, 2004, **93**–**95**, 615–618.

89 E. F. Iliopoulou, S. D. Stefanidis, K. G. Kalogiannis, A. Delimitis, A. A. Lappas and K. S. Triantafyllidis, *Appl. Catal. B Environ.*, 2012, **127**, 281–290.

90 V. M. Akhmedov and S. H. Al-Khowaiter, *Catal. Rev.*, 2007, **49**, 33–139.

91 D. B. Bukur and X. Lang, *Ind. Eng. Chem. Res.*, 1999, **38**, 3270-3275.

92 D. B. Bukur, X. Lang, D. Mukesh, W. H. Zimmerman, M. P. Rosynek and C. Lii, *Ind. Eng. Chem. Res.*, 1990, **29**, 1588–1599.

93 M. Baranak, B. Gürünlü, A. Sarıoğlan, Ö. Ataç and H. Atakül, *Catal. Today*, 2013, **207**, 57–64.

94 F. A. N. Fernandes, *Chem. Eng. Technol.*, 2005, **28**, 930–938.

95 S. Gamba, L. a. Pellegrini, V. Calemma and C. Gambaro, *Catal. Today*, 2010, **156**, 58–64.

96 C. Bouchy, G. Hastoy, E. Guillon and J. a. Martens, *Oil Gas Sci. Technol.*, 2009, **64**, 91–112.

97 W. Yu, B. Wu, J. Xu, Z. Tao, H. Xiang and Y. Li, *Catal. Letters*, 2008, **125**, 116–122.

98 V. M. Akhmedov and S. H. Al-Khowaiter, *Catal. Rev. Sci. Eng.*, 2002, **44**, 455–498.

99 H. Schulz, *Catal. Today*, 2014, **228**, 113–122.

100 H. Schulz, *Catal. Today*, 2013, **214**, 140–151.

101 E. Iglesia, S. C. Reyes and R. J. Madon, *J. Catal.*, 1991, **129**, 238–256.

102 G. Bozga and I. T. A. and R. E. Bozga, *Recent Patents Catal.*, 2013, 2, 68–81.

103 Z. Azizi, M. Rezaeimanesh, T. Tohidian and M. R. Rahimpour, *Chem. Eng. Process.*

Process Intensif., 2014, **82**, 150–172.

104 C. Arcoumanis, C. Bae, R. Crookes and E. Kinoshita, *Fuel*, 2008, **87**, 1014–1030.

105 Z. Wang, T. He, J. Li, J. Wu, J. Qin, G. Liu, D. Han, Z. Zi, Z. Li and J. Wu, *Fuel*, 2016, **186**, 587–596.

106 K. Saravanan, H. Ham, N. Tsubaki and J. W. Bae, *Appl. Catal. B Environ.*, 2017, **217**, 494–522.

107 I. A. Kurzina, S. I. Reshetnikov, N. I. Karakchieva and L. N. Kurina, *Chem. Eng. J.*, 2017, **329**, 135–141.

108 M. Farsi, R. Eslamloueyan and A. Jahanmiri, *Chem. Eng. Process. Process Intensif.*, 2011, **50**, 85–94.

109 W. Lu, L. Teng, and W. Xiao, *Int. J. Chem. React. Eng.* , 2003, **1**, 1.

110 A. Bakopoulos, *Chem. Eng. Sci.*, 2006, **61**, 538–557.

111 G. R. Moradi, R. Ghanei, and F. Yaripour, *Int. J. Chem. React. Eng.*, 2007, **5**, 1–8.

112 L. L. Murrell, F. M. Dautzenberg, R. A. Overbeek and B. J. Tatarchuk, *US Patent 20020068026*, 2002.

113 X. Cheng, H. Yang and B. J. Tatarchuk, *Catal. Today*, 2016, **273**, 62–71.

114 D. L. S. Nieskens, A. Ciftci, P. E. Groenendijk, M. F. Wielemaker and A. Malek, *Ind. Eng. Chem. Res.*, 2017, **56**, 2722–2732.

115 X. D. Peng, A. W. Wang, B. A. Toseland and P. J. A. Tijm, *Ind. Eng. Chem. Res.*, 1999, **38**, 4381–4388.

116 A. C. Sofianos and M. S. Scurrell, *Ind. Eng. Chem. Res.*, 1991, **30**, 2372–2378.

117 S. Ilias and A. Bhan, *ACS Catal.*, 2013, **3**, 18–31.

118 K. Fujimoto, *J. Catal.*, 1985, **94**, 16–23.

119 T. Fischer-tropsch, 1979, **273**, 268–273.

120 R. Dagle, V. Lebarbier and J. L. Adarme, 2013, **PNNL-22984**, 94.

121 R. A. Dagle, J. A. Lizarazo-adarme, V. Lebarbier, M. J. Gray, J. F. White, D. L. King and D. R. Palo, *Fuel Process. Technol.*, 2014, **123**, 65–74.

122 K. Fujimoto, K. Asami, H. Saima, T. Shikada and H. Tominaga, *Ind. Eng. Chem. Prod. Res. Dev.*, 1986, **25**, 262–267.

123 W. O. Haag, R. M. Lago and P. G. Rodewald, *J. Mol. Catal.*, 1982, **17**, 161–169.

124 A. Takeuchi and J. Katzer, *J. Phys. Chem.*, 1981, **1**, 937–939.

125 G. J. Hutchings and R. Hunter, *Catal. Today*, 1990, **6**, 279–306.

126 K. A. Ali, A. Z. Abdullah and A. R. Mohamed, *Renew. Sustain. Energy Rev.*, 2015, **44**, 505–518.

127 M. Sheng, H. Yang, D. R. Cahela, W. R. Yantz, C. F. Gonzalez and B. J. Tatarchuk, *Appl. Catal. A Gen.*, 2012, **445**–**446**, 143–152.

128 D. K. Harris, D. R. Cahela and B. J. Tatarchuk, *Compos. - Part A Appl. Sci. Manuf.*, 2001, **32**, 1117–1126.

129 Q. Gu, R. T. Henderson and B. J. Tatarchuk, *Eng. Appl. Comput. Fluid Mech.*, 2015, **9**, 567–576.

130 C. D. Chang, *Catal. Today*, 1992, **13**, 103–111.

131 S. Lee and A. Sardesai, *Top. Catal.*, 2005, **32**, 197–207.

132 S. Yurchak, in *Methane Conversion*, eds. D. M. Bibby, C. D. Chang, R. F. Howe and S. B. T.-S. in S. S. and C. Yurchak, Elsevier, 1988, vol. 36, pp. 251–272.

133 U. Olsbye, S. Svelle, M. Bjrgen, P. Beato, T. V. W. Janssens, F. Joensen, S. Bordiga and K. P. Lillerud, *Angew. Chemie - Int. Ed.*, 2012, **51**, 5810–5831.

134 H. Schulz, *Catal. Today*, 2010, **154**, 183–194.

135 S. M. Campbell, D. M. Bibby, J. M. Coddington, R. F. Howe and R. H. Meinhold, *J. Catal.*, 1996, **161**, 338–349.

136 S. M. T. Almutairi, B. Mezari, E. A. Pidko, P. C. M. M. Magusin and E. J. M. Hensen, *J. Catal.*, 2013, **307**, 194–203.

137 Q. Sheng, K. Ling, Z. Li and L. Zhao, *Fuel Process. Technol.*, 2013, **110**, 73–78.

138 A. A. Rownaghi and J. Hedlund, *Ind. Eng. Chem. Res.*, 2011, **50**, 11872–11878.

139 Z. Wan, W. Wu, W. Chen, H. Yang and D. Zhang, *Ind. Eng. Chem. Res.*, 2014, **53**, 19471–19478.

140 A. A. Rownaghi, F. Rezaei and J. Hedlund, *Microporous Mesoporous Mater.*, 2012, **151**, 26–33.

141 M. Ogura, S. Y. Shinomiya, J. Tateno, Y. Nara, M. Nomura, E. Kikuchi and M. Matsukata, *Appl. Catal. A Gen.*, 2001, **219**, 33–43.

142 F. Bauer, H. Ernst, E. Geidel and R. Schödel, *J. Catal.*, 1996, **164**, 146–151.

143 G. Lietz, K. H. Schnabel, C. Peuker, T. Gross, W. Storek and J. Völter, *J. Catal.*, 1994, 148, 562–568.

144 S. Fathi, M. Sohrabi and C. Falamaki, *Fuel*, 2014, **116**, 529–537.

145 X. G. Y. He, M. Liu, C. Dai, S. Xu, Y. Wei, Z. Liu, *Chinese J. Catal.*, 2013, **34**, 1148–1158.

146 M. Bjørgen, F. Joensen, M. Spangsberg Holm, U. Olsbye, K. P. Lillerud and S. Svelle, *Appl. Catal. A Gen.*, 2008, **345**, 43–50.

147 J. C. Groen, J. A. Moulijn and J. Pérez-Ramírez, *J. Mater. Chem.*, 2006, **16**, 2121–2131.

148 J. C. Groen, T. Bach, U. Ziese, A. M. Paulaime-Van Donk, K. P. De Jong, J. A. Moulijn and J. Pérez-Ramírez, *J. Am. Chem. Soc.*, 2005, **127**, 10792–10793.